Stimulated Brillouin scattering
Its generation and applications in optical fibre

by

David Culverhouse

A thesis submitted for the Degree of

Doctor of Philosophy

University of Kent at Canterbury

February 1992

Physics Laboratory

The University

CANTERBURY

Kent

This thesis is dedicated to Patricia, my mother and my father

Contents

Acknowledgements

The experimental and theoretical work presented in this thesis was performed under the joint supervision of Professor D.A. Jackson and Doctor P.St. J. Russell and supported by the Hyatt-Woolfe studentship. In particular I will always be indebted to Dr. P. St. J. Russell for his guidance, endless support and encouragement during difficult times and also for his advice throughout the more theoretical aspects of this work.

I am also grateful to members of the Applied Optics group, past and present, for their valuable discussion. Those who deserve a special mention are Kyriacos Kalli who became a close colleague during those twelve long months in our successful efforts to finally fabricate a ring resonator, Dr. J. Rogers who contributed towards the final revisions made to this thesis and who could always be relied upon in a last minute crisis and similarly Professor J. Brown.

I would also like to express my gratitude to Mr. D. Riley, Mr. J. Howes and the technicians in the mechanical and electronics workshops and also to those non academic members of staff who, better than anybody, could always make you believe that things weren't as bad as they seemed.

Glossary of abbreviations and mathematical terms

Abbreviations

SBS	Stimulated Brillouin scattering
BSBS	Backward stimulated Brillouin scattering
FSBS	Forward stimulated Brillouin scattering
FSR	Free spectral range
CFP	Confocal Fabry Perot
GT	Glan Thompson
CCR	Cross coupled fibre ring resonator
DCR	Direct coupled fibre ring resonator
F	Finesse
DM	Dual moded
PD	Photo-detector
PZT	Piezzo-electric transducer

Mathematical terms

k_L	Wave-vector (m^{-1}) of the laser/pump wave
k_B	Wave-vector (m^{-1}) of the Brillouin wave
K_o	Wave-vector (m^{-1}) of the longitudinal acoustic phonon
K_F	Wave-vector (m^{-1}) of the flexural acoustic wave
ω_L	Angular frequency ($rads^{-1}$) of the laser/pump wave
ω_B	Angular frequency ($rads^{-1}$) of the Brillouin wave
Ω_o	Angular frequency ($rads^{-1}$) of the longitudinal acoustic phonon
Ω_F	Angular frequency ($rads^{-1}$) of the flexural acoustic phonon
f_L	Frequency (Hz) of the laser/pump wave
f_B	Frequency (Hz) of the Brillouin wave
f_o	Frequency (Hz) of the longitudinal acoustic phonon
f_F	Frequency (Hz) of the acoustic flexural wave
Δf_{BT}	Beat frequency (Hz) generated by mixing two BSBS signals
$n_{L/B}$	Refractive index of the pump and Brillouin modes
c	The speed of light (ms^{-1})
$v_{gL/B}$	Pump/Brillouin group velocity (ms^{-1})
v_{go}	Longitudinal phonon group velocity (ms^{-1})
v_{gF}	Flexural phonon group velocity (ms^{-1})
v_o	Longitudinal phonon phase velocity (ms^{-1})
v_F	Flexural wave phase velocity (ms^{-1})
v_e	Flexural wave extensional wave phase velocity (ms^{-1})
v_t	Flexural wave shear velocity in silica (ms^{-1})
λ_L	Laser/pump wavelength (m)
λ_B	Brillouin wavelength (m)
Λ_o	Longitudinal acoustic phonon wavelength (m)

Λ_F	Flexural acoustic phonon wavelength (m)
α	Optical attenuation (m^{-1})
α_o	Longitudinal acoustic phonon absorption (m^{-1})
α_F	Flexural acoustic phonon absorption (m^{-1})
τ_o	Longitudinal acoustic phonon lifetime (s)
$g_{BO}(f_B)$	SBS Brillouin gain (m^{-1})
$\bar{g}_{BO}(f_B)$	Explicit definition for the BSBS Brillouin gain (m/W)
$g_{BF}(f_B)$	FSBS Brillouin gain (m^{-1})
$\bar{g}_{BF}(f_B)$	Explicit definition for the FSBS Brillouin gain (m/W)
Δf_L	Full width at half maximum laser/pump linewidth (Hz)
Δf_B	Full width at half maximum spontaneous Brillouin linewidth (Hz)
L_{coh}	Laser coherence length (m)
L	Fibre length (m)
L_{eff}	BSBS effective interaction length (m)
L_i	FSBS effective interaction length (m)
A_L	Electric field amplitude of the laser/pump wave (V)
A_B	Electric field amplitude of the Brillouin wave (V)
E_{TOT}	Total electric field (V)
A_o	Slowly varying longitudinal acoustic phonon amplitude
A_F	Slowly varying flexural phonon amplitude
E_S	Total energy stored (J)
W	Average energy per unit volume (Jm^{-3})
T	Temperature (K)
K_B	Boltzman's constant (JK^{-1})
h	Plank's constant (Js)
ε_r	Relative dielectric permittivity
ε_o	Dielectric permittivity of free space (Fm^{-1})
ε	Dielectric permittivity of the medium (Fm^{-1})
E	Youngs modulus (Nm^{-2})
s	Strain
r_{eq}	Modal spot radius (m)
A_{eq}	Equivalent modal spot size (m^2)
a	Fibre radius (m)
a_L	Normalised and dimensionless laser field amplitude
a_B	Normalised and dimensionless Brillouin field amplitude
a_o	Normalised and dimensionless acoustic phonon field amplitude
a_F	Normalised and dimensionless flexural wave field amplitude
P_L	Total power of pump/laser wave (W)
P_B	Total power of Brillouin wave (W)
P_o	Total power of longitudinal acoustic phonon (W)
P_F	Total power of flexural acoustic phonon (W)
P_{TOT}	Total power of the system (W)
κ_L	Coupling coefficient for the laser/pump wave
κ_B	Coupling coefficient for the Brillouin wave

κ_o	Coupling coefficient for the longitudinal acoustic wave
κ_F	Coupling coefficient for the flexural acoustic wave
C_o	Frequency parameter in BSBS (ms^{-1})
C_F	Frequency parameter in FSBS (ms^{-1})
G_B	Brillouin gain multiplication factor (m/W)
s_o	Normalised spontaneous BSBS power
s_F	Normalised spontaneous FSBS power
P_{th}	Threshold power (W)
γ_o	Directional coupler loss
k	Tuning coupling coefficient for directional coupler
k_r	Resonant coupling coefficient
E_i	Complex field amplitude at the i^{th} port for a directional coupler
L_b	Intermodal beat length (m)
$e_L(r,\phi)$	Dimensionless transverse mode profile for the laser/pump wave in dual moded fibre
$e_B(r,\phi)$	Dimensionless transverse mode profile for the Brillouin wave in dual moded fibre
ϕ_L	Phase of laser (radians)
ϕ_B	Phase of Brillouin wave (radians)
ϕ_F	Phase of acoustic flexural wave (radians)
Ψ	Relative phase ϕ_L - ϕ_B -ϕ_F (radians)
Q	Overlap integral
χ	Poisson ratio
L_{opt}	Optical path length (m)
M_d	Induced electrostrictive driving moment (Nm)
Δp	Electrostrictive stress (Nm^{-2})
ρ	Mass density (kgm^{-3})
I	Second moment of inertia (m^4)

Abstract

In the work presented in this thesis, the generation of stimulated Brillouin scattering and its applications in optical fibres is theoretically and experimentally investigated. The study pursues three special cases:

i) Backward stimulated Brillouin scattering in long fibre lengths
ii) Backward stimulated Brillouin scattering in high finesse all fibre ring resonators
iii) Forward stimulated Brillouin scattering in dual moded single core fibres.

Stimulated Brillouin scattering (SBS) occurs for relatively low input powers in monomode optical fibres, as the power density is very high because of the relatively small core size. For applications such as optical communications, SBS is seen as a potentially deleterious effect because it can limit the maximum optical power transmitted by the fibre and hence decrease the distance between repeaters. SBS, however, can also be used to advantage in optical fibres, for example to produce amplification.

In this thesis the comprehensive study of SBS in relation to other non-linear scattering mechanisms in optical fibres leads to the derivation of explicit definitions for the Brillouin gain and the Brillouin threshold. The study of SBS in high finesse all fibre ring resonators also demonstrates how threshold powers can be reduced, typically, from milliwatts observed in long fibre lengths to microwatts. Because Brillouin scattering is primarily a result of the interaction of the incident optical beam with spontaneously generated (thermal) fluctuations in the density of the medium, the spectral features show a considerable variation with temperature thus providing a mechanism with sufficient sensitivity to realise tunable microwave generation and frequency shifting devices. Finally, the observation of stimulated Brillouin scattering in a forward direction (FSBS) in dual moded single-core fibre is also reported. Frequency shifts in the order of 17MHz are observed in optical fibre supporting LP_{01} and LP_{11} modes at 514.5nm. The phenomenon is examined here in detail and the governing differential equations of the three wave parametric process (involving pump/laser, Brillouin signal and acoustic flexural wave phonon) is derived and solved. FSBS is possible because, although the overlap integral between a fibre flexural mode and the light is small, the phonon lifetime is much longer than in conventional SBS. FSBS may also be the first example of a non-linear effect which is enhanced by *increasing* the optical mode area at constant pump power.

Chapter 1

Introduction

1.1 Historical background

When light passes through matter weak random scattered radiation appears. In the early 16th century, Leonardo da Vinci prophetically suggested scattering by particles of air as the explanation for the blueness of the sky. The idea was pursued by many scientists including Newton and Tyndall who tried with only limited success to identify the particles responsible for the scattering. Lord Rayleigh[1], following a suggestion by Maxwell, finally proved that the air molecules themselves were responsible for the blueness of the sky. After three centuries of thought a correct and unambiguous explanation to this phenemenon and all known properties of scattering - frequency dependence, critical opalescence, index of refraction etc.- became a reality. Then came the anti-climax that usually follows the insertion of the last jagged piece in a jig-saw puzzle; most physicists turned their attention elsewhere.

A few didn't. In 1922 Brillouin[2] predicted that if monochromatic radiation was allowed to scatter from an optical medium, side bands would appear. He went on to theorize that the bands would result from a Doppler shift due to the generation of a sound wave produced by the light wave as it encountered molecules in its path. The frequency shift would be a function of the angle of observation and of the sound velocity in the medium. In 1923 Smekal[3] considered, in the Bohr theory approximation, the scattering of light by a system having two quantised energy levels and predicted the effect to be discovered in 1928 by Raman[4]. Working independently in Russia, Mandelstam and Landsberg[5] discovered the same phenomenon in quartz; the appearance of lines in the spectrum in addition to those from the source. In 1930 Gross[6] confirmed the theory of Brillouin, demonstrating that the Doppler shifted frequencies appeared as predicted for both liquids and solids.

In 1934, Placzek [7] wrote a lengthy and excellent review paper on the Raman effect. Just as Lord Rayleigh's explanation of the elastic scattering 35 years earlier had resulted in a virtual halt to further work in this area, Placzek's paper seemed to mark the end of an era in frequency shifted spectra. Most fundamental Raman problems seemed now to be so well understood that research ground to a halt and pertinent papers in the Physical Review virtually disappeared.

Light scattering research was adrenalised once again with the invention of laser sources in the 1960's[8]. Not only was the physical chemist handed a new, more powerful and cleaner source but, equally important, the physicist was furnished with means of testing rigorously the theories of Placzek, Rayleigh and Brillouin. Phenomena such as directional effects in scattering processes and inelastic scattering from very small cross sections which had previously defied measurement could now be studied easily with laser sources. The great level of current enthusiasm in such investigations is evident from the impressive number of laboratories and scientists engaged in related light scattering experiments.

1.2 Elastic and non-elastic scattering mechanisms

When light passes through an optical medium it is scattered due to fluctuations in the dielectric constant. Static fluctuations (i.e. inclusions, impurities etc.) scatter the light elastically and hence there is no frequency shift. Dynamic fluctuations give rise to frequency shifted components in the scattered light spectrum; these fluctuations arise due to several causes of which the most important are:

i) spontaneously generated fluctuations in the density of the medium

ii) molecular vibrations.

The spectrum of the light scattered from density fluctuations is composed of a central Rayleigh line and a frequency shifted Brillouin line. The Rayleigh line is broadened by non-propagating density fluctuations, i.e.thermal diffusion. The Brillouin lines are caused by light being scattered from adiabatic pressure fluctuations

i.e. hypersonic thermal phonons. The Brillouin shift depends upon the bulk modulus of the material, the temperature and other thermodynamic variables; for liquids and solid polymers the frequency shifts are ~5GHz, and for hard optical materials such as quartz, > 10GHz. At these high frequencies, the propagation of the phonon is highly damped and the width of the Brillouin lines are directly related to the acoustic loss in the medium which again depends on the thermodynamic quantities.

The spectrum of the light scattered from the molecular vibrations, usually termed Raman scattering, is composed of discrete lines associated with vibrations of individual molecules - i.e. optical phonons. The frequency shifts of the Raman lines are several orders of magnitude greater than are those for the Brillouin lines, but the scattering cross-section is typically 10^{-3} times less than for the Rayleigh -Brillouin triplet in the same medium.

The intensity of stimulated Brillouin scattering (BSBS) in optical fibres, first observed by Ippen and Stolen in the 1970's[9], depends upon several factors of which the most important are power density, the interaction length which is related to but is less than the physical length of the fibre, the core dopants, and the source linewidth. In normal bulk materials the generation of BSBS requires intense pulses of laser light, whereas it can be readily generated in monomode optical fibres with very modest narrow bandwidth continuous wave (cw) sources. This is primarily due to the very small core size of these fibres. For example, cw lasers of output power ~1mW focussed into a 5 micron core fibre produces an intensity of about 4kW/cm^2 . These and other such general considerations are discussed more fully in chapter 2, where the concept of SBS is introduced by first analysing the conservation laws of energy and momentum. Expressions for the Brillouin gain and Brillouin threshold are then more fully developed and incorporated into the analysis given in chapter 3.

1.3 Outline of thesis

In the previous sections a brief discussion of stimulated Brillouin

scattering in the context of other non-linear fibre effects has been given. The general considerations for BSBS are given in chapter 2. In chapters 3, 4 and 5 three situations where BSBS occurs are theoretically and experimentally investigated. In chapter 3, the generation of BSBS in long fibre lengths is analysed and experimental data presented in order to characterise the variation of the Brillouin frequency shift with temperature. In chapter 4 the high circulating power densities observed in high finesse all-fibre ring resonators are exploited in order to reduce the typical input threshold powers from the mW's needed in long fibre lengths to μW's. Chapter 5 presents a new phenomenon discovered for the first time during work on this thesis, namely intermodal stimulated Brillouin scattering in a forward direction (FSBS) in dual moded (DM) fibres. This phenomenon is examined in detail and the governing differential equations of the three wave parametric process derived and solved. FSBS is possible because, although the overlap integral between a fibre flexural mode and the light is small, the phonon lifetime is much longer than in conventional BSBS. FSBS may also be the first example of a non-linear effect which is enhanced by increasing the optical mode area at constant pump power. The application of BSBS in order to realise both microwave generation and frequency selective devices is presented in chapter 6. The novel aspect of these applications is the exploitation of a non-linear scattering mechanism in optical fibres to realise a vital function required for heterodyne signal processing in fibre optic based interferometric systems. The method investigated for microwave generation and frequency shifting uses a very low loss fibre ring resonator illuminated with a narrow linewidth source, L_1, with the resonator field stabilised electronically at resonance. The backscattered light from the ring will be at a frequency of $(f_L - f_{SBS}(1))$ where f_L is the laser frequency and $f_{SBS}(1)$ is the frequency of the generated sound wave. If L_1 is also used to illuminate a second ring (again stabilised at resonance) a second SBS signal will be produced at $(f_L - f_{SBS}(2))$. As these new optical signals are generated in optical fibres they can be used as the signal and reference beams for any fibre optic based sensor or measurement system. When these output signals are combined, the resulting carrier frequency will be at $(f_{SBS}(1) - f_{SBS}(2))$. This

frequency difference can be controlled either by using different fibres in the rings or by varying the temperature of one of the ring resonators. Similarly, a GHz microwave signal can be produced by mixing the BSBS signal generated within a fibre ring cavity with the original pump source at a fibre coupler and detecting the beat signal at a photo-detector. The manufacture of the fibre ring resonator is discussed in appendix A; it has found numerous applications, as will be discussed in chapters 3 and 6. Such applications include optical filters, delay lines, and optical spectrum analysers. Conclusions are finally drawn in chapter 7.

References: Chapter 1

1. Lord Rayleigh: "On the light from the sky, its polarisation and colour", Philos.Mag., vol.41, pp.107-120, 1871.
2. Brillouin, L., Ann.de Phys., (Paris), vol.17, p.88. 1922.
3. Smekal, A.: "The quantum theory of dispersion", Naturwiss, vol.11, p.873, 1923.
4. Raman, C.V.: "On the molecular scattering of light", Proc. Royal Society of Lon., vol.A101, pp.63-80, 1928.
5. Landsberg, G., and Mandelstam, L., Naturwiss, vol.16, p.57, 1928.
6. Gross, E.: "Change of wavelength of light due to elastic heat waves of scattering in liquids", Nature, vol.126, p.201, 1930.
7. Placzek, G.: "Rayleigh - Streuung und Raman effeckt", Marx's Handbuch der Radiologie V1, vol.2, p.209, 1934.
8. Chio, R.Y., Townes, C.H., and Stoicheff, B.P.: "Stimulated Brillouin scattering and coherent generation of intense hypersonic waves", Phys.Rev.Lett., vol.12, p.592, 1964.
9. Ippen, E.P., and Stolen, R.H.: "Stimulated Brillouin scattering in optical fibres", Appl.Phys.Lett., vol.21, p.539, 1972.

Chapter 2

Stimulated Brillouin scattering:general considerations

2.1 Introduction

Backward stimulated Brillouin scattering (BSBS) is a non-linear process that can occur in optical fibres at power levels much lower than those of other non-linear processes. It leads to the generation of a backward propagating Stokes wave that carries most of the input power once the Brillouin threshold is reached and it is because of this that BSBS can be detrimental for optical communication systems. At the same time, it can also be useful in applications such as fibre Brillouin lasers[1] and amplifiers[2]. This chapter addresses the general conditions needed to observe BSBS. In section 2.2 the relevance of the phonon dispersion relation (for both acoustic and optical phonons) is explained and the roles of acoustic and optical phonons in both BSBS and stimulated Raman scattering (SRS) discussed. Section 2.3 describes the general conservation laws of momentum and energy which are so fundamental to BSBS, whilst the significance of the spectral width of the laser line relative to the spontaneous Brillouin linewidth is discussed in section 2.4, and its implications, when the laser line is broadened, on the Brillouin gain. Conclusions are drawn in section 2.5.

2.2 Dispersion relation for acoustic phonons

Stimulated Brillouin scattering is similar in broad outline to stimulated Raman scattering in as much as it leads to the generation of a Stokes wave down-shifted from the frequency of the incident pump wave by an amount determined by the non-linear medium. There are, however, major differences. For example, the Stokes wave propagates backwards when BSBS occurs; this is in contrast with SRS which occurs in both directions. The Brillouin Stokes shift (~10GHz) is smaller by three orders of

magnitude than that occurring in SRS and the threshold pump power for BSBS depends on the spectral linewidth associated with the pump wave. It can be as small as ~1mW for a continuous wave pump or for relatively long pump pulses (width > 1μs); in contrast with SRS, BSBS nearly ceases to exist for pump pulses of width <10ns. All of these differences stem from a single fundamental fact: acoustic phonons participate in BSBS whereas optical phonons participate in SRS.

The difference between optical and acoustic phonons is most easily understood from the dispersion diagram for phonons in the lattice[3]. This is clearly shown in figure 2.1 where, for a crystal having two atoms per primitive cell, new features are revealed. For example, Sodium Chloride has two kinds of atoms of mass m and M and which are separated by a distance d. The reduced mass is 60×10^{-27}Kg and the elastic force constant[4] for the crystal is about $15 Nm^{-1}$. For each polarisation mode in a given propagation direction the dispersion relation ω (angular frequency) versus K (wave-vector) develops two branches known as the acoustical and optical branches. In the case of transverse optical branches (TO) the atoms vibrate against each other, but their centre of mass is fixed. When two such atoms carry opposite charges a motion of this type can be excited by the electric field of a light wave, hence the term optical branch. Consequently SRS involves rapidly accelerating charges resulting in an electromagnetic wave being radiated. In the case of BSBS the atoms (and their centre of mass) move together, as in long wavelength vibrations; hence the use of the term acoustic branch. With the consequent shift in mass, light scattered from the lattice results in a frequency that is down converted described by a Doppler shift.

2.3 General Conservation Laws

The process of SBS can be described classically as a parametric interaction between the pump wave, the Stokes wave and an acoustic wave. Thermally activated and spontaneous phonons in the dielectric medium weakly Bragg scatter the incoming laser / pump light leading to spontaneous Brillouin scattering. A slowly moving

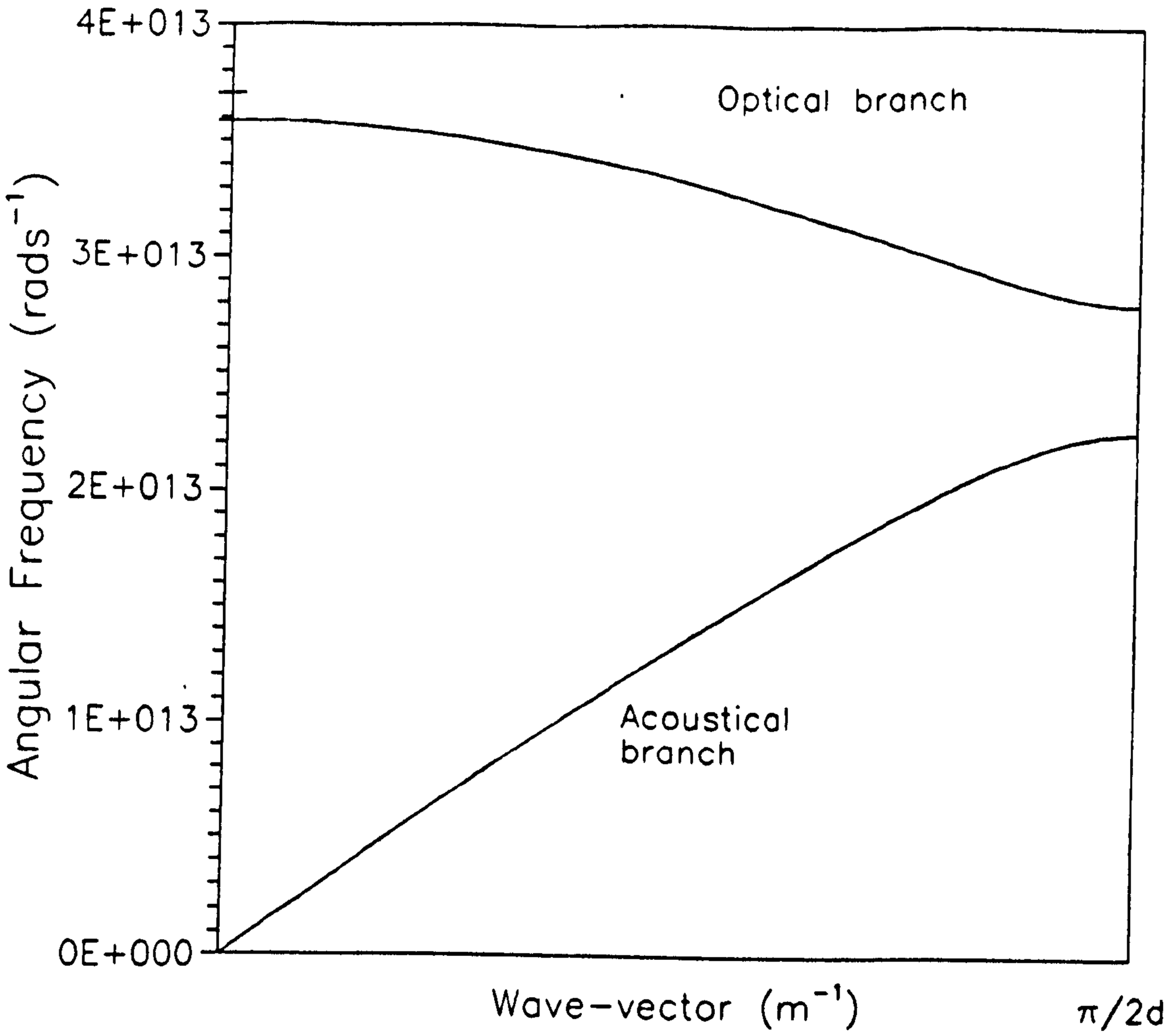

Figure 2.1

Dispersion relations for the two modes of transverse oscillation in a diatomic crystal structure. It can be seen that the dispersion relationship for optical phonons is fairly flat when $K<<\pi/2d$, thus allowing SRS in both directions. This is in contrast to BSBS which can only propagate backwards in an optical fibre.

interference fringe pattern is then generated by the constructive interference between the pump wave and the counter propagating Stokes light; this fringe pattern co-propagates with the pump wave and travels at the acoustic phonon velocity. At electric field strengths greater than 10^4 volts per cm the process of electrostriction takes place and results in the periodic contraction of the dielectric medium and energy is subsequently depleted from the optical waves. Because the pump field is periodic, when the dielectric medium is relaxed the energy, instead of simply being dissipated, is carried away by a phase matched acoustic phonon and leads to an increased phonon lifetime. The scattering strength of the acoustic phonon is then enhanced and when the gain exceeds the phonon loss the process becomes stimulated and both the phonon and the Brillouin waves experience exponential gain. Electrostriction then, describes the mechanism by which energy is transferred between three waves travelling at vastly different speeds - in this case between two waves travelling at the speed of light and another at the speed of sound. The same process can be viewed quantum mechanically as when the annihilation of a pump photon creates simultaneously a Stokes photon and an acoustic phonon. Since both the energy and momentum must be conserved during each scattering event, the frequency and the wave-vectors are related by:

Conservation of momentum:

$$k_L = k_B + K_O \tag{2.3.1}$$

Conservation of energy:

$$\hbar\omega_L = \hbar\omega_B + \hbar\Omega_O$$

$$f_O = f_L - f_B \tag{2.3.2}$$

where K_O, k_L and k_B are the wave-vectors of the phonon, pump and Brillouin waves at frequency f_O, f_L and f_B and angular frequency Ω_O, ω_L and ω_B. The conservation of momentum is shown schematically in figure 2.2. From figure 2.2 it is clear that the

Conservation of:

Energy: $\omega_L = \omega_B + \Omega_o$

Momentum: $k_L = k_B + K_o[\omega_L n_L = -\omega_B n_B + (\Omega_o \frac{c}{v_o})]$

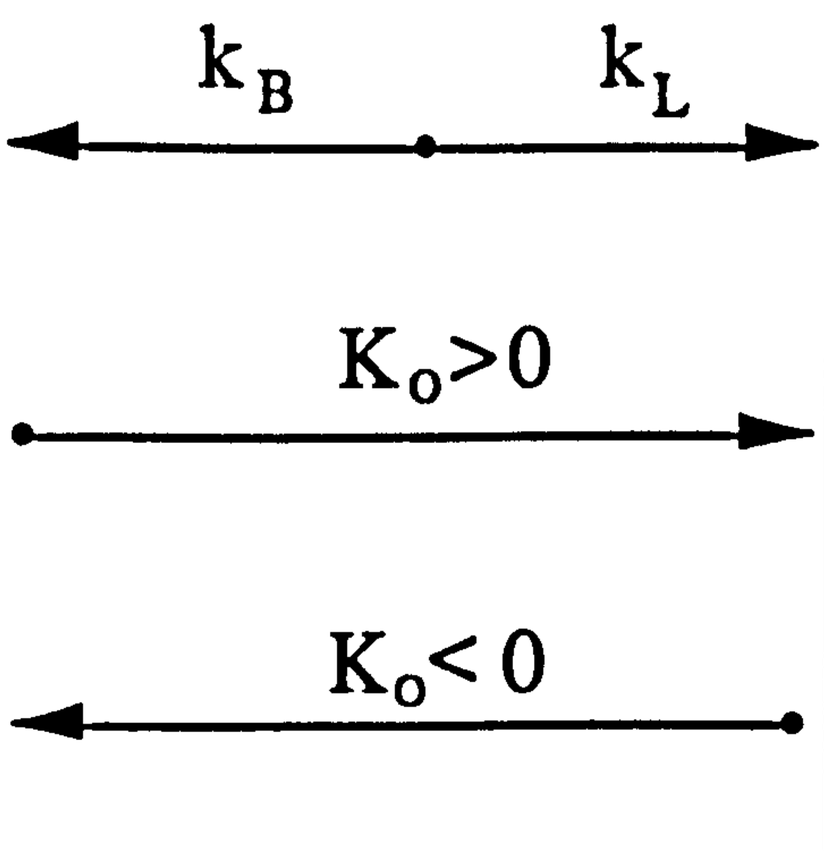

$\Delta\omega$	Spontaneous	Stimulated
<0	✓	✓
>0	✓	✗

Figure 2.2

It is clearly shown that whilst both forward and backward propagating phonons are applicable to the generation of the Stokes and anti-Stokes waves in spontaneous scattering, in BSBS only a forward propagating phonon will satisfy the phase matching condition. This corresponds to a Stokes wave downshifted in frequency and where the change in angular frequency, $\Delta\omega$, from the pump to the Brillouin signal is determined by the phonon frequency, Ω_o.

long K vector describing those phonons that are phase matched to the travelling fringe pattern generated by the counter propagating pump and Brillouin waves have a small wavelength, Λ_o, (sub-microns). This follows from eqn.(2.3.1):

$$\frac{2\pi}{\Lambda_o} = \frac{\Omega_o}{v_o} = \frac{\omega_L n_L}{c} + \frac{\omega_B n_B}{c}$$

$$\frac{2\pi}{\Lambda_o} = \frac{\omega_L(n_L+n_B)}{c} - \frac{\Omega_o n_B}{c} = \frac{\Omega_o}{v_o} \approx \frac{2\omega_L n_L}{c} \qquad (2.3.3)$$

where $\Omega_O << \omega_L$ and the approximation that $n_L \approx n_B$ is made. Equation (2.3.3) describes the length of the grating, i.e. the acoustic phonon wavelength, Λ_o. For example, a pump wavelength of λ_L = 514.5nm and refractive index n = 1.46 yields $\Lambda_o \approx 0.2\mu m$. Because the acoustic wave is well collimated, travelling in the fibre core along the fibre axis, the acousto-optic overlap integral tends to unity. This is because the wavelength of the phonon is small compared to the core radius and therefore is not diffracted. This, along with the phonon within the fibre core is illustrated in figure 2.3. From eqn.(2.3.3) the acoustic frequency is clearly given by:

$$f_o = \frac{2v_o n}{\lambda_L} \qquad (2.3.4)$$

where eqn.(2.3.4) describes the frequency of the acoustic phonon and hence the downshift in frequency of the backward propagating Stokes wave in relation to the pump. The acoustic velocity, v_o, in the dielectric medium is also assumed to be non dispersive, i.e.the acoustic velocity is independent of frequency f_o. For example at λ_L = 514.5nm, n = 1.46 and v_o = 5760ms^{-1} the acoustic frequency $f_o \approx$ 32.7GHz. However, spontaneous or thermal Brillouin scattering in the forward direction can occur in optical fibres. This happens because the guided nature of acoustic waves leads to the relaxation of the wave-vector selection rule. As a result a small amount of Stokes light is generated in the forward direction and the phenomenon is referred to as guided

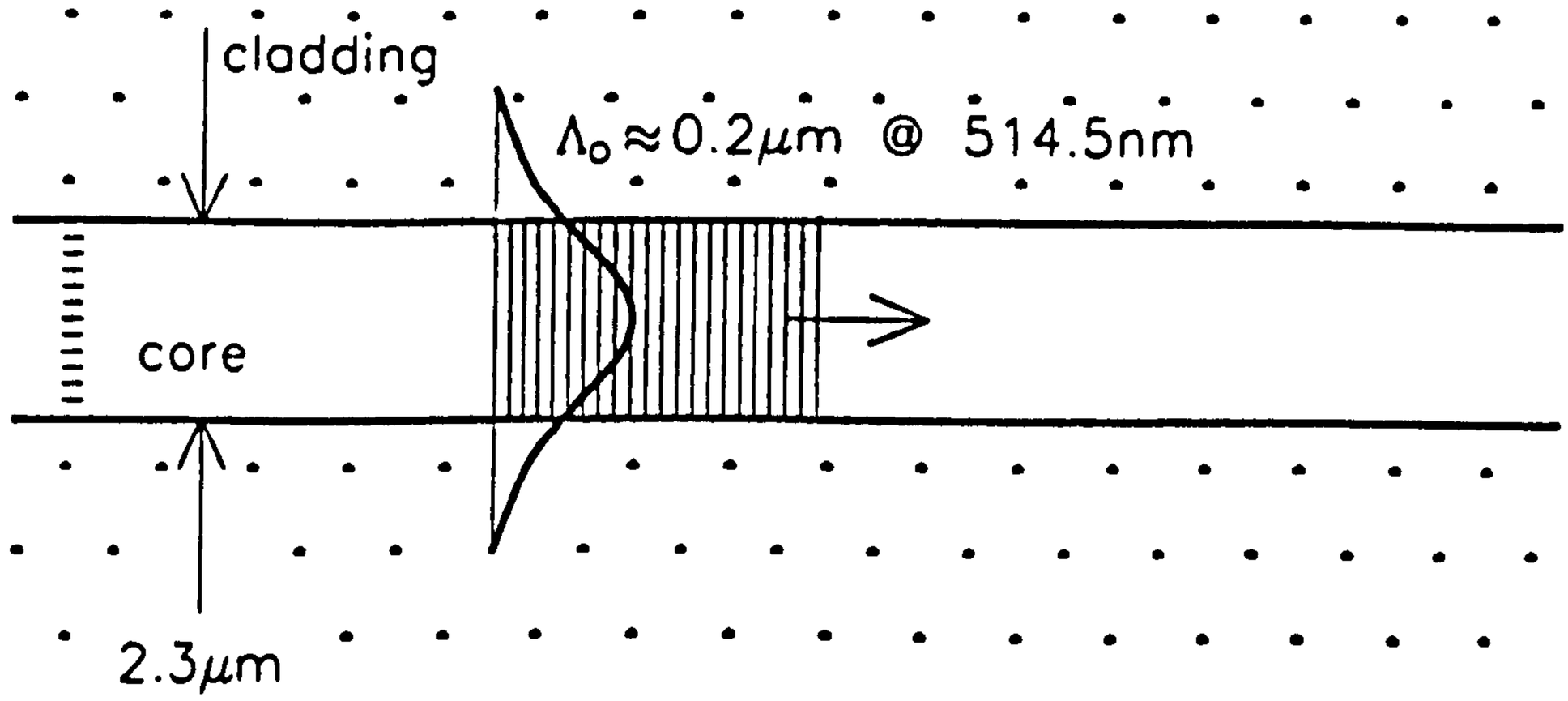

Figure 2.3

The longitudinal acoustic phonon is seen to be well collimated within the fibre core. This is attributed to the phonon wavelength, Λ_o, being much smaller than the fibre spot size and hence the phonon wave is not diffracted from the fibre axis. Consequently the optical and acoustical power overlap in the case of BSBS is close to unity and this is reflected by the high conversion efficiencies involved.

acoustic wave Brillouin scattering.The Stokes spectrum shows multiple lines with frequencies ranging from 10MHz - 1000MHz[6]. This is in contrast to Raman scattering which, because of the flat character of the dispersion relation for optical phonons near the centre of the Brillouin zone (see figure 2.1), permits forward stimulated scattering. In other words the pump and downshifted Stokes wave exist as two co-propagating and coherent electromagnetic waves. The fact that they are co-propagating describes an interaction that occurs instantaneously. The fact that they are electromagnetic waves propagating at the speed of light eliminates the need for phase matching. Conversely the counter propagating nature of the Stokes and pump waves in the example of BSBS is not an instantaneous process and the energy transfer to an elastic or acoustic phonon is dependent on the coherent interference of the formentioned waves. It is this phase matching requirement for BSBS in an isotropic medium (fused quartz) where two waves are propagating at vastly different velocities that forward stimulated scattering is prohibited.

2.4 Significance of the spectral width of the laser line

Similar to the case of SRS the growth of the Stokes wave can be characterised by the Brillouin gain coefficient $\bar{g}_{BO}(f_B)$ measured in m/W. The peak values occur at $f = f_B$. However, in contrast with SRS, the spectral width Δf_B of the spontaneous Brillouin scattering is very small. The absorption is related to the phonon lifetime τ_o and the bandwidth Δf_B by $\alpha_o = \Delta f_B / v_o = 1/v_o\tau_o$. For fused quartz the spectral width is typically 150MHz, but the Brillouin gain spectrum for silica fibre can differ significantly from that observed in bulk silica because of the guided nature of the optical modes and the presence of dopants in the fibre core[7]. The phonon linewidth is typically 15-20MHz at the optical communication wavelength λ_L = 1300nm. This small Brillouin gain spectrum is in contrast to the 5THz linewidth of optical phonons. In fact if the acoustic waves are assumed to decay as $\exp(-\tau/\tau_o)$ the Brillouin gain has a Lorentzian spectral profile given by[8]:

$$\bar{g}_{BO}(f) = \frac{(\Delta f_B/2)^2}{(f-f_B)^2+(\Delta f_B/2)^2}\,\bar{g}_{BO}(f_B) \qquad (2.4.1)$$

where Δf_B is the full width at half maximum. In fact this is a very good approximation and the comparison between the experimental and theoretical Lorentzian spectral profiles are clearly shown in chapter 6, figure 6.3. The explicit definition for the Brillouin gain (m/W), denoted by $g_{BO}(f_B)$, is (see eqn.(3.2.4)):

$$\bar{g}_{BO}(f_B) = \frac{\{\pi(\partial\epsilon_r/\partial s)\}^2\ 2v_o}{\lambda_L n_L n_B E c\ \ \Lambda_o \Delta f_B} \qquad (2.4.2)$$

where $\partial\epsilon_r/\partial s$ is the influence of electrostriction and the change in dielectric permittivity with strain, $\lambda_L = \lambda_B$ the pump wavelength, c the velocity of light, $n_L = n_B$ the refractive index, E Youngs modulus, v_o the acoustic velocity in silica, Λ_o the acoustic wavelength and Δf_B the Brillouin linewidth. Experiments carried out using a single mode argon ion laser[9] show that f_B = 34.7 GHz and Δf_B = 54MHz at 486nm. These experiments also indicate that Δf_B depends on the Brillouin shift and varies as f_B^2. The narrowing of the Brillouin gain signal profile with an increase of λ_L cancels the decrease in gain apparent from eqn.(2.4.2). As a result the Brillouin gain is nearly independent of the pump wavelength. Typical values of $\bar{g}_{BO}(f_B)$ give $\bar{g}_{BO}(f_B)$ = 5.0×10^{-11}m/W. This value is larger by nearly three orders of magnitude compared with the Raman gain coefficient[8] and is in agreement with other predictions[9] for values of the Brillouin gain.

Equation (2.4.2) for the Brillouin gain is obtained under steady state conditions and is valid for a continuous wave pump (pulse width $T_o >> \tau_o$) whose spectral width Δf_L is smaller than the Brillouin gain linewidth Δf_B. For a pump pulse width $T_o << \tau_o$, the theory of transient BSBS[10] shows that the Brillouin gain is substantially reduced compared with that obtained from eqn.(2.4.2). If the pulse width becomes much smaller than the phonon lifetime the Brillouin gain is reduced below the Raman gain

and such a pump pulse generates a forward propagating Raman pulse through SRS. Even for a cw pump the Brillouin gain is substantially reduced if the spectral width Δf_L exceeds Δf_B. This can be the case for a multi-mode pump. It can also happen for a single-mode pump whose phase varies rapidly on a time scale shorter than the phonon lifetime τ_o. Detailed calculations[11] show that the Brillouin gain under broad band pumping conditions depends on the relative magnitudes of the pump coherence length, defined by $L_{coh} = c/n\Delta f_L$, and the BSBS interaction length, $L_{eff} = (1 - \exp(-\alpha L))/\alpha$, defined as the distance over which the Stokes amplitude grows appreciably. In the case of optical fibres where $L_{eff} >> L_{coh}$ and where the interaction length is comparable to the fibre length the gain is significantly reduced. In the specific case of a pump having a Lorentzian spectral profile of width (FWHM) Δf_L, the Brillouin gain spectrum is still given by eqn (2.4.1), but with a peak gain[11]:

$$\bar{g}_{BO}` = \frac{\Delta f_B}{\Delta f_B + \Delta f_L} \bar{g}_{BO}(f_B) \qquad (2.4.3)$$

Eqn.(2.4.3) clearly indicates how the gain is reduced as the pump linewidth is increased. In the limit where $\Delta f_L << \Delta f_B$ then the peak gain is simply $\bar{g}_{BO}(f_B)$. In this regime any fluctuation between the pump and Brillouin signals can be accommodated by the phonons population. In other words the phonon is fast enough i.e. excited and absorbed sufficiently quickly, to be such that its relationship with the pump is always satisfied. As the pump linewidth is broadened the phonon is less able to respond to any change in phase. As Δf_L becomes much larger than Δf_B the power coupled into the Stokes wave is negligible and the threshold for other non-linear effects such as SRS are reached sooner.

2.5 Discussion

Although a more detailed discussion of the mechanism of BSBS will follow in

chapter 3, the broad outline of Brillouin scattering and the coupling of energy between three waves travelling at vastly different velocities has been given. In the following chapters three special cases of Brillouin scattering will be theoretically and experimentally examined: in chapter 3 BSBS in long lengths of fibre is considered and in chapter 4 BSBS in fibre ring resonators is discussed. The latter exploits the high circulating intensities within the ring configuration such that the threshold powers are reduced, typically, from milliwatts to microwatts. A third category, namely forward stimulated Brillouin scattering (FSBS), where a Stokes wave co-propagates with the pump as opposed to the counter-propagating nature in BSBS, is also examined and presents an entirely new phenomenon. This new phenomenon is examined in detail in chapter 5. It exploits the fact that an optical fibre is able to support simultaneously two non-degenerate propagating modes at the same optical frequency and, whereas frequency shifts in the order of GHz are observed in BSBS, in FSBS frequency shifts in the order of MHz are observed.

References: Chapter 2

1. Stokes, L.F., Chodorow, M., and Shaw, H.J.: "All fibre stimulated Brillouin ring laser with sub-milliwatt pump threshold ", Opt.Let., vol.7, p.509, 1982.
2. Atkins, C.J., Cotter, D., Smith, D.W., and Wyatt, R.: "Application of Brillouin amplifaction in coherent optical transmission", Electron.Lett., vol.22, p.556, 1986.
3. Kittel: "Introduction to Solid State Physics", 5th Edition. pp 109-116, 1976.
4. Pain, H.J.: "The Physics and Vibrations of waves", second edition, Wiley Press, p.130, (1979).
5. Butcher, C.J.F.: "Theory of Electric Polarisation", second edition, vol.1.pp. 289-326, 1978.
6. Shelby, R.M., Levenson, M.D., and Bayer, P.W.: "Guided acoustic wave Brillouin scattering", Physics Review, vol.B31, pp. 5244-5252, 1985.
7. Tkach, R.W., Chraplyvy, A.R., Drossier, R.M.: "Spontaneous Brillouin scattering for single mode optical fibre characterisation", Electronics Letters, Vol 22. pg. 1011,1986.
8. Stolen, R.H., Ippen, E.P. and Taynes, A.R. Applied Physics Letters, vol.20, p.162, 1972.
9. Heiman, D., Hamilton, D.S., and Hellworth, R.W.: "Brillouin scattering measurements in optical glasses", Physics Review B, vol.19, p.6583, 1979.
10. Tang, C.L.: "Saturation and spectral characteristics of the Stokes emission in the stimulated Brillouin process", Journal of Applied Physics, vol.37, p.2945, 1966.
11. Lichtman, E., Friesman, A.A.: "Stimulated Brillouin scattering excited by a multi-mode laser in single mode optical fibre", Journ. Opt.Commun., vol.64, p.544, 1987.

Chapter 3

Backward stimulated Brillouin scattering in straight fibres

3.1 Introduction

The classical description of conventional backward stimulated Brillouin scattering (BSBS) has been given in chapter 2. It has been described as a parametric interaction involving the pump (laser) wave, the Stokes wave and a longitudinal acoustic wave. The acoustic wave is driven (i.e. given gain) by the process of electrostriction which is the result of the periodic modulation of the density of the non linear medium at high field strengths and which leads to phonon gain. It is when the gain of the acoustic wave exceeds its attenuation loss that the process becomes stimulated and the scattering strength becomes significantly enhanced for small increments of input power.

The aims of this chapter is to present the results of theoretical and experimental investigations in the special case of BSBS in straight fibres. The concept of BSBS in optical fibres is well studied - consequently the relevant expressions defining the three coupled amplitude equations in normalised form will simply be stated in section 3.2. However, the analysis is similar in broad outline to chapter 5 where a detailed investigation of forward stimulated Brillouin scattering (FSBS) in dual moded optical fibres is presented as an entirely new phenomenon. Similarly expressions leading to explicit definitions for the Brillouin gain and Brillouin threshold power will be stated; a comparison with stimulated Raman scattering is also made. Experimental results feature in section 3.3. In sub-section 3.3.1 the experimental observation of BSBS and the observed experimental threshold power and its effect with temperature are both discussed whilst in sub-section 3.3.2 the effect of temperature on the Brillouin frequency shift is reported.

3.2 Power-normalised coupled wave equations, gain and threshold for BSBS

The coupled wave equations governing BSBS are well studied[1] and are summarised in normalised form in eqn.(3.2.1):

$$\frac{\partial a_L}{\partial z} + \frac{\alpha}{2} a_L = -j\,\kappa_L\, a_o a_B \qquad \text{(a)}$$

$$\frac{\partial a_B^*}{\partial z} - \frac{\alpha}{2} a_B^* = -j\,\kappa_B a_L^* a_o \qquad \text{(b)} \qquad (3.2.1)$$

$$\frac{\partial a_o}{\partial z} + \frac{\alpha_o}{2} a_o = -j\,\kappa_o\, a_L a_B^* \qquad \text{(c)}$$

where the coupling coefficients κ_L, κ_B and κ_o are defined by:

$$\kappa_L = \omega_L/c_o \;;\; \kappa_B = \omega_B/c_o \text{ and } \kappa_o = \Omega_o/c_o \qquad (3.2.2)$$

and where the velocity c_o is given by the expression:

$$c_o = \frac{n_L n_B}{(\partial\varepsilon_r/\partial s)} \sqrt{\left(\frac{8 v_{gL} v_{go} v_{gB} E A_{eq}}{P_{tot}}\right)} \qquad (3.2.3)$$

The normalised amplitudes are given by a_m where $m = L, B,$ or o and the phenomenological absorption has been incorporated. The other symbols are defined by E the Youngs modulus, A_{eq} the equivalent modal area, $n_L = n_B$ the mode refractive index, $(\partial\varepsilon_r/\partial s)$ the electrostrictive parameter, P_{tot} the total power and v_{gm} the group velocity of the pump, Stokes and phonon waves of angular frequency ω_L, ω_B, Ω_o. The coupled wave equations given in eqn.(3.2.1), normalised for power, denote how coupling between any two waves fuels the third wave. The feature common to all three equations is that all three waves have to exist prior to the regime of stimulated scattering; this is satisfied by spontaneous scattering whereby thermal phonons are

generated by localised variations in the refractive index profile along the fibres length and are attributed to environmental changes in the temperature. Furthermore, these equations also reflect the power that fuels the process of electrostriction, i.e. the power of the acoustic wave. In contrast to the power coupled into the optical waves, the power of the acoustic wave is negligible and this is evident when examining the coupling coefficients given in eqn.(3.2.2). Merely on account of the frequency, f_o (GHz), of the phonon wave being much smaller than the optical frequencies (THz) can this point be verified. However, whilst the coupled energy is very small, what enables such a mechanism to be so effective is the large momentum of the phonon wave (as shown in figure 2 chapter 2) and this explains how conversion efficiencies approaching 70%[1] between the pump and the Brillouin signals can take place.

The normalised coupled wave equations in eqn.(3.2.1) can be solved analytically[2,3]. In the example of FSBS, chapter 5, and in order to provide a thorough analysis this is included, but here, for the purpose of estimating an explicit definition for the Brillouin gain considerable physical insight is gained if pump depletion is neglected. In order that the Brillouin gain can be estimated, the approximation (Shen's approximation)[4] is safely made such that in eqn.(3.2.1c), $\partial a_o/\partial z = 0$. This leads to a Brillouin gain (m/W) given by:

$$\bar{g}_{BO} = \frac{g_{BO}A_{eq}}{P_{tot}} = G_B\frac{2}{\Lambda_o\alpha_o}\,(\mathrm{m/W}) \qquad (3.2.4)$$

where

$$G_B = \frac{\{\pi(\partial\varepsilon_r/\partial s)\}^2}{\lambda_B c n_L n_B E} \qquad (3.2.5)$$

and where the symbols have their previously defined meanings. In the following experiments, typical values are[5] $\lambda_L = 514.5\mathrm{nm}$, $c = 3\times10^8\ \mathrm{ms}^{-1}$, $n_L = n_B = 1.46$, $E = 73\mathrm{kNmm}^{-2}$ and $(\partial\varepsilon_r/\partial s)$, (see eqn. (5.3.3)), = 3.3. This yields $G_B = 4.5\times10^{-12}\mathrm{m/W}$. Theoretical plots for the Brillouin gain, $\bar{g}_{BO}$, are featured in figure (5.5), but for $\Lambda_o = 0.176\mu\mathrm{m}$, (eqn.(2.3.3)), and $\alpha_o = 1\times10^6\ \mathrm{m}^{-1}$, the Brillouin gain $\bar{g}_{BO} \sim 5\times10^{-11}\mathrm{m/W}$

and is in good agreement with other authors[6] which quote a similar value. In contrast the Raman gain[7] is smaller by three orders of magnitude, $\bar{g}_{RO} = 1.9.10^{-13}$m/W. However, because SRS is predominantly forward propagating and not constrained to the same stringent phase matching conditions, as the laser linewidth is broadened the Stokes and pump wave continue to maintain mutual coherence over long fibre lengths. As the linewidth of the pump begins to exceed the linewidth of the spontaneous Brillouin gain curve, the Brillouin gain falls below that for Raman scattering which will subsequently become the dominant non-linear scattering process.

Following Smith[8] in defining the threshold as occurring when the Brillouin signal equals $P_L(z) = \exp(-\alpha z)$, the threshold power P_{th} is a solution of:

$$P_{th} = \frac{f_L \Delta f_L K_B T}{f_o} \exp\left(\frac{\bar{g}_{BO} P_{th} L_{eff}}{\pi r_{eq}^2}\right) \qquad (3.2.6)$$

and where $L_{eff} = (1-\exp(-\alpha L))/\alpha$ and describes the fibre length over which the Stokes field grows appreciably and is less than the physical length because of the fibre attenuation. The equivalent injected power at $z = L$ is found to be $s_O = f_L \Delta f_L K_B T / f_o$. The Brillouin threshold can also increase by a factor between 1 and 2 depending on whether the pump and Stokes waves maintain their polarisation along the fibre or not. An increase of a factor of two in the Brillouin threshold occurs when the polarisation is completely scrambled[9]. For a laser linewidth $\Delta f_L = 25$MHz, $\lambda_L = 514.5$nm, $T = 293$°C and $f_o = 32$GHz, the equivalent injected power, s_O, turns out to be 1.8nW. The threshold power for identical parameters and fibre length $L = 500$m and Brillouin gain $\bar{g}_{BO} = 5.10^{-11}$m/W give $P_{th} = 30$mW. This is in excellent agreement with other authors, eg. Smith[8] where for the same fibre parameters a threshold value of 34mW is derived. It is also within good experimental agreement of the proceeding section. The Brillouin threshold can also be compared to the threshold of stimulated Raman scattering. Under the assumption of a Lorentzian Raman gain spectrum, the critical pump power can be given by[8], $\bar{g}_{RO} P_{th} L_{eff} / A_{eff} = 16$. The numerical factor 16 is only

approximate and depends on the exact value of the Raman gain bandwidth; for the previously stated values the threshold for the onset of SRS is P_{th} = 7.6W. Clearly for the regime of small scattering cross sections, long fibre lengths of low loss fibres and narrowband lasers, BSBS is the dominant non-linear effect.

The computed threshold powers for the above parameters, but for different fibre lengths is shown in figure 3.1. Clearly long fibre lengths significantly favour SBS because of the lower thresholds required. This can be attributed to the backward propagating Brillouin wave experiencing a greater overall gain on account of the longer interaction length. However, for lengths greater than the effective length, L_{eff}, the variation in the Stokes amplitude becomes increasingly less marked as the fibre loss exceeds the overall Brillouin gain. On the other hand if the same efficiencies of conversion are to be achieved for fibre lengths shorter than L_{eff} then, from figure 3.1, it is seen that greater input powers are necessary.

3.3 Experimental results

3.3.1 Experimental observation

The experimental configuration shown schematically in figure 3.2 was used to measure the Brillouin frequency shift at λ_L = 514.5nm. Light from an argon laser running single frequency, Δf_L = 25MHz, was launched, via a beam splitter, into 500m of single core fibre. The laser was protected from any back reflection by a Glan Thompson prism (GT) and quarter wave plate configured such that the polarisation of any back reflected light incident to the GT from the fibre face was rotated by 90°. Light back reflected from the fibre (Rayleigh + BSBS) was then optically resolved by a scanning confocal Fabry Perot (CFP) with a free spectral range (FSR) of 2GHz (±30 MHz). Light reflected from the fibre end was then passed into the CFP and used as a frequency reference. Figure 3.3 shows the experimental observation of BSBS at 514.5nm. It shows a frequency shift of 32.8GHz (±0.48GHz). It is also necessary to appreciate that because the CFP has a fixed FSR the observed BSBS signal will occur

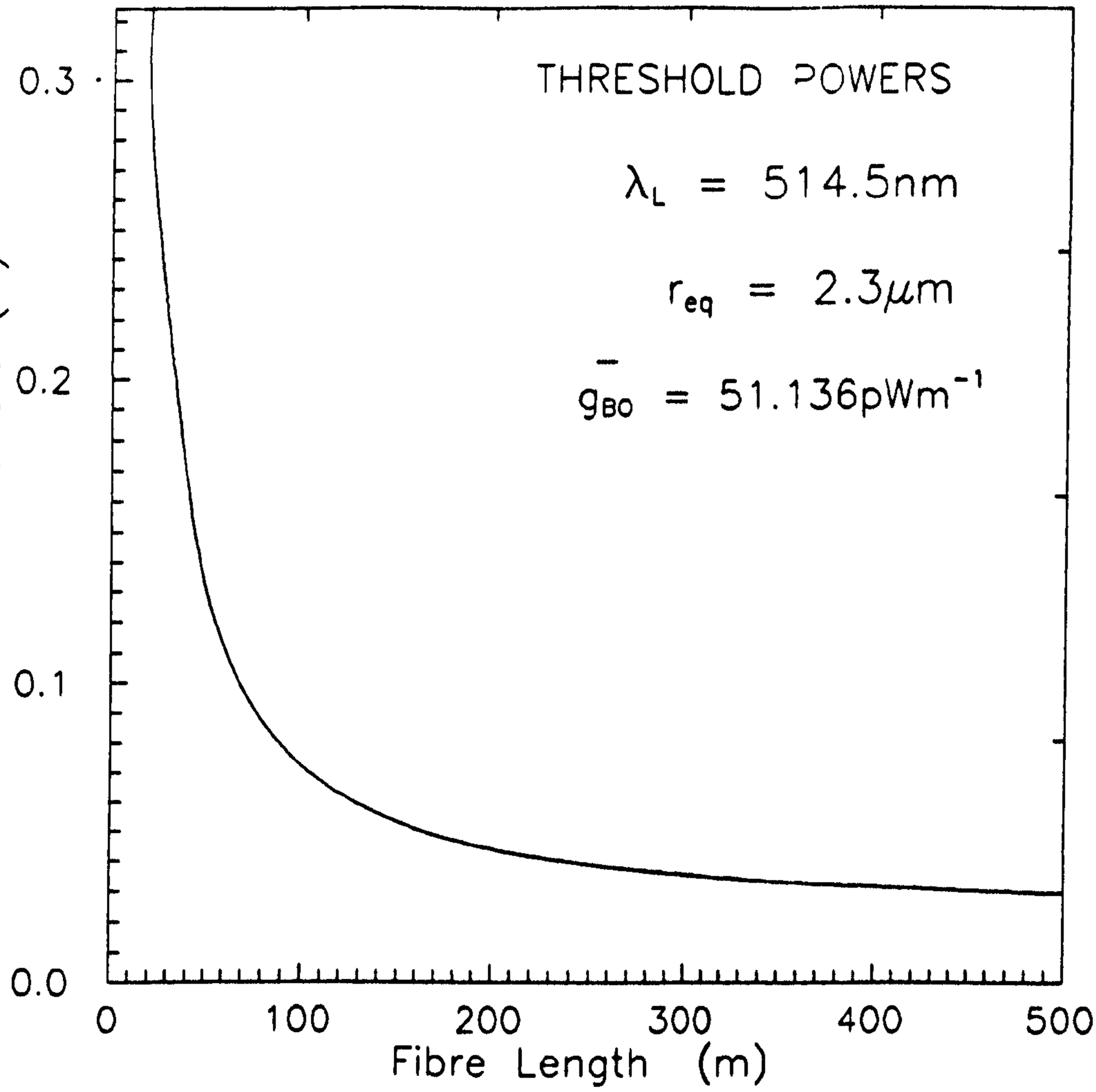

Figure 3.1

Computed threshold powers derived from eqn.(3.2.6). Clearly for given fibre parameters and launched power, long fibre lengths significantly favour BSBS.

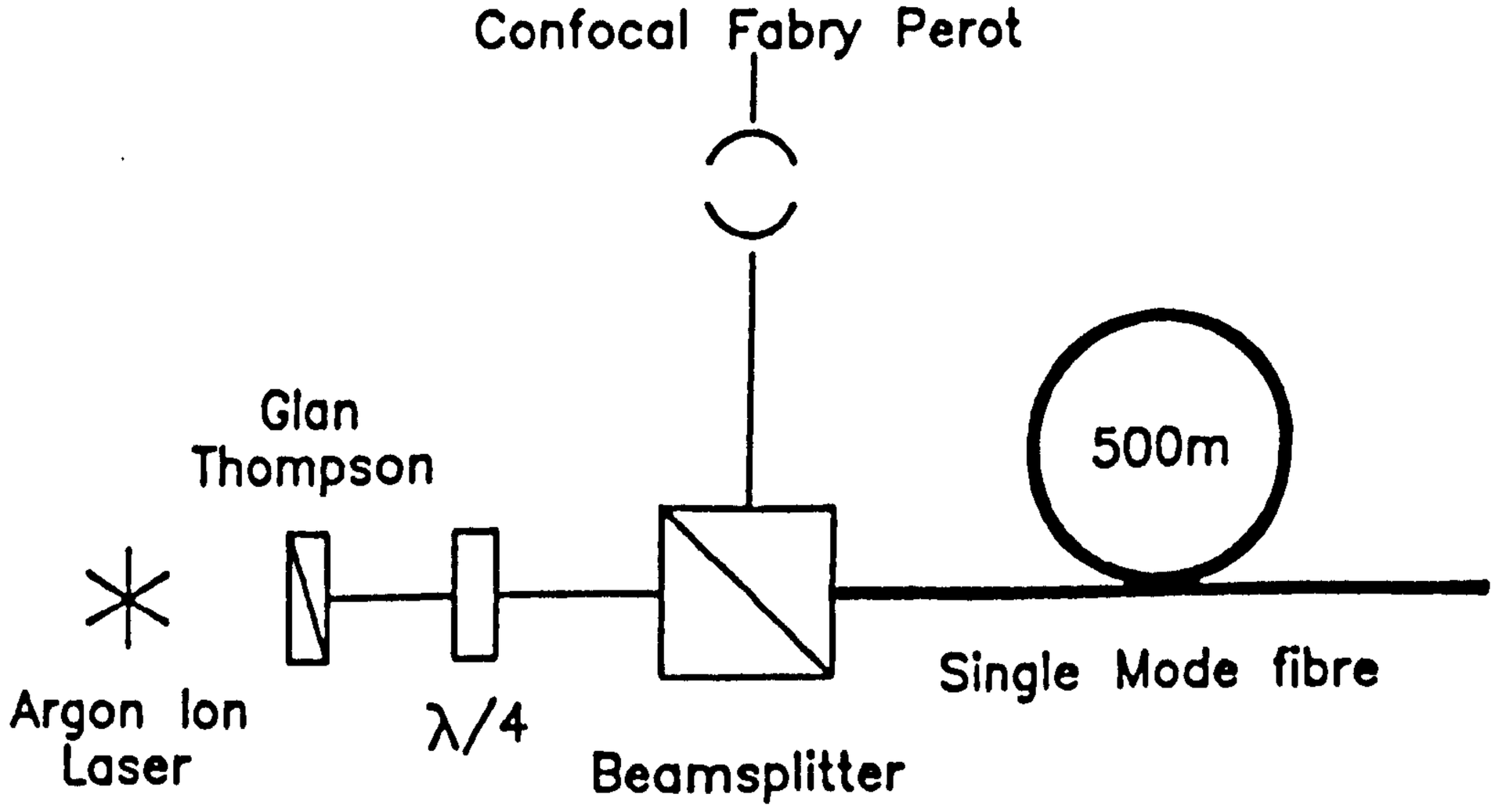

Figure 3.2

Experimental configuration for the generation and detection of BSBS in 500m of single mode fibre at λ_L = 514.5nm. The signal is resolved optically by a confocal Fabry Perot (FSR = 2GHz±30MHz) and the laser protected from any back reflection by a Glan Thompson prism and quarter wave plate.

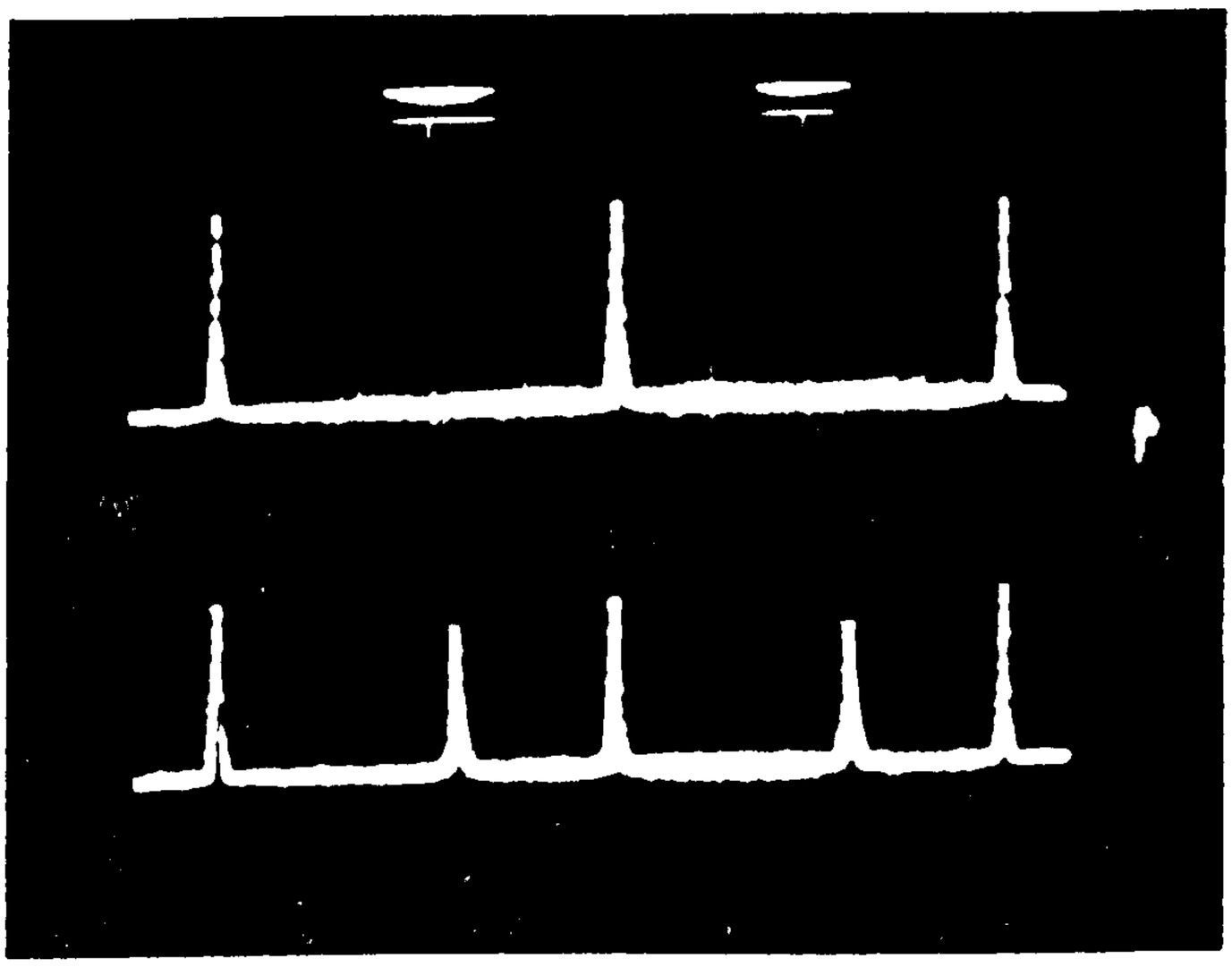

Figure 3.3

Experimental observation of BSBS at 514.5nm. In the upper trace the laser line is resolved optically by a confocal Fabry Perot with a FSR equal to 2GHz (±30MHz). The lower trace, whilst illustrating the unshifted laser line, also shows the BSBS signal which can be seen to be shifted in frequency by 32.8GHz (±33MHz) from the laser. The BSBS signal is the larger of the two peaks and the smaller peak, the pump, acts as a reference. This result is in good agreement with the theoretically predicted value of 32.7GHz as given by eqn.(2.3.4)

in a multiple order; i.e. m x (FSR) + 0.8GHz (±33MHz), where m is an integer. Theoretically from eqn.(2.3.4) the shift is expected to be 32.7GHz Whilst the FSR of the CFP limits the direct comparison between the theoretical and experimental result to be made, Hill[10] measured the frequency shift to be 33GHz. The difference between this value and the result from figure 3.3 is attributed to the difference in acoustic velocities in the fibre core and cladding, but nonetheless it is in good agreement with our experimental value and confirms that theoretically predicted in eqn.(2.3.4).

The threshold value for which the SBS signal was generated in figure 3.3 was experimentally observed at 45±0.5mW. This is indicated in figure 3.4. For the experimental configuration shown in figure 3.2, the SBS and transmitted signals were measured as the launched power was increased. The fibre loss at λ_L = 514.5nm was measured as 20dB/km by cutting the fibre back without disturbing the launch. Figure 3.4 indicates a conversion efficiency of 20% for a launch power of 100mW. The observed threshold of 45±0.5mW is in good agreement with that theoretically predicted (~30mW) by eqn.(3.2.6) and it is also in good agreement with other authors. Stolen[9] measured the Brillouin threshold at 524.5nm as 130mW; however, this was for a fibre length of 395m and a fibre loss of 43dB/km. The discrepancy between the experimental and theoretically predicted value is certainly a result of the variation in the characteristics of the fibre used, i.e. fibre spot size and the fibre dopants.

The sub-section following will consider the effects of temperature on the Brillouin frequency shift. However, it is appropriate here to discuss briefly the effect of temperature on the threshold power. Equation (3.2.6) suggests, because the phonons are thermally generated, the "seed power" will increase with an increase in temperature and thereby reduce the threshold power before the onset of stimulated Brillouin scattering. At room temperature the seed power has been calculated as 1.8nW, but by increasing the temperature by 100°C this increases to 2.4nW; the computed threshold powers as a function of temperature for an effective length of 380m are shown in figure 3.5. As expected the Brillouin threshold decreases for an increase in temperature and results indicate a sensitivity of ~3.7μW per degree Celsius. This result, because of the

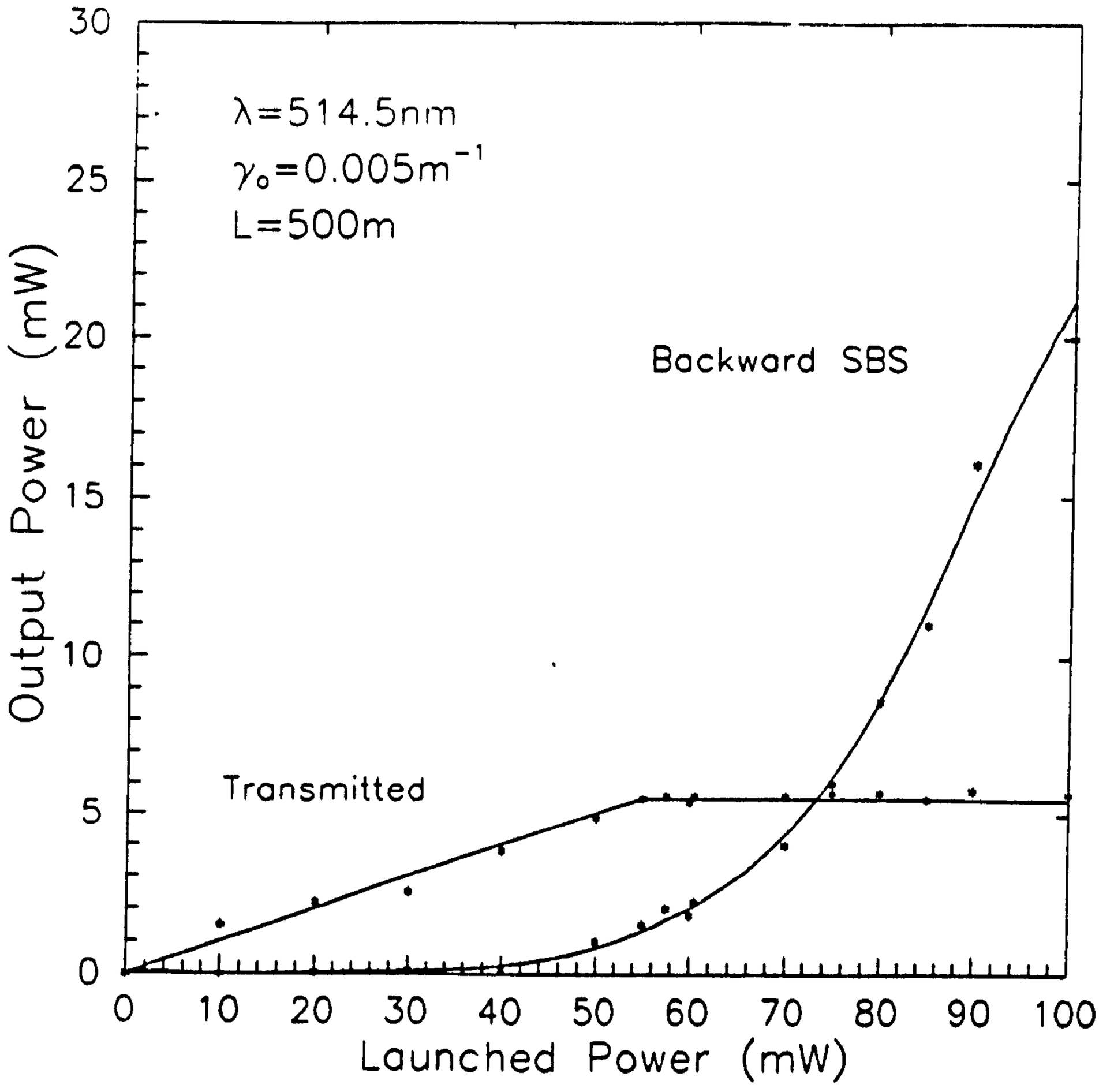

Figure 3.4

Backward SBS and transmitted power measured for increased launched powers (mW). For a fibre length of 500m and attenuation of 20dB/km the threshold power at λ_L = 514.5nm was measured to be 45±0.5mW. This value was determined by simultaneously measuring the launched power when the Brillouin signal was first observed at the confocal Fabry Perot, as shown in figure 3.3.

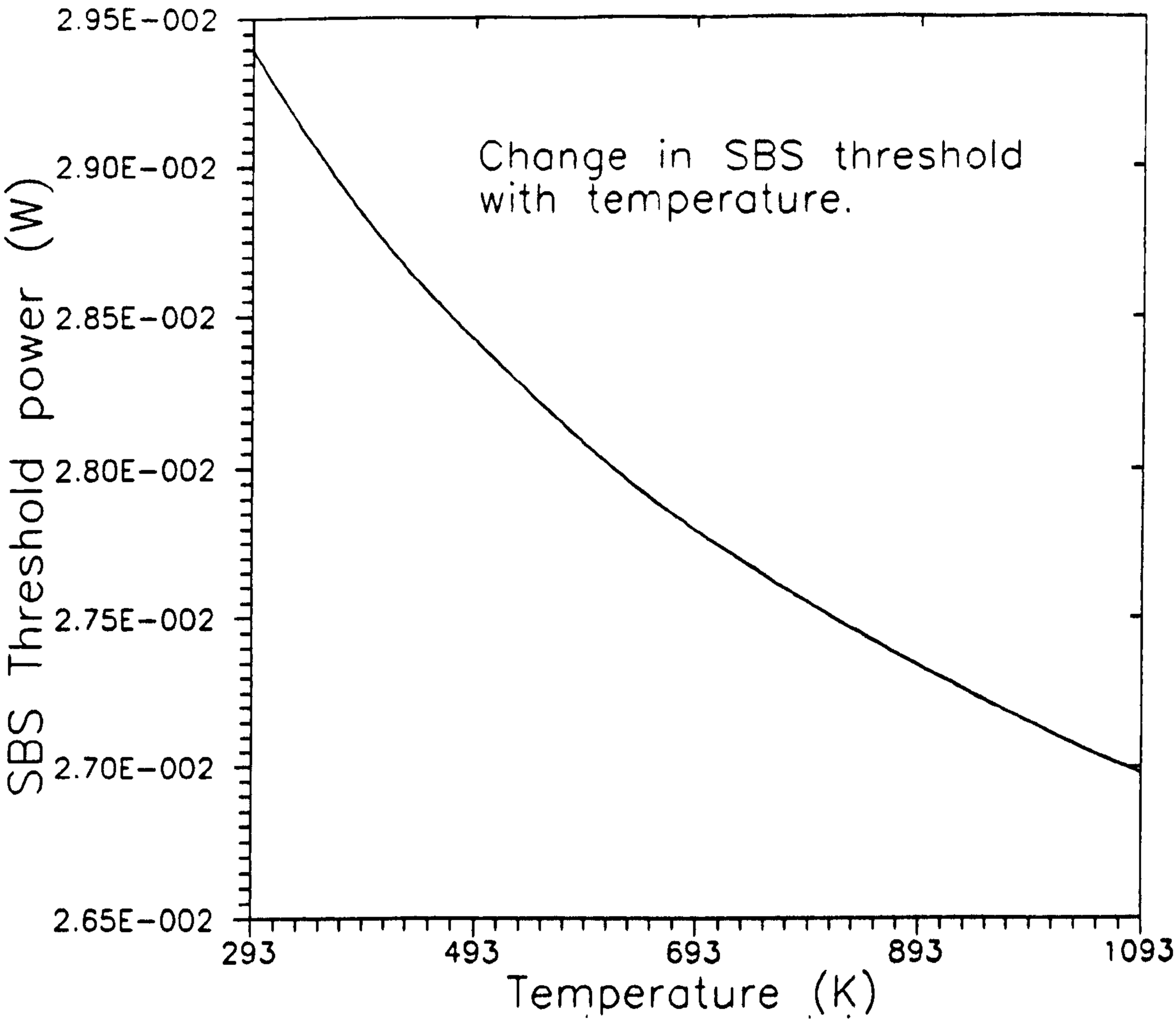

Figure 3.5

Threshold powers as a function of increased temperature computed from eqn.(3.2.6)

and for an effective length of 381m. The results confirm the experimental difficulty to observe a change in threshold power for localised temperature changes along the fibres length. The sensitivity of the threshold power is 3.7μW per °C and is seen to decrease for increased temperatures.

small sensitivity confirms the difficulty described in the following sections of detecting any change in the Brillouin threshold power as the fibre is heated.

3.3.2 Effects of temperature and core refractive index on the Brillouin frequency shift

It was discussed in section 3.3.1 when comparing Smith's observation for the Brillouin frequency shift to that in figure 3.3 that any change in the refractive index of the fibre core was fundamental to the Brillouin shift. This will be illustrated in this section which anticipates chapter 6 and the application of BSBS in order to realise a) a tunable microwave generator by heterodyning the pump with the Brillouin signal, and b) a frequency shifter by heterodyning two SBS signals in order to generate a low frequency beat signal. The experimental configuration shown in figure 3.6 is similar in broad outline to that in figure 3.2. Two spools of single core fibre, each having different core refractive indices, were initially at room temperature. Light from a single frequency argon laser operating at 514.5nm was launched, via the beam splitter, simultaneously into both fibres. The Glan Thompson and quarter wave plate isolated the laser from optical feedback. The backscattered stimulated Brillouin signal from the two fibres were combined on the first beam splitter and intensity divided at the second beam splitter to enable the optical and heterodyne spectra of the light to be simultaneously measured using a high resolution confocal Fabry Perot and an electronic spectrum analyser. The reflected pump line from one of the fibre ends was passed into the CFP and used as a frequency reference. The optical spectra resolved by the CFP are shown in figure 3.7. Fibre 1 as shown in figure 3.3 indicates a frequency shift of 32.8GHz (±33MHz) whilst fibre 2, to the right of the unshifted Rayleigh line, shows a frequency shift of 32.042GHz (±33MHz). The two backscattered BSBS signals were also detected on a high speed PIN photo-diode and the spectrum of its output current was analysed with a HP8596A RF spectrum analyser. Figure 3.8 shows the resulting power spectrum at room temperature where a very strong <1MHz wide peak at 760MHz is easily identified. The frequency of this peak clearly corresponds to the

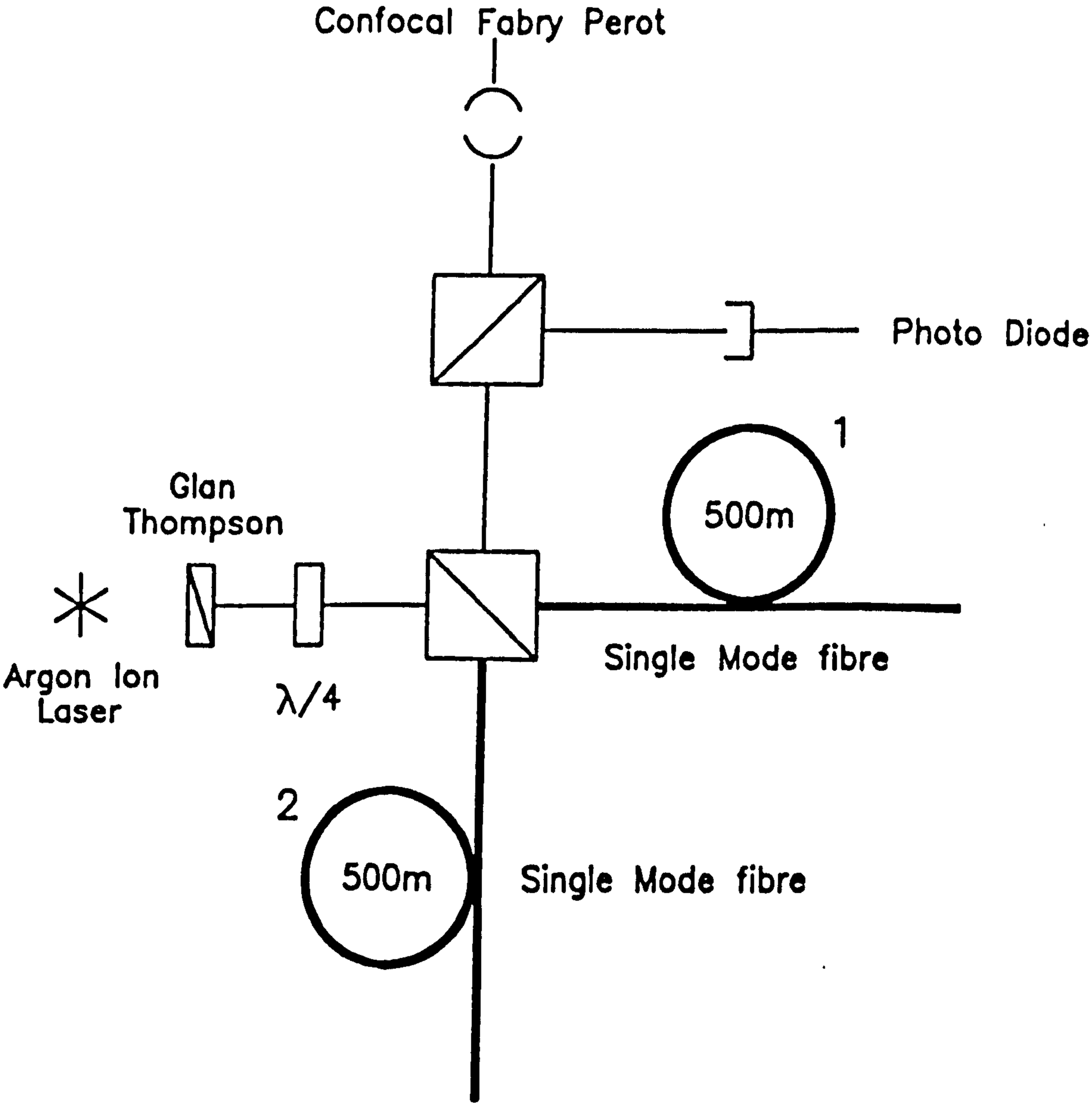

Figure 3.6

Experimental configuration : the two backscattered stimulated Brillouin shifted signals from the two 500m spools of single mode fibre were analysed with a scanning CFP with a FSR of 2GHz. The beat frequency was detected by a photo-detector and investigated with an electronic RF spectrum analyser.

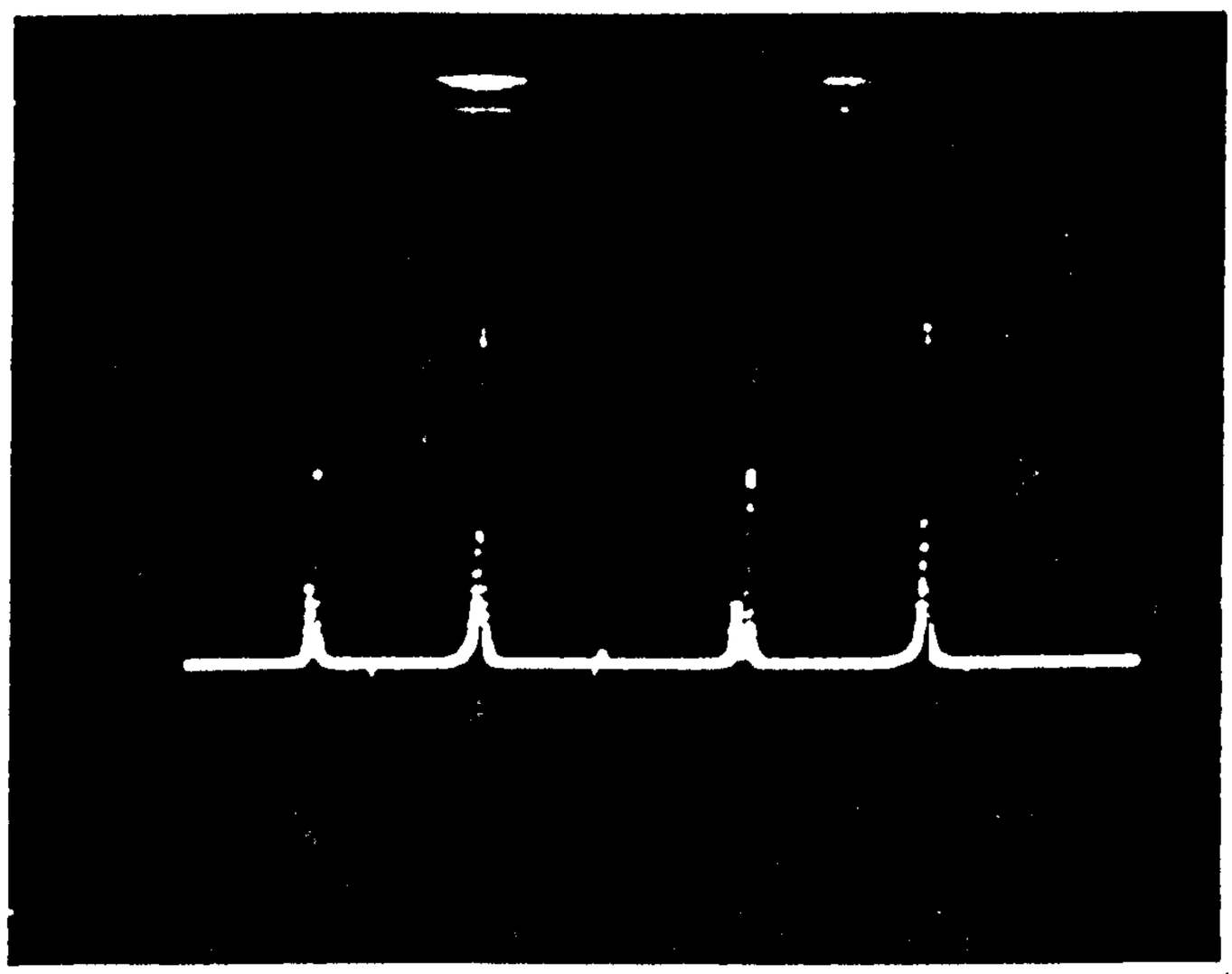

Figure 3.7

The optical spectrum of the light analysed by the CFP. The frequency shift of each stimulated line relative to the (small) pump line is 32.8GHz (±33MHz), fibre 1, and 32.042GHz (±33MHz) for fibre 2 and where the Rayleigh line is the small signal to the left of fibre 2. This corresponds to a beat frequency at room temperature of ~761.4MHz as shown in figure 3.8.

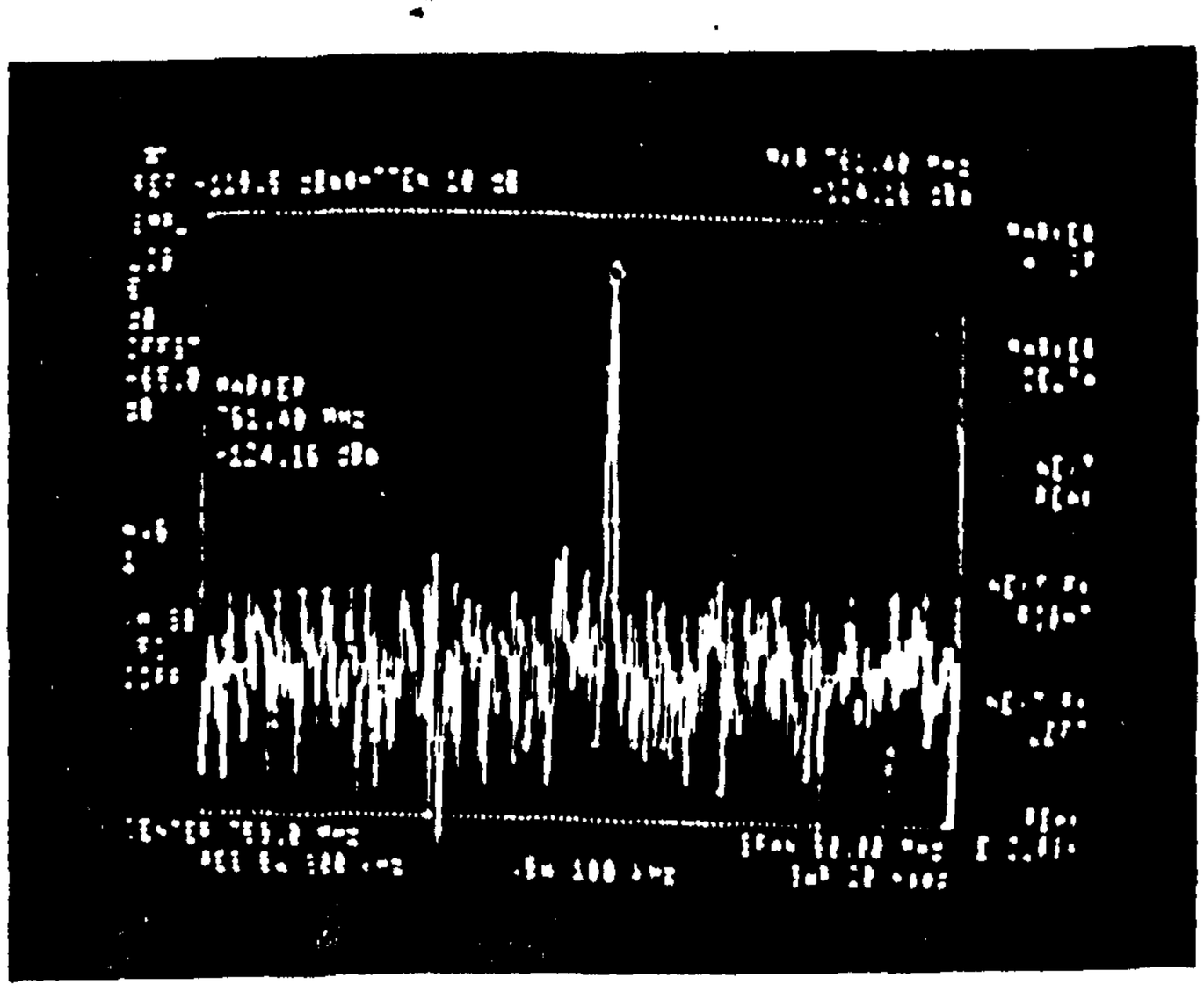

Figure 3.8

The heterodyne frequency at 761.4MHz generated at the photo-diode.

difference frequency between the two BSBS signals; thus one may conclude that optical heterodyning is occurring. The narrow linewidth of the heterodyne signal also confirms that although the scattering is occurring in different fibres a considerable degree of temporal coherence between the stimulated signals must be retained.

Finally the beat frequency was monitored whilst the temperature of one of the fibres was increased, and the temperature of the other fibre being held constant. The result of this experiment is shown in figure 3.9 where two traces are superimposed. The low frequency peak (748MHz) corresponds to the beat frequency when both fibres were at the same temperature and the high frequency peak ~800MHz when the differential temperature on account of heating fibre 2 is 10°C. This corresponds to a frequency shift of 5.2MHz per°C. The sensitivity of the phonon frequency and hence the Brillouin frequency shift with temperature is largely the result of the change in refractive index with temperature and this becomes clear when examining eqn.(2.3.4). Although the frequency shift is dependent on the acoustic velocity this parameter has been shown to change by only 7% for the temperature range 20°C to 1620°C, and therefore accounts for 14MHz of the difference frequency generated at the photo-diode when fibre 2 is heated.

3.7 Conclusion

This chapter has verified experimentally the dependence of the fibre parameters on the Brillouin frequency shift. It has also verified experimentally that a strong heterodyne beat signal with a narrow linewidth can be produced by mixing two BSBS signals generated in separate optical fibres. The beat frequency is shown to vary rapidly with temperature. It would thus appear that this phenomenon could be exploited to realise a tunable microwave generator with a large frequency range by heterodyning the pump and Brillouin signal and secondly a tunable frequency shifter by heterodyning two BSBS signals. In practice these systems would be based upon solid state laser sources rather than argon lasers. This subject is taken up in chapter 6 where BSBS in fibre ring

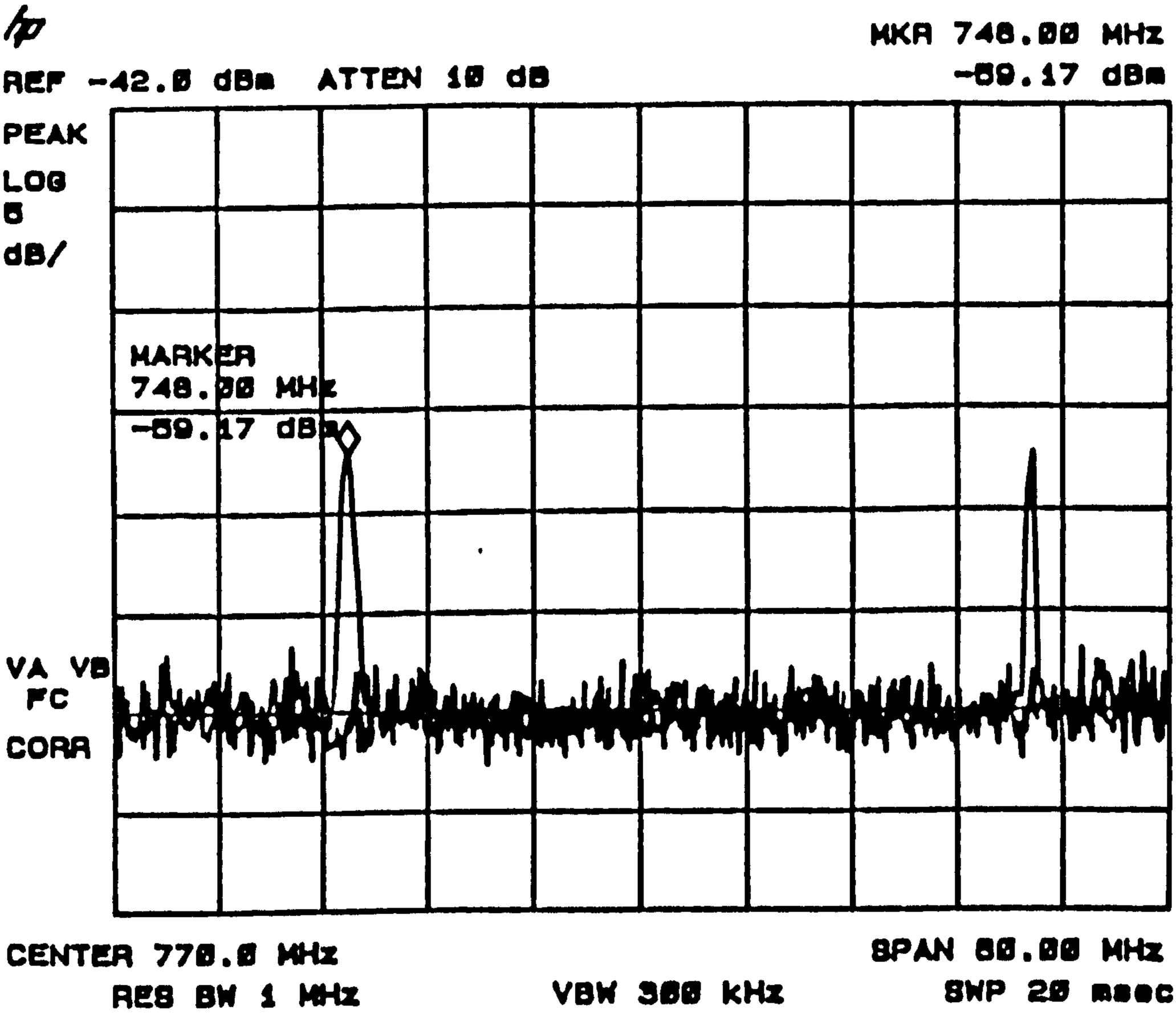

Figure 3.9

The lower frequency peak (748MHz) corresponds to the beat frequency when both fibres were at room temperature. The higher frequency peak (800MHz) corresponds to the beat frequency when fibre 2 was heated by 10°C.

lasers is exploited in order to realise a more practical device than has otherwise been explained here. The subject of BSBS in ring resonators and the high circulating power densities that they offer such that the threshold powers for BSBS can be drastically reduced is the discussion that now follows in chapter 4.

References: Chapter 3

1. Cotter, D.: "Stimulated Brillouin Scattering in Monomode Optical Fibre", J.Opt.Comm., vol.4, no 1, pp 10-19, 1983.
2. Tang, C.L.: "Saturation and Spectral Characteristics of The Stokes Emission in The Stimulated Brillouin Process", J.Appl.Phys., vol. 37, p 2945, 1966.
3. Enns, R.H., and Batra, I.P.: "Saturation and Depletion of Stimulated Light Scattering", Phy.Lett., vol. 28A, p 591, 1969.
4. Shen, Y.R.: "Principles of Non-Linear Optics", p 188, Wiley, 1984.
5. American Institute of Physics Handbook, edited by D.C.Gray ,McGraw - Hill Book Co., Inc., New York, 1965 second edition.
6. Pelous, J., and Vacher, R.: "Thermal Brillouin Scattering Measurements of The Longitudinal Hypersound in Fused Quartz From 77-300K", Solid State Commun, vol.16, pp 279 - 283, 1975.
7. Yeung, J., and Yariv, A.: "Theory of CW Raman Oscillation in Optical Fibres", J.Opt.Soc.Am., vol.69, no.6, 1979.
8. Smith, R.G.: "Optical Power Handling Capacity of Low Loss Optical Fibres as Determined by Stimulated Raman and Brillouin Scattering", Appl.Opt., vol.11, p 2489, 1972.
9. Stolen, R.H.: "Polarisation Effects in Fibre Raman and Brillouin Lasers", IEEE. J.Quantum Electronics, vol.QE - 15, no.10, 1979.
10. Hill, K.O., Johnson, D.C., and Kawasaki: "C.W.Generation of Multiple Stokes and Anti - Stokes Brillouin Shifted Frequencies", Appl.Phy.Lett., vol.29, no.3, 1976.
11. Bucaro, J.A., and Dady, H.D.: "High Temperature Brillouin Scattering in Fused Quartz", J.Appl.Phys., vol.45, no 12, 1984.

Chapter 4

Stimulated Brillouin scattering in fibre ring resonators

4.1 Introduction

To perform some of the basic functions required in any optical system, components have been developed such as polarisation controllers[1], modulators[2], passive filters[2] and fibre amplifiers[2]. Added to this, another important function is the transfer of signal power between two optical fibres. Various approaches have been investigated by different authors using either multi-mode or single-mode fibres and these have led to several coupler geometries. Some of the approaches rely on evanescent wave coupling[3,4]which require that the fibre cores be brought close to each other to make possible the interaction of the evanescent fields which extend just outside the fibre cores.

The reason why low loss couplers are important here is that their manufacture is essential regarding the fabrication of a high finesse fibre ring resonator[5]. Whilst optical resonators have important practical and potential applications, e.g. optical sensors[6,7] and frequency selective devices[8,9], the single mode all fibre ring resonator has been widely used in the fabrication of all fibre ring lasers[10,11], passive resonator gyroscopes[12,13], laser diode linewidth stabilisation [14]and as fibre amplifiers[15,16]. When a long coherence source is used the intense circulating power in the loop is ideal for the generation of non linear effects and in particular, because of the narrow linewidth of excitation, (<100MHz), stimulated Brillouin scattering. The generation of SBS in a ring resonator can be considered as a lasing process in which the pump wave strongly amplifies a counter propagating Stokes wave giving a frequency shifted output (eqn.(2.3.4)). BSBS fibre lasers, first investigated by Hill et al[17,18], have also been realised in both hybrid bulk/fibre[17,19]and all fibre versions[11,20]. The all fibre ring resonator geometry has the advantages of very low round trip loss (~ 0.03 dB)

coupled with a significant enhancement of the circulating power over the input power, thus realising extremely high finesse ring resonators exhibiting BSBS thresholds at powers as low as 35μW [21]. In the next section it will be shown that the threshold power is limited by the finesse of the resonant cavity or its Q value. In order to enhance the circulating power density inside the ring, and consequently minimise the threshold value, the finesse (a function of the loss of the device) has to be made as large as possible.

The all fibre ring resonator can take one of two configurations. Whilst their manufacture is discussed fully in appendix A, both geometries are discussed in section 4.2 and the transfer function of the cross coupled ring resonator is derived. The effects of a variable coupling coefficient and the resonant cavity loss on the finesse and contrast of the transfer function is also emphasised. The threshold powers are expressed in section 4.3, and the effect of the number of modes (states) under the Brillouin gain curve is discussed in section 4.4. Experimental results feature in section 4.5. In sub-section 4.5.1 the experimental observation of BSBS is discussed. In sub-section 4.5.2 a comparison is made between the experimentally observed threshold power and the theoretically predicted value from section 4.3. The results of increased pump powers above threshold and the change in finesse which results from the counter propagating BSBS generating a loss within the cavity is also considered. The effect of larger FSR's, (i.e. longer loop lengths) is similarly discussed. Conclusions are drawn in section 4.6.

4.2 Transfer function and finesse for all fibre ring resonators

The design of a single mode optical fibre ring resonator can take one of two forms:

a) A length of fibre can be formed into a closed loop to constitute a low loss cavity, figure 4.1(A), and such a configuration is referred to as a cross coupled ring

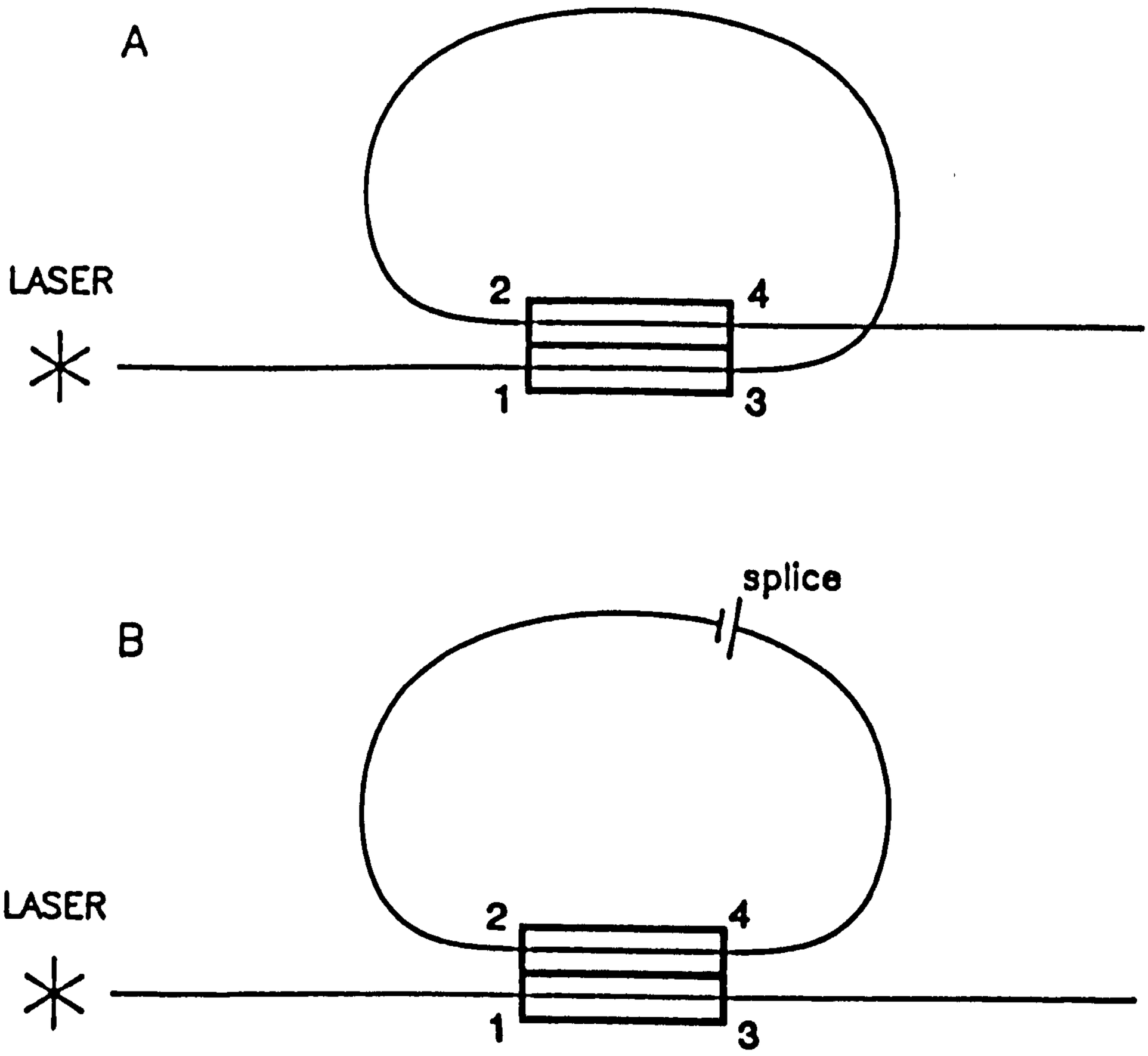

Figure 4.1

Configurations illustrating, above, the cross coupled (CCR) and below the direct coupled (DCR) all fibre ring resonator. The CCR is limited by the insertion loss of the coupler halves and relies on a coupling coefficient tending to unity. This is in contrast to the DCR, below, which is limited by the splice loss and relies on a coupling coefficient tending to zero.

resonator (CCR). This configuration relies on a coupling coefficient tending to unity and is limited by the lumped loss of the coupler halves. If the directional coupler has a large coupling coefficient, light trapped in the ring will couple from port 2 to port 3 and will continue to circulate. Similarly light introduced to the input port 1 will couple mostly to the output port 4. Now consider the case when the fibre loop length is adjusted for constructive interference (addition) between coherent components entering port 3 from ports 1 and 2. The small fraction of light from port 2 to port 4 will destructively interfere with the light coupling from port 1 to port 4 (bearing in mind there is a $\pi/2$ phase shift on coupling). The circulating field will grow until an equilibrium is reached. With an optimum value of coupling that depends on losses, the two destructively interfering components emerging from port 4 are equal in amplitude and completely cancel each other. From an energy conservation point of view the circulating power grows until the power dissipated by the losses in the loop equals the input power at port 1. If the cavity length is now modulated, the power emerging from port 4 will show a series of sharp minima whenever the input optical frequency matches the resonant condition. The behaviour is similar to a Fabry Perot-type resonator whose reflected power has sharp minima at resonance. For a directional coupler of this type to function properly the directional coupler must have a low insertion loss (< 0.1dB) and, because the optimum value of coupling depends on losses, a variable coupling coefficient is desirable. In the following experiments an evanescent field coupler is used; its method of fabrication is discussed fully in appendix A. Essentially a single strand of optical fibre is bound into two slotted quartz blocks a distance L apart. Each fibre is then ground and polished to within a few micrometers of the fibre core. The two units are then placed in contact and orientated as in figure 4.1(A). Coupler tuning is accomplished by sliding one block over the other in order to vary the core to core separation and to optimise the coupling coefficient.

b) Alternatively, the direct coupled fibre ring resonator (DCR) shown in figure 4.1(B) consists of a single mode directional coupler where the principal fibre has ports (1) and (3) and the ends of ports (2) and (4) of the coupled fibre are spliced together to

form a complete loop. This configuration relies on a coupling coefficient tending to zero. An input launched into port 1 may be coupled into port 4 from which it is guided along the fibre loop and reaches port 2. Part of the light at port 2 will be coupled into port 3 and part of it will proceed to port 4 to complete a round trip. In the steady state a dynamic equilibrium is established between the waves travelling in the principal fibre, 1-3, and those coupled into the coupled fibre, 2-4. When light is launched into port 1, and a perfect resonant state is established, much optical energy circulates in the loop. In the optimum resonant condition the output intensity is equal to zero in a similar manner to that described for the CCR. Under these conditions a little energy continues to be coupled into the fibre loop from port 1 in order to maintain a resonance and satisfy the losses inherent to the device. The theory is developed in an identical manner to that now described for the CCR.

The directional coupler is modelled as a perfect (lossless) device with an added lumped loss that is independent of the coupling coefficient. Referring to figure 4.1(A), the fractional coupler intensity loss, γ_o, is given by:

$$|E_3|^2 + |E_4|^2 = (1 - \gamma_o)[\,|E_1|^2 + |E_2|^2\,] \qquad (4.2.1)$$

where E_i is the complex field amplitude of the i^{th} port. Typically, γ_o, varies between 3 and 5 % [4]. The complex amplitudes in the fibre after the coupled mode interactions are related to the incident field amplitudes by:

$$|E_3| = (1 - \gamma_o)^{\frac{1}{2}}\,[\,(1-k)^{\frac{1}{2}} E_1 + j\sqrt{k}E_2\,] \qquad (4.2.2)$$

$$|E_4| = (1 - \gamma_o)^{\frac{1}{2}}\,[\,j\sqrt{k}E_1 + (1-k)^{\frac{1}{2}} E_2\,]$$

where k is the (intensity) coupling coefficient. No coupling corresponds to $k = 0$, whereas $k = 1$ gives complete cross coupling; j denotes a phase change for the coupling term. E_2 and E_3 are further related by :

$$E_2 = E_3 \exp(-\alpha L/2)\exp(j\beta L) \qquad \beta = n\omega/c \qquad (4.2.3)$$

where $\alpha/2$ is the fibre's (amplitude) attenuation coefficient, n the fibre's refractive index, ω the optical frequency and c the speed of light. Essentially eqn.(4.2.3) describes E_2 differing from E_3 because of a loss and a phase change attributed to the loop length L.

Equations (4.2.2) and (4.2.3) can be solved for E_4/E_1 in terms of γ_o, k, αL and βL. For a resonant situation we require real and imaginary parts of E_4/E_1 to vanish. This yields two necessary resonant conditions. The first is:

$$\beta L = q2\pi - \pi/2 \qquad (4.2.4)$$

where q is any integer. Note that from eqns.(4.2.2) the directional coupler has a $\pi/2$ phase shift, so that the collected phase around the ring is $q2\pi$. The second condition required for resonance specifies the coupling coefficient, denoted by k_r, and which is a limitation of the device - i.e. the losses.

$$k_r = (1 - \gamma_o)\exp(-\alpha L) \qquad (4.2.5)$$

It is clear from eqn.(4.2.5) that the limitation of the device is the insertion loss of the coupler halves, $(1-\gamma_o)$, and that, by comparison, the attenuation of the fibre length ($\sim 0.023 m^{-1}$) is negligible; note also that the round trip intensity loss is also given by $(1 - k_r)$. With this value of coupling, eqns.(4.2.2) and (4.2.3) yield for the output and circulating intensities when $k = k_r$:

$$\left|\frac{E_4}{E_1}\right|^2 = (1 - \gamma_o)\left[1 - \frac{(1 - k_r)^2}{(1 + k_r)^2 - 4k_r\sin^2(\frac{\beta L}{2} - \frac{\pi}{4})}\right] \qquad (4.2.6)$$

$$\left|\frac{E_3}{E_1}\right|^2 = \left[\frac{(1- \gamma_o)(1 - k_r)}{(1 + k_r)^2 - 4k_r\sin^2(\frac{\beta L}{2} - \frac{\pi}{4})}\right] \qquad (4.2.7)$$

Equation (4.2.6) gives a zero resonator output when the cavity finesse satisfies the resonance conditions, $\beta L/2 + \pi/4 = m\pi.$, and also when $k = k_r$. Hence the need for a varying coupling coefficient, k, such that it can be tuned to the resonant coupling coefficient of the cavity k_r. If the cavity length, L, is modulated the resonator behaves as a scanning optical spectrum analyser. When a single frequency light is incident the output of the resonator will be a series of sharp minima whenever the ring length matches the resonant conditions. This is clearly shown in figure 4.2 where the circulating and output intensities as a function of phase are computed from eqns.(4.2.6) and (4.2.7). The finesse of the cavity for the given parameters $\gamma_0 = 0.01$ and $\alpha = 0.0023\text{m}^{-1}$, is $F = 200$. More importantly, however, is the enhanced circulating power within the cavity. When the output intensity is zero the circulating power is amplified; for the given parameters the power enhancement is seen to be ~ 64 times the launched power. This power amplification is clearly expressed in eqn.(4.2.8). It is this characteristic that makes high finesse ring resonators ideal for the generation of non linear effects and in particular BSBS[11,20]. Experimentally these results will be confirmed in section (4.3), but it should be appreciated that because the circulating power is confined within the cavity, detecting it directly is made difficult. The significance of a low coupler insertion loss is illustrated in figure 4.3. Clearly the finesse (the free spectral range divided by the half width at half maximum) decreases for greater insertion losses. This results in a smaller circulating density and consequently higher threshold powers for the onset of SBS. This is more clearly shown in section 4.3. The final and important characteristic for the generation of BSBS in ring resonators is a variable coupling coefficient. At resonance ideally all the light should be trapped within the cavity and this is satisfied when $k = k_r$. Figure 4.4, computed from eqn.(4.2.6), shows the output transfer function for when this equality is no longer satisfied. When $k = 0.85k_r$, firstly the contrast diminishes to ~20% and secondly the finesse of the cavity is dramatically reduced from 200 to 20. Both of these factors have implications on the threshold powers and require greater launched powers in order to generate BSBS. The desirability of a variable coupling ratio highlights the

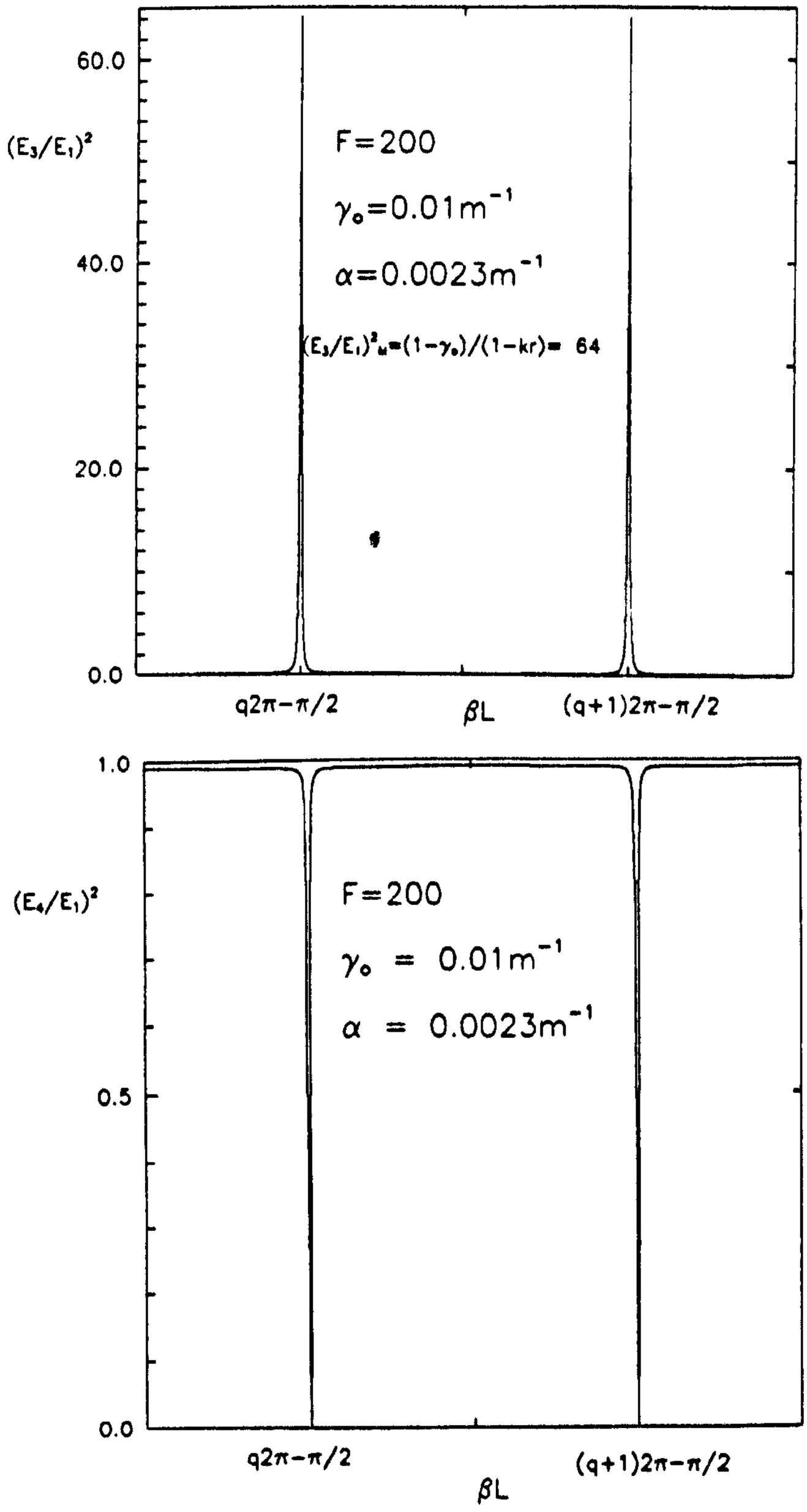

Figure 4.2

Transfer function for the circulating power $|E_3/E_1|^2$ within the ring, given above, and the output of the resonator, $|E_4/E_1|^2$, below. The transfer functions are computated from eqns.(4.2.6) and (4.2.7) for a fibre loss α = 0.0023m^{-1} and insertion loss γ_o = 0.01m^{-1} thus giving a finesse of ~ 200

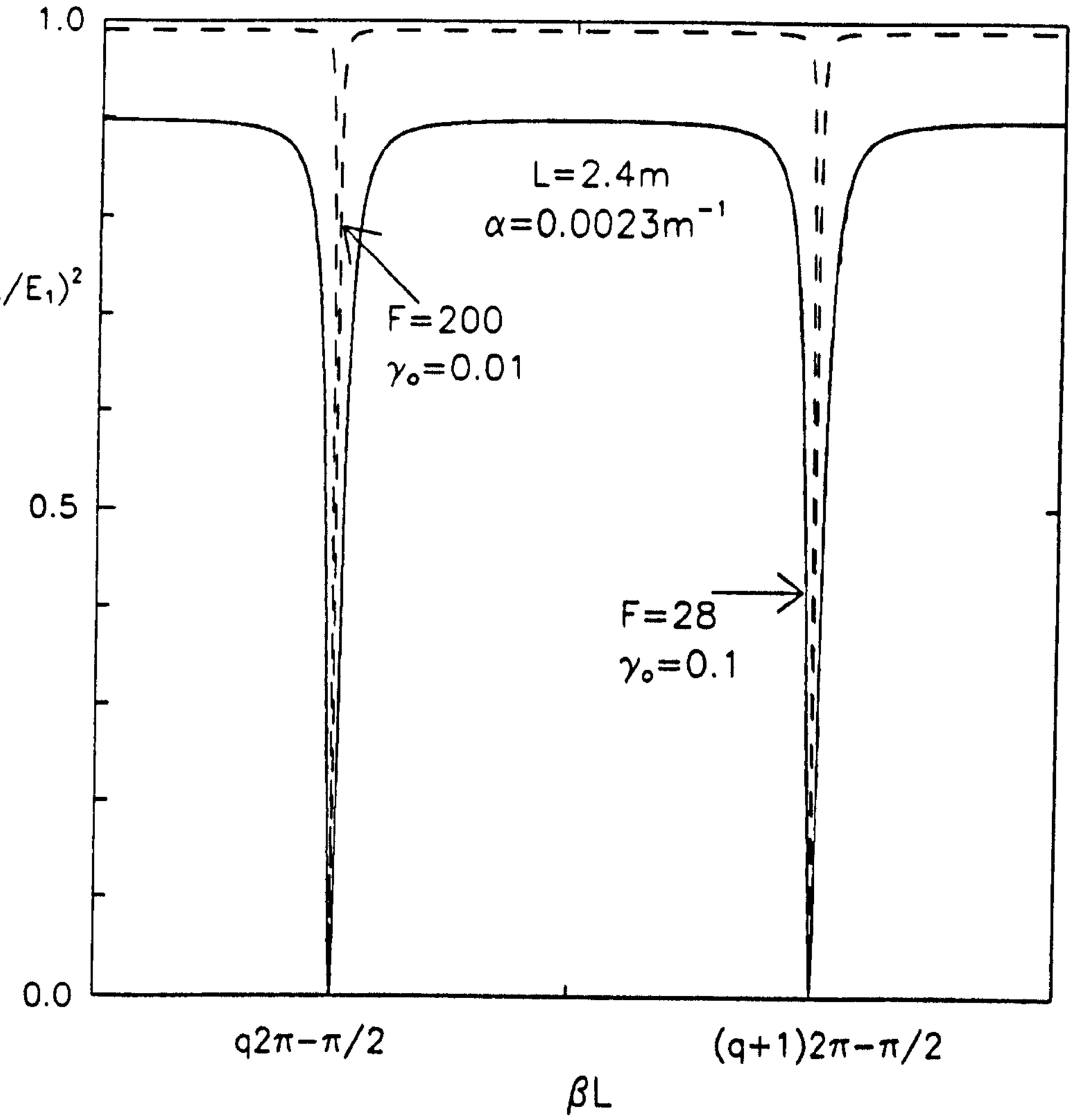

Figure 4.3

The significance of the insertion loss of the directional coupler. For the given parameters in figure 4.2, $\gamma_o = 0.01$ which gives a finesse of ~ 200. However, for a lumped loss of $\gamma_o = 0.1$, the finesse falls to 28. The circulating power density within the ring subsequently deteriorates and results in a higher threshold in order to generate BSBS.

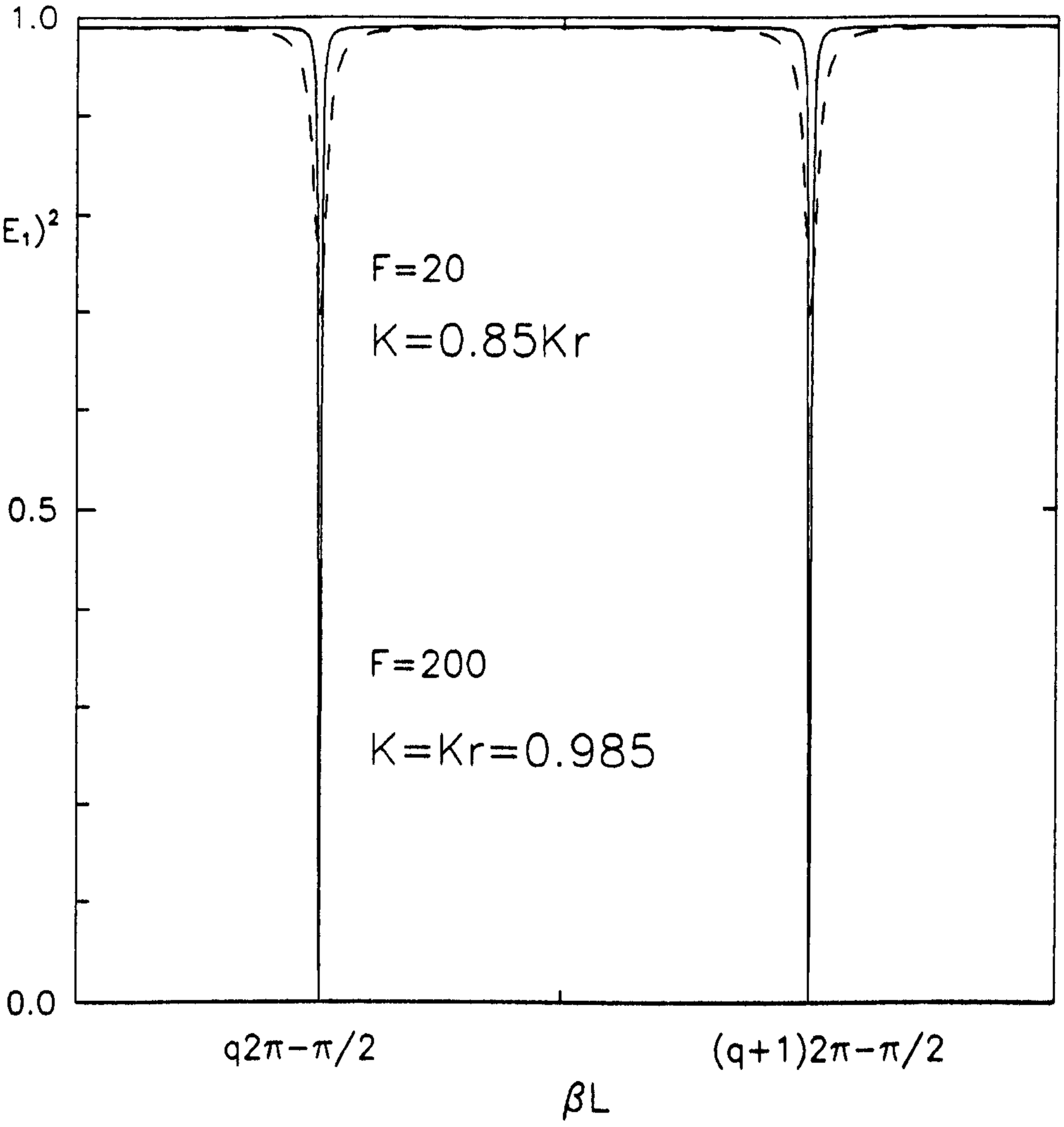

Figure 4.4

The significance of a variable coupling ratio: for $k = k_r$ and for the given parameters in figure 4.2, the resonator has a finesse of ~200. However, for a coupling coefficient $k = 0.85k_r$, the finesse is reduced to F~20, whilst the contrast is reduced to a 20% modulation depth. Both of these characteristics supress the threshold power for the onset of SBS.

major disadvantage of the DCR. In the case of the CCR the couplers are polished for maximum coupling and it is therefore always possible to detune the device and match k and k_r and thereby realise the high finesse and contrast required for the generation of BSBS. However, in the example of the DCR, because the coupler halves are polished for minimal coupling, it is impossible to "up-tune" the device in order to compensate for the splice. In theory the DCR should be easier to manufacture, but in practice the full potential of the resonator is best achieved when the fibre from a single length is closed in low loss manner.

From figure 4.2 and eqns.(4.2.6) and (4.2.7), it is seen that for the CCR, at resonance, $\sin^2[(\beta L/2) - (\pi/4)] = 1$.The output intensity is then zero and consequently the circulating intensity is given by:

$$\left|\frac{E_3}{E_1}\right|^2_{MAX} = \frac{(1 - \gamma_o)}{(1 - k_r)} \qquad (4.2.8)$$

Hence from eqn.(4.2.8) in order that the circulating power intensities within the cavity be maximised, a coupling coefficient tending to unity and as near a lossless device as possible are desired. The power enhancement shown in figure 4.2 is now more clearly defined by eqn.(4.2.8). The free spectral range (FSR) of the resonator is c/nL. By equating eqn.(4.2.7) to $1/2|E_3/E_1|^2_{MAX}$ defined in eqn.(4.2.8), the fullwidth at half maximum is found to be:

$$\Delta f = \frac{c}{nL}\left[1 - \frac{2}{\pi}\sin^{-1}\left[1 - \frac{(1 - k_r)^2}{4k_r}\right]^{\frac{1}{2}}\right] \qquad (4.2.9)$$

For k_r near to unity, Δf is, to a very good approximation (within 2% for $k_r > 0.8$)[5]:

$$\Delta f = \frac{c}{nL}\frac{(1 - k_r)}{\pi\sqrt{k_r}}$$

and the cavity finesse is therefore:

$$F = \frac{FSR}{\Delta f} = \frac{\pi\sqrt{k_r}}{(1 - k_r)} \qquad (4.2.10)$$

This is analogous to the finesse of a flat Fabry Perot etalon of mirror reflectively R and spacing L, giving $F = \pi\sqrt{R}/(1 - R)$[22]; note that the etalon and fibre resonator have a fractional loss per unit length of $(1 - R)/L$ and $(1 - k_r)/L$, respectively. Eqn.(4.2.10) shows that the finesse of the ring resonator is heavily dependent on the coupling constant k_r of the device. For a given ring resonator the fibre loss $\exp(-\alpha L)$ is a constant, therefore, from eqn.(4.2.5) it is seen that decreasing the insertion loss, γ_o, of the directional coupler is the only way to achieve a high finesse ring resonator.

4.3 Threshold powers

If the circulating pump power is above the stimulated Brillouin lasing threshold, a backward propagating Brillouin shifted wave will build up from noise and circulate in a direction opposite to the pump (see chapter 2.3). Therefore, when the pump frequency is at resonance for the ring, a resonant mode near the peak Brillouin gain is automatically present allowing the Brillouin shifted wave to circulate simultaneously. For the CCR, port 1, figure 4.1(A), becomes the output port for this wave. Because the coupling constant is near to unity, only a small fraction of the circulating Brillouin power emerges from port 1. To determine a threshold level for BSBS, pump power depletion that is due to the Brillouin scattering is neglected. This is the same assumption made in chapter 3.5 and is also made by Smith[23]. The stimulated Brillouin scattering gain along the fibre of perimeter length, L, is given by, (see eqn.(3.2.4)), $\exp(\bar{g}_{BO}P_C L_{eff}/A)$, where $L_{eff} = [\,1 - \exp(-\alpha L)]/\alpha$ is the effective gain length and is slightly less than L because of the linear fibre attenuation of the pump; the round trip transmission seen by the stimulated Brillouin wave (with no gain present) is the product of the fibre transmission $\exp(-\alpha L)$ and the net coupler transmission from port 3 to port 2. The latter transmission is actually the coupler power transmission $(1 - \gamma_o)$ multiplied by the coupling coefficient, k_r, because only the fraction k_r of the Brillouin wave

remains in the fibre ring while the fraction (1 - k_r) leaves the ring through port 1. Thus the stimulated Brillouin wave round trip transmission is $[(1 - \gamma_o)\exp(-\alpha L)]^2$. The threshold condition for stimulated Brillouin oscillation (transmission x gain = 1) i.e. the backward propagating Stokes wave equals the pump wave as given by Smith, is therefore:

$$[(1 - \gamma_o)\exp(-\alpha L)]^2 \exp(\bar{g}_{BO} P_C L_{eff}/A) = 1 \qquad (4.3.1)$$

To a good approximation we have $(1 - \gamma_o) = \exp(-\gamma_o)$ and $(1 - \alpha L) = \exp(-\alpha L)$. The threshold circulating pump power, P_c, from eqn.(4.2.8) can now be expressed below where eqn.(4.2.10) defining the finesse has also been incorporated to give:

$$P_c threshold = \frac{2A}{\bar{g}_{BO} L}(\gamma_o + \alpha L) \approx \frac{2A}{\bar{g}_{BO} L}\frac{\pi}{F} \qquad (4.3.2)$$

The threshold input power, when incorporating eqn.(4.2.8) into the above finally yields:

$$P_i threshold = \frac{2A}{\bar{g}_{BO} L}\frac{(\gamma_o + \alpha L)^2}{(1 - \gamma_o)} \approx \frac{2A}{\bar{g}_{BO} L}\frac{\pi^2}{F^2} \qquad (4.3.3)$$

Equation (4.3.3) clearly shows the importance of a low loss, high finesse fibre resonator. From eqn.(3.2.4), the gain at λ_L = 633nm can be calculated to be $\bar{g}_{BO}$ = 3.355×10^{-11} m/W. This is in excellent agreement with Stokes[13]. Hence for a fibre core radius, r_{eq} = 2.3μm, a fibre loop length, L = 2.4m, and a finesse of 200, the threshold power is theoretically found to be 100μW. This is in contrast to a linear length of fibre of 500m (L_{eff} = 316m for $\alpha = 0.002\text{m}^{-1}$) where, for identical fibre parameters, a threshold power of, see eqn.(3.2.6), 20mW is predicted. Hence it is clearly seen that the enhanced power density generated within the fibre ring resonator reduces the

launched powers necessary for the onset of SBS by a factor of ~400. However, it should again be emphasised that because of a coupling ratio tending to unity (for a finesse of 200, $k_r = 0.98$) only 2% of the SBS signal is output at port 1, figure 4.1(a).

4.4 Effect of modes (states) available under the Brillouin gain curve

The free spectral range (FSR) for an all fibre ring resonator is given by c/nL, where c is the speed of light, n the refractive index, and L the fibre cavity loop length. The FSR defines the spacing between modes within the resonant cavity; hence the density of states, i.e. the number of modes per unit frequency, is simply the inverse of the FSR. Therefore, by increasing the loop length, the resonant cavity is able to support a greater number of modes. For a loop length of 1m, the FSR of the cavity ($3x10^8/1.46$ x 1) is ~200MHz and for a loop length of 4m the FSR ($3x10^8/1.46$ x 4) is ~50MHz and the density of states is increased by a factor of 4. This suggests that the cavity can resonate at integer values of the FSR. This characteristic is significant when designing the all fibre ring resonator in order to generate SBS as it is necessary that a resonance of the cavity falls under the spontaneous Brillouin gain curve. The linewidth of the spontaneous Brillouin signal is typically 100 MHz in fused quartz, such that for a loop length of 1m (FSR ~ 200MHz) the possibility of BSBS being generated at all is minimal as it is unlikely that the cavity will resonate under the gain curve and, if it does, the chances are that it will not resonate where the gain is maximum - the centre of the gain curve. Thus for BSBS to be generated greater launch powers would be necessary. On the other hand, for a loop length of 4m (FSR ~ 50MHz) it is guaranteed that the cavity will resonate under the gain curve and BSBS will be generated for a given threshold power determined by the gain. As the density of states is increased further still, the position is reached where multiple BSBS lines can be generated under the gain curve and there will exist competition between the lasing modes for the pump power.

4.5 Experimental results

4.5.1 Observation of BSBS in all fibre ring resonator

The experimental configuration given in figure 4.5 is for a CCR of length 2.4m which was fabricated from Lightwave Technology fibre and has a core radius of 2.3μm. As shown, part of the fibre length was wound about a piezo-electric cylinder that can expand radially to modulate the phase. A polarisation controller consisting of two rotatable fibre loops, each acting as a 1/4 wave plate[1], was used to counter any birefringence induced in the ring resonator. Thus the polarisations entering the coupler from the laser, port 1, and the fibre ring, port 2, will be the same. A single frequency long coherence He-Ne laser (λ_L = 633nm) was used to excite the resonator. A low frequency triangular waveform (50Hz) was applied to the phase modulator and the output at port 4 was monitored by a photo-diode. In this way the fibre resonator behaves like a scanning Fabry Perot interferometer. The oscilloscope trace shown in figure 4.6(a) shows the resonant behaviour (output dropping to zero) twice during each linear stretch of the fibre. The output minima being equal to zero is clearly shown in figure 4.6(b) where the oscilloscope trace clearly indicates a 100% modulation depth. Although the theoretical value of the finesse, eqn.(4.2.10), was derived for the circulating intensity maxima it is clear from eqns.(4.2.6 & 7) that the theoretical calculation governing the finesse applies equally to the output maxima. A finesse of 200 was measured from figure 4.6. By cutting the fibre back, a lumped insertion loss of γ_o = 0.011 was determined. For a fibre loss of -10dB/km (0.0023 m^{-1}), eqn.(4.2.5) gives the resonant coupling coefficient, k_r, of the device as 0.9837. This yields a finesse, eqn.(4.2.10), of 188 which is in excellent agreement with the observed finesse of 200 reported above.

When the output from the ring resonator drops to zero, the circulating power within the ring is a maximum. This high circulating power density leads to the generation of a backward propagating BSBS signal from port 1 and which can be detected by a scanning confocal Fabry Perot (FSR = 2GHz), figure 4.7. In practice it is

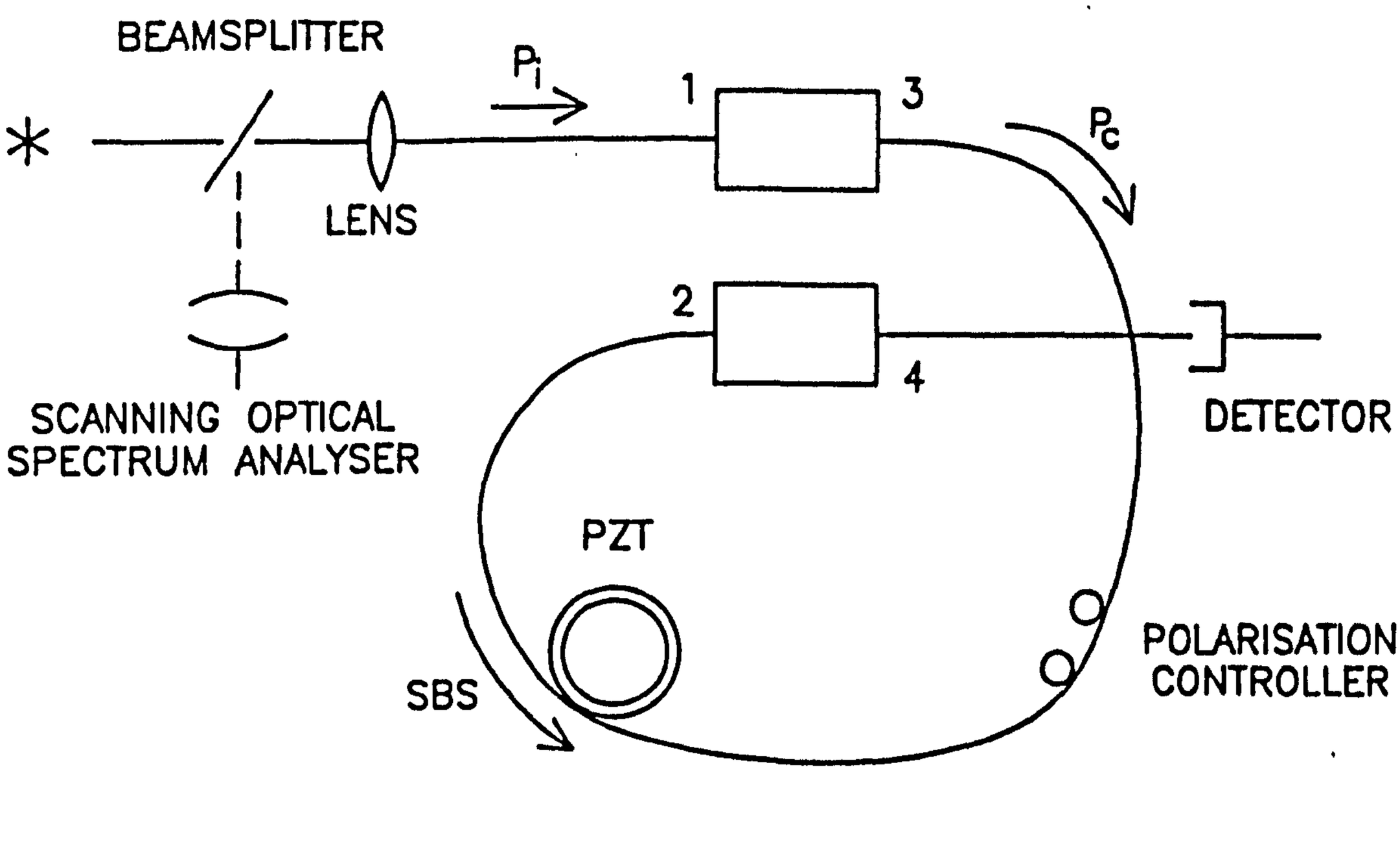

Figure 4.5

All fibre stimulated Brillouin ring laser showing input pump power P_i, resonant circulating pump power P_c, and backward travelling stimulated Brillouin wave.

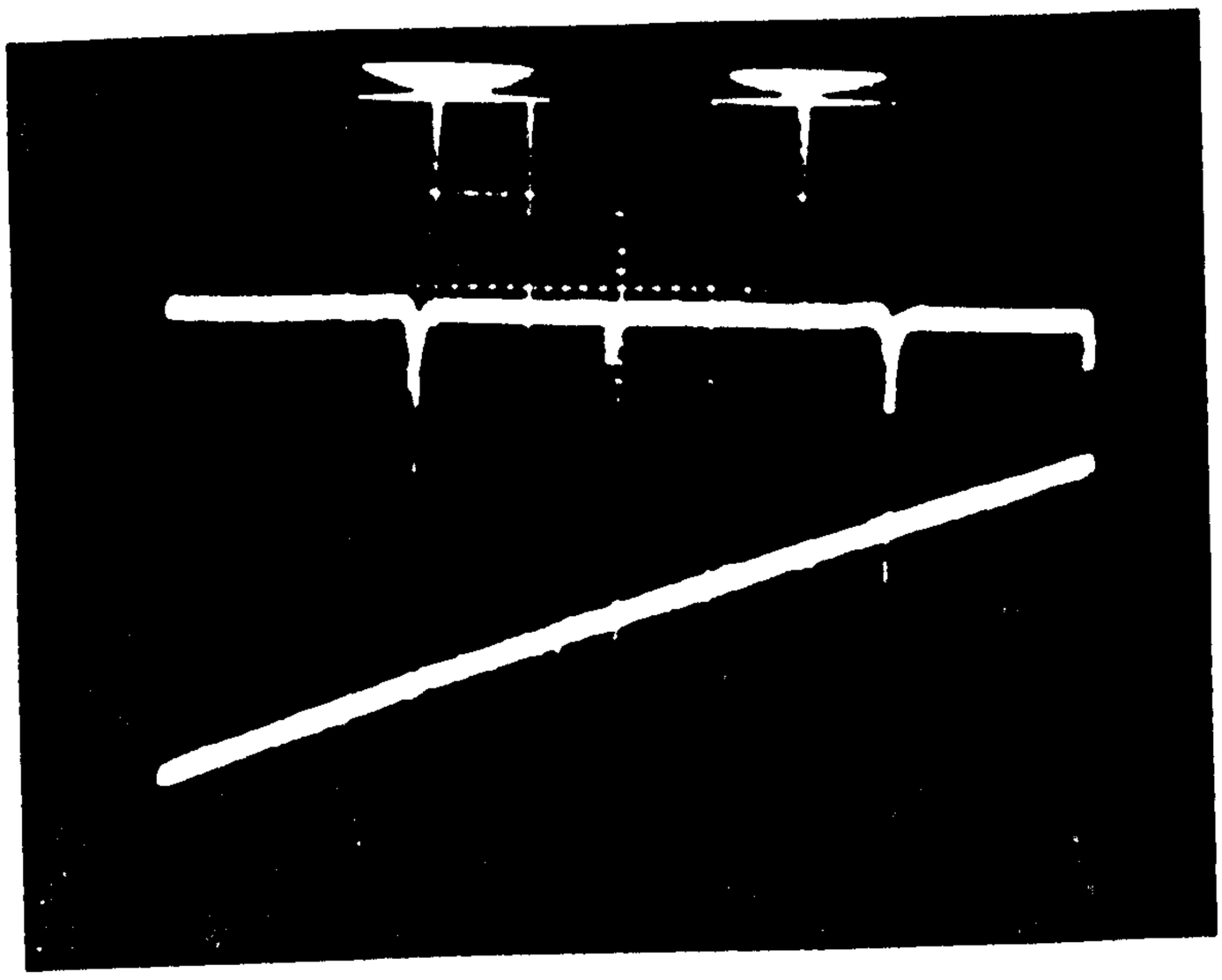

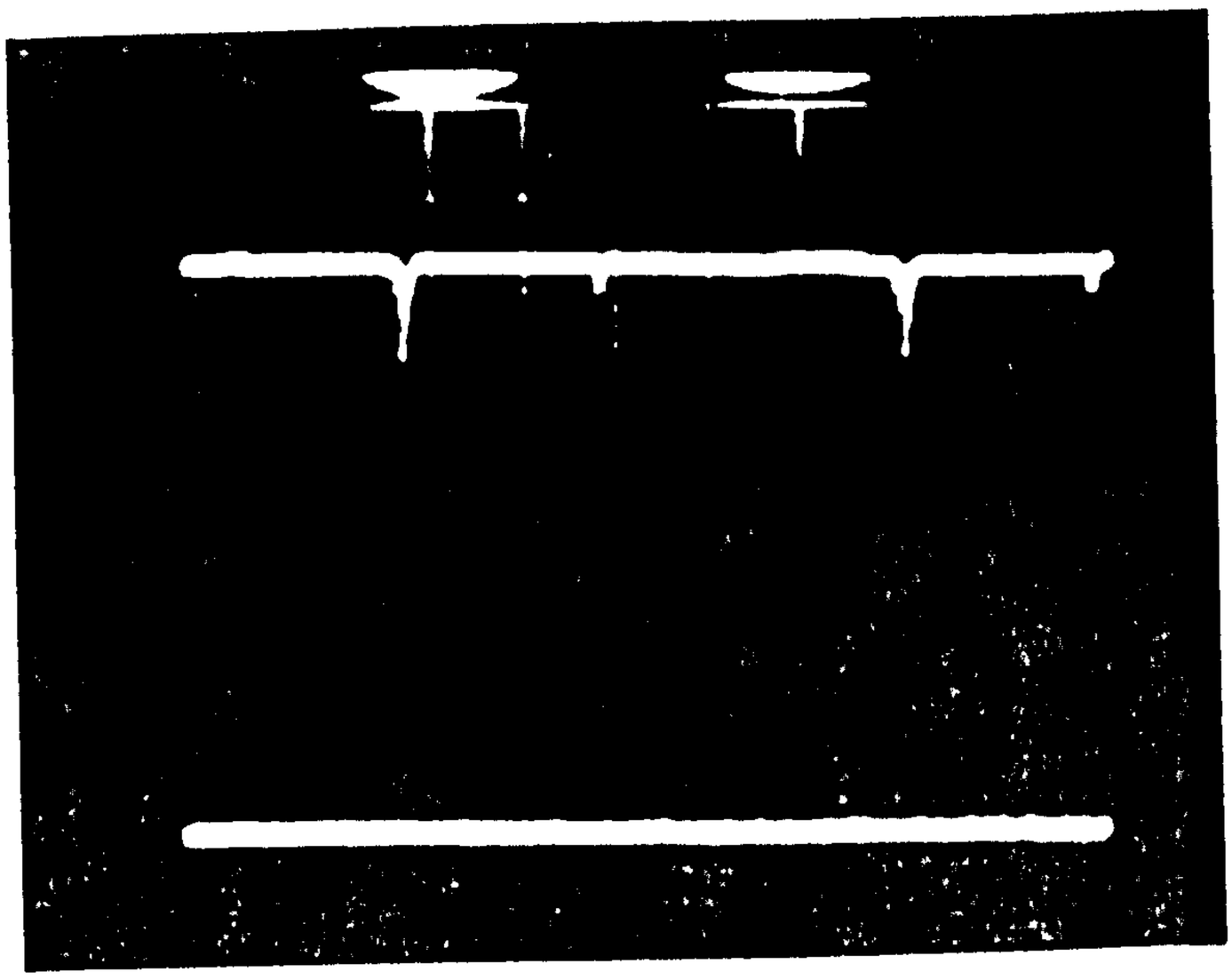

Figure 4.6

Above, the output spectrum of a CCR resonator. A finesse of 200 is measured and the saw-tooth waveform over two orders is clearly shown. Below, the output spectrum of a CCR resonator in order to illustrate 100% contrast. The base line is shown.

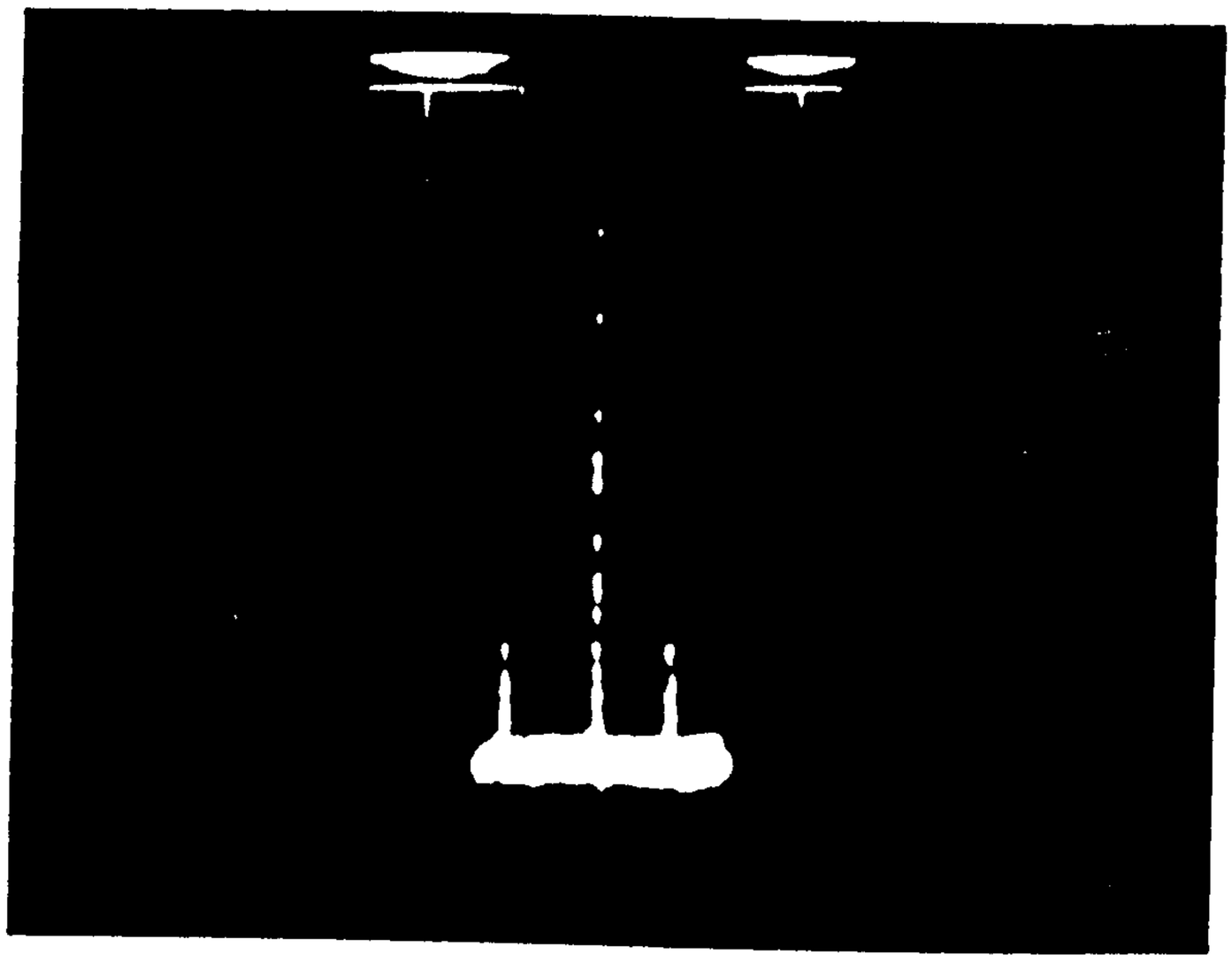

Figure 4.7

The BSBS spectrum at λ_L = 633nm generated in a 2.4m loop ring resonator and detected by a confocal Fabry Perot (FSR = 2GHz±30MHz). The BSBS signal is the intense line and the smaller peaks are the unshifted Rayleigh lines.

better to allow the phase of the resonator to be modulated thermally. It then drifts through the resonance more slowly and allows the BSBS to be generated over a longer time interval. The BSBS signal in figure 4.7 is the more intense line whilst the smaller peaks indicate the back reflected pump/Rayleigh light. It is also seen that the SBS signal is very narrow. This narrowing of the BSBS laser line is typical of stimulated emission in any resonant cavity and is a feature common to all lasers. The extent by which the SBS line is narrowed is a function of the number of circulations of the pump line within the cavity which in turn depends on the finesse. Similarly for any laser the bandwidth of the stimulated emission is a function of the reflectivity of the mirrors. If the mirrors of the lasing cavity were removed whilst a broad band source continued to be incident to the 'exciting medium' then the light emitted would be accordingly broad. However, with the mirrors replaced and multiple passes made by the pump, then the lasing line is found to narrow as the peak gain is enhanced during each pass. Similarly, for a ring resonator, for each circulation the spontaneous gain is enhanced with the result that the maximum gain draws in all the pump power and the SBS line is progressively narrowed. Hence, because the Stokes wave is generated inside the ring, it will have the spectral characteristics of the cavity. Thus one can expect the output of an SBS laser to exhibit linewidth narrowing if the intrinsic linewidth is smaller than the pump and intrinsic bandwidth of the Brillouin gain. An estimation of the Brillouin linewidth generated within a ring resonator cavity is made in chapter 6 and an upper bound optical limit set. More reliably the stimulated Brillouin laser will have a spectral width ~2KHz and an intrinsic linewidth of less than 30Hz[24]. This broadening is determined primarily by the residual acoustic and thermal fluctuations of the fibre cavity. Clearly the free running linewidth can be reduced by precisely controlling the laser environment.

4.5.2 Threshold comparison between experiment and theory

In the previous section the all fibre resonator was scanned by applying a low frequency (50Hz) sawtooth waveform to a piezo-electric cylinder. This alternately stretched and contracted the fibre length such that the phase of the laser was monitored

over an optical cycle. When the resonant phase matching condition was satisfied the circulating power density within the ring was maximised and the output was zero. For the fibre ring resonator to be a viable device for generating BSBS, a lock-in system has to be designed in order that the high circulating power stored is kept to its maximum value; then any random temperature drifts and its influence on the resonant phase matching condition can be compensated for. Quite simply, the lock-in used in these experiments compared the phase difference between the input and output signals of the resonator which, if the resonant condition is to be maintained, should be equal to an integer, m, of 2π, i.e. $2\pi m$. A summer at the output measured the phase difference, ϕ_t, between the output and the input giving an error signal to the controller. The controller then produces a signal, V_c, to the PZT causing it to produce a phase, ϕ_p, by stretching the fibre which will then cancel, ϕ_t, thus leaving the output unaffected by the disturbance and equal to the input.

With the lock-in system incorporated into figure 4.5, i.e. the system locked for maximum circulating power in the ring such that the resonator is no longer scanned, the backward propagating Brillouin wave can be easily measured for varying launched powers. This is shown in figure 4.8 for a ring resonator of loop length 2.4m and a finesse of 180. The threshold power at λ_L = 633nm is seen to be 165μW and exhibits a maximum conversion efficiency of 25% for a launched power of 350μW .This is in good agreement with the theoretically predicted threshold power of 125μW given by eqn.(4.3.3). The discrepancy between the two values can be attributed to i) the polarisation between the counter propagating Stokes and pump waves being scrambled along the interaction length[25]. This can increase the observed threshold value by a factor of between 1 and 2 above the theoretically predicted value; and ii) that it has to be appreciated that the value of the gain incorporated into eqn.(4.3.3) is the peak gain. The chances that the fibre ring cavity will resonate at this peak gain are small, as it is more than likely that the resonant mode will be displaced from this central frequency. The effect of a smaller gain coefficient in eqn.(4.3 3) will be to increase the theoretically predicted threshold power. For example, if the fibre ring cavity were to resonate at the

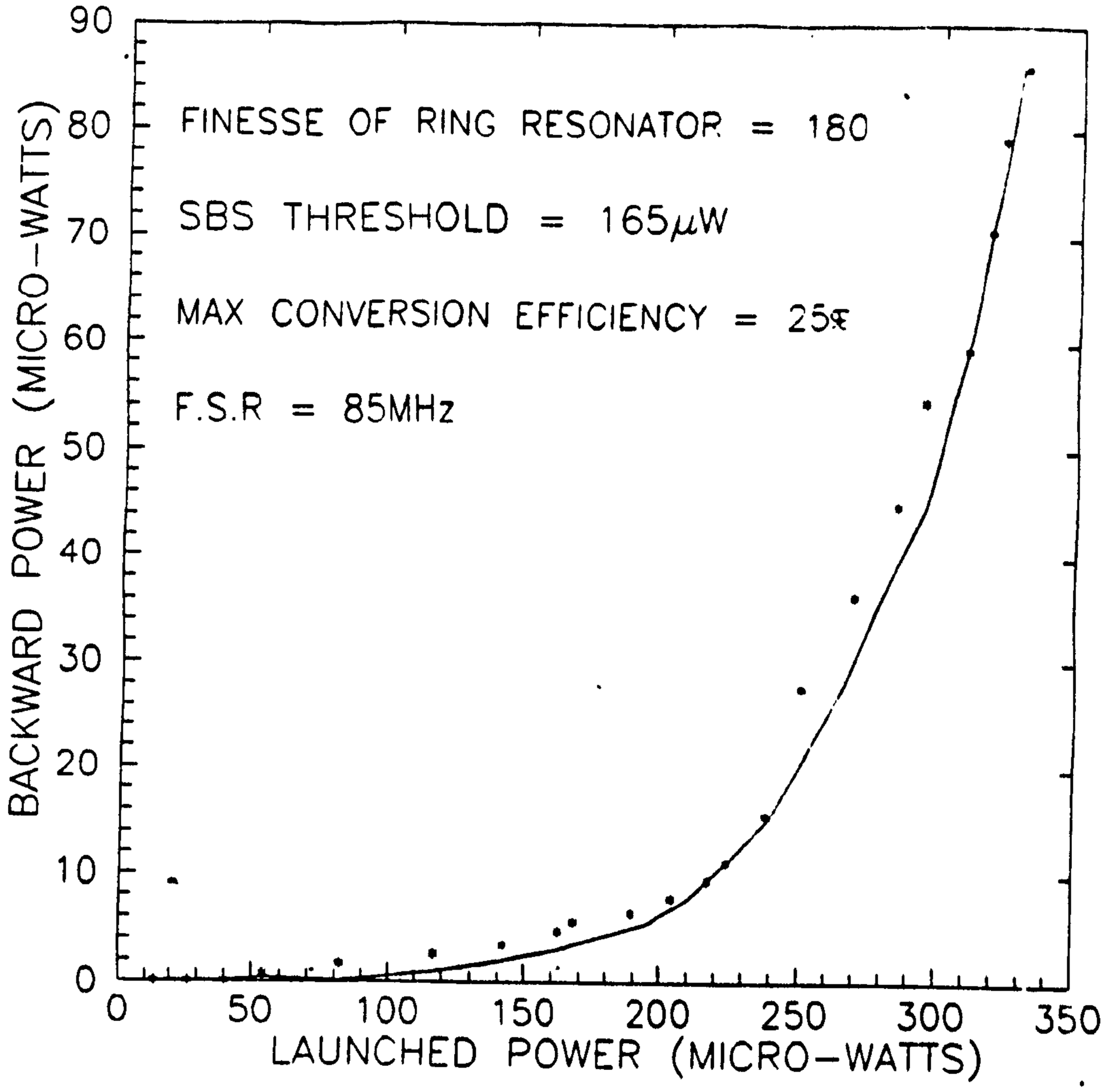

Figure 4.8

Level of BSBS power at λ_L = 633nm detected as a function of increased launched power. The fibre ring resonator has a finesse of 180, a loop length of L = 2.4m and a threshold power of 165±10μW. The threshold power was determined by simultaneously measuring the launched power when the Brillouin signal was first observed at the confocal Fabry Perot, as shown in figure 4.7.

half width half maximum intensity, where $\tilde{g}_{BO} = 1.68\text{x}10^{-11}$m/W, then the theoretical threshold power for BSBS would be $P_{th} = 251\mu$W, which would be greater than that observed experimentally. Nonetheless, eqn.(4.3.3) serves as a useful indication when predicting the threshold powers required for the onset of BSBS in fibre ring lasers.

The significance of the gain, $\tilde{g}_{BO}$ (m/W), is also relevant as regards the fibre loop length. From eqn.(4.3.3) and for a given finesse, one would immediately infer that a longer loop length, L, would be more favourable for the generation of BSBS. Although for a fixed gain this would be true, one also has to remember that by increasing the fibre loop length, the FSR of the device is also changed and hence where the cavity resonance overlaps the Brillouin gain curve. This effect and the influence of the gain profile will prove to be more significant than increased fibre lengths for a fixed finesse; i.e. by marginally increasing the fibre loop length, one may well discover that the threshold power is increased, as has been experimentally observed.

Above threshold, the generation of BSBS constitutes a cavity loss because of pump depletion. If the coupling ratio is kept constant at a value optimised at powers below the BSBS lasing threshold, then, as the input power is increased above this threshold, the measured finesse of the device and the depth of the transfer function decrease. The decrease in the resonant notch depth is directly proportional to the amount of BSBS generated within the ring. This observation simply corresponds to when the coupling constant no longer matches the new increased losses, and the device is thus progressively overcoupled. This effect of increased levels of BSBS for increased launched powers is shown in figure 4.9 where the measured changes of observed finesse and modulation depth are recorded. The fibre parameters are the same as those given in figure 4.8. This can also be interpreted by the change in measured finesse and modulation depth, as above threshold (165μW) their change with increased launched powers become most significant and confirm the results obtained by Kadiwar[26] for a polarisation maintaining ring resonator. They also confirm those results theoretically predicted in figure 4.4 where the effects resulting from a mismatch between k and k_r are analysed.

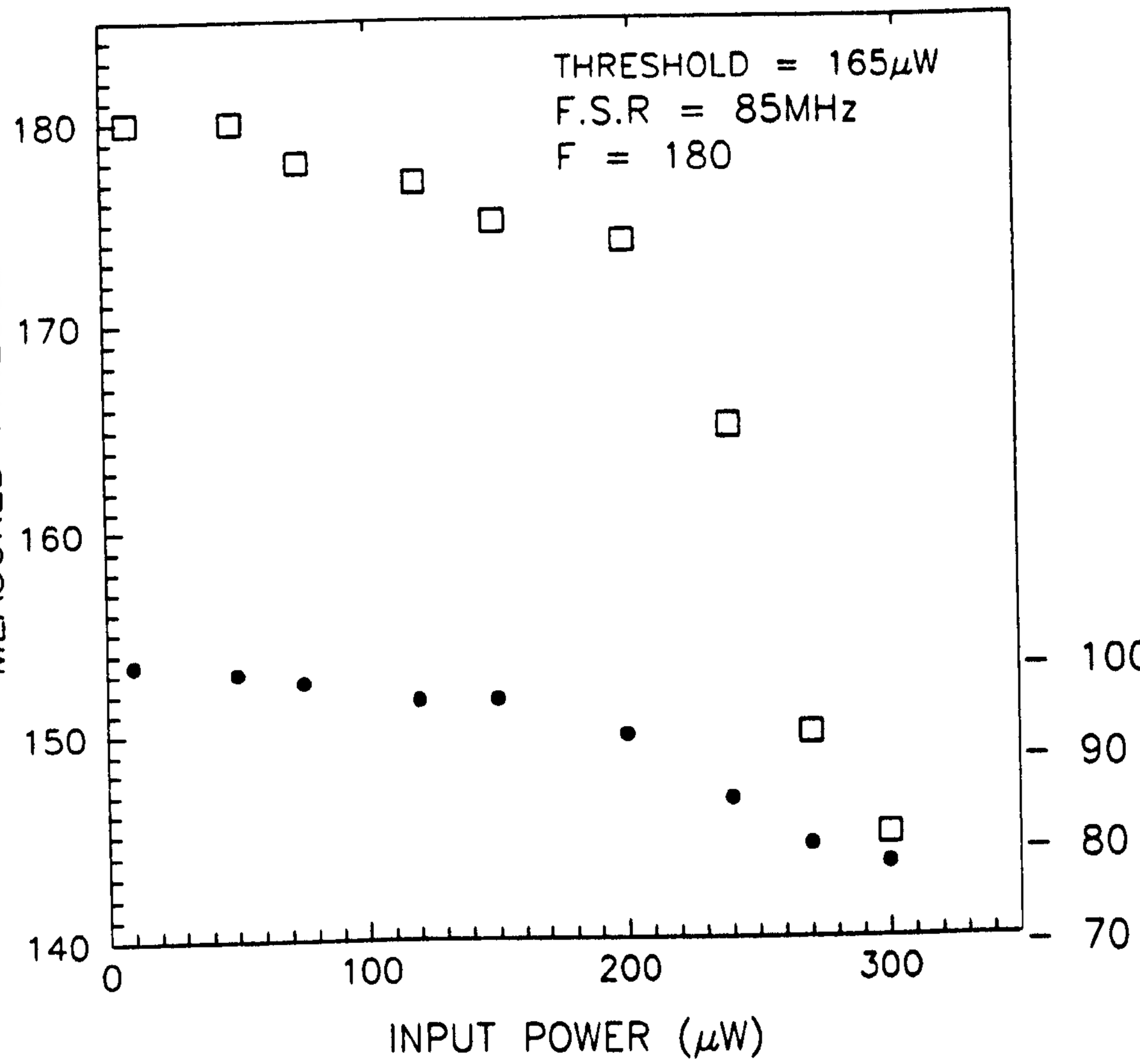

Figure 4.9

Observed variations in the measured finesse (squares) and the modulation depth (filled circles) with input power for a fixed coupling constant (optimised at low powers) for a 2.4m ring resonator at $\lambda_L = 633$nm.

4.6 Conclusions

The generation of BSBS in fibre ring resonators has been examined in detail. Most significant is the reduction of the threshold powers necessary for the onset of BSBS from mW's to μW's on account of the intense circulating powers within the cavity. This application of fibre ring resonators and also their use as high resolution optical interferometers is pursued in chapter 6. In the next chapter an entirely new phenomenon, namely intermodal forward Brillouin scattering (FSBS) is discussed and whilst FSBS has much in common with BSBS, there are also significant differences.

References: Chapter 4

1. Lefevre, H.C.: "Single - mode fibre fractional wave devices and polarisation controllers", Electron. Lett., vol.16, p.778, 1980.
2. Dakin. J., Culshaw, B.: "Optical Fibre Sensors: Principles and Components", Artech House, 1988.
3. Bergh, R.A., Kotler, G., and Shaw, H.J.: "Single mode fibre optic directional coupler", Electron. Lett., vol.16, p 260, 1980.
4. Digonnet, M.J.,and Shaw, H.J.: "Analysis of a tunable single mode optical fibre coupler", IEEE J.Quantum.Electron, vol.QE-18, no.4, 1982.
5. Stokes, L.F., Chodrow, M., Shaw, H.J.: "All single mode fibre resonator", Opt. Lett., vol.7, no.6, pp.288-290, 1982.
6. Petuchowski, S.K., Giallorenzi, T.G., and Sheem, S.K.: "A sensitive fibre optic Fabry Perot interferometer", IEEE.J.Quantum.Electron., vol.QE-17, pp.2168-2170, 1981.
7. Shupe, D.M.: "Fibre resonator gyroscope: sensitivity and thermal non reciprocity", Appl.Opt., Vol.20, pp.286-289, 1981.
8. Reston, K.R.: "Simple spectral control technique for external cavity laser transmitters", Electron.Lett., vol.18, pp.1092-1094, 1982.
9. Mallinson, S.R.: "Fibre optic coupled Fabry Perot wavelength de-multiplier", Electron.Lett., vol.21, pp.121-122, 1985.
10. Sorin, W.V., and Yu, M.H.: "Single mode fibre ring dye laser", Opt.Lett., vol.10, pp.550-522, 1985.
11. Stokes, L.F., Chodorow, M., and Shaw, H.J.: "All fibre stimulated Brillouin ring laser with sub-milliwatt pump threshold", Opt.Lett., vol.7, pp.509-511, 1982.
12. Meyer, R.F., Ezekiel,S, Stowe, D.W.,and Tekippe, V.J.: "Passive fibre optic ring resonator for rotation sensing", ibid., vol.8, pp.644-646, 1983.

13. Bergh, R.A., Lefevre, H.C., and Shaw, H.J.: "An overview of fibre optic gyroscopes", IEEE.J.Lightwave Technol., vol.LT-2, pp.91-107, 1986.

14. Tai, S., Kyuma, K., and Nakayama, T.: "Spectral linewidth of external - cavity laser diode stabilised by a fibre optic ring resonator", Appl.Phys.Lett., vol.47, pp.439-440, 1985.

15. Atkins, C.G., Cotter, D., Smith, D.W., and Wyatt, R.:Application of Brillouin amplification in coherent optical transmission", Electron.Lett., vol.22,p.556, (1986).

16. Olsson, N.A., and Van Der Ziel, J.P.:"Characteristics of a semi-conductor laser pumped Brillouin amplifier with electronically controlled bandwidth", J.lightwave Technol, Vol. L.T-5, p.147, (1987).

17. Hill, K.O., Kawasaki, B.S., and Johnson, D.C.: "CW Brillouin laser", Appl. Phys.Lett., vol.28, pp.608-699, 1976.

18. Kawasaki, B.S., Johnson, D.C., Fujii, Y., and Hill, K.O.: "Band width - limited operations of a mode locked Brillouin parametric oscillator", ibid., vol.32, pp.429-431, 1978.

19. Bar - Joseph, I., Dienes, A., Friesem, A.A., Lichtman, E., Warrts, R.G., and Yaffe, H.H.: "Spontaneous mode locking of single and multi-mode pumped SBS fibre lasers", Opt. Commun., vol.59, pp.296 - 298, 1986.

20. Bayvel, P., Halley, J., Kadiwar, R., and Giles, I.P.: "Theoretical and experimental investigation of all fibre Brillouin laser", ECOC.Conf.Proc.Pt.1, IEE.Conf.Publ.292, pp.292 - 294, 1988.

21. Zarinetchi, F., Smith, S.P., and Ezikiel, S.: "SBS fibre optic laser gyroscope", Opt.Lett., vol.16, no.4, p.229, 1991.

22. Levi, L,: "Applied Optics", Wiley, 1968.

23. Smith, R.G.: "Optical power handling capacity of low loss optical fibres as determined by stimulated Raman and Brillouin scattering", Appl. Opt.,vol.11, no.11, pp.2489-2494, 1972.

24. Smith, S.P., Zarinetchi, F., and Ezekiel, S.: "Narrow linewidth stimulated

Brillouin fibre laser and applications", Opt. Lett., vol.16, no.6, p 393, 1991.

25. Stolen, R.H.: "Polarisation effects in fibre Raman and Brillouin lasers", IEEE. J.Quant.Electron., vol.QE - 15, no.10, pp.1157-1160, 1979.

26. Kadiwar, R., and Giles, I.P.: "Effects of stimulated Brillouin scattering on the performance of polarisation maintaining all fibre ring resonators", Opt.Lett., vol.14, no.6, 1989.

Chapter 5

Forward stimulated Brillouin scattering

5.1 Introduction

In this chapter a detailed analysis is presented of a new non-linear effect observed recently for the first time[1] - Intermodal stimulated Brillouin scattering in a forward direction (FSBS) in dual moded (DM) fibres. FSBS differs from the guided acoustic wave Brillouin scattering reported by Shelby et al[2] and which is discussed in chapters 2 and 3 in being based on genuine collinear phase matching between three distinct guided waves and in displaying a stimulated threshold. The recent growth of interest in DM optical fibres for a variety of non-linear switching and modulation schemes[3-8] owes its origin to the long interaction lengths that are possible in fibre waveguides and to the interesting new experimental possibilities offered by a structure that supports two non degenerate co-propagating modes at the same optical frequency. These factors give DM fibre waveguides unique advantages over bulk optics for the study of new non-linear optical phenomena. Some recent examples include all optical switching in twin core[3], Hi-Bi[4] and periodically rephased mismatched dual core fibres[5,6]. DM fibres have also been used to form acousto-optical frequency shifters[7,9] by exciting flexural waves on them and switching the acoustic wavelength to the intermodal beat length. Detailed analysis[8,10] of these devices are of direct relevance to the present study of FSBS; intermodal beating (between Brillouin and pump light) excites (via electrostriction) a flexural wave that in turn couples power between the modes.

This chapter is organised as follows: in section 5.2 general comparisons with BSBS are made and the underlying physical intuitive basis and the momentum and energy conservation requirements considered. The derivation of the coupled wave equations are the subject of section 5.3.Intermodal beating between the LP_{01} and LP_{11}

modes at different frequencies is treated in subsection 5.3.1 and the wave equation for the low frequency flexural waves obtained in subsection 5.3.2. Intermodal coupling via flexural microbending is analysed in subsection 5.3.3 and the full set of differential equations describing the parametric interaction, normalised to power, obtained in subsection 5.3.4. In subsection 5.3.5 approximate analytical expressions for the Brillouin gain are found having made the standard approximation of a short phonon lifetime. In section 5.4 the threshold power for the onset of FSBS is derived. Computer modelled solutions for the full set of the three cw equations are given in section 5.5, which also considers the approximate solutions for short phonon lifetimes and their comparison with the exact solutions for longer phonon lifetimes. The experimental observation of FSBS is made in section 5.6, and in section 5.7 conclusions analysing the unique features of FSBS are summarised.

5.2 General comparisons with BSBS

Two basic conservation laws must be obeyed for Brillouin scattering to occur (see chapter 2.3). The first is conservation of energy:

$$\hbar \omega_L = \hbar \omega_B + \hbar \Omega_F \tag{5.2.1}$$

and the second conservation of momentum:

$$k_L = k_B + K_F \tag{5.2.2}$$

where ω_L, ω_B and Ω_F are the radian frequencies and k_L, k_B and K_F the wavevectors of the pump/laser, Brillouin and acoustic waves. In addition to these conservation laws, there must exist two non-degenerate normal modes at the pump optical frequency. In a single mode optical fibre, only two modes satisfying this condition are available - the backward and forward propagating ones; hence the Brillouin signal appears in the backward direction. In a DM fibre, by contrast, the LP_{01} and LP_{11} modes satisfy this condition making permissible the generation of an intermodal SBS signal in the

forward direction.

The physical basis underlying FSBS is a circular loop of cause and effect. Spontaneous acoustic phonons (flexural waves in this case) generate, through the strain optical effect, weak travelling refractive index gratings in the fibre core. Those phonons whose wavelength $\Lambda_F = v_F/f_F$ (where v_F is their phase velocity and f_F their frequency) equals the intermodal beat period L_b will weakly Bragg scatter the light between the fibre modes, causing Stokes and anti-Stokes frequency conversion from the pump into the Brillouin signals. The pattern of moving interference fringes generated by intermodal frequency mixing of the Stokes and pump modes has points of constructive interference that alternate to and fro across the fibre core, see figure 5.1. This creates via electrostriction a moving periodically reversing moment wave whose wavelength matches that of the original spontaneous phonon. If, in addition, the spatial registration of the moment wave relative to the acoustic wavefront is correct, the spontaneous acoustic wave will experience gain. This in turn increases the scattering strength into the Brillouin wave, thus closing the loop of cause and effect. If the electrostrictive gain over the phonon coherence length is greater than the acoustic loss, then FSBS can occur; both the acoustic and Brillouin waves will then experience exponential gain.

In FSBS the direction of the phonon wave depends on whether the frequency down conversion is LP_{01} - LP_{11} or vice versa, figure 5.2. Unlike backward BSBS, where the threshold power depends strongly on the laser linewidth, chapter 2.4, in FSBS this condition is considerably relaxed, permitting a multi-frequency laser pump to be used. This is because the pump and Brillouin waves propagate along exactly the same optical path and hence can maintain mutual coherence over very long lengths of fibre.

5.3 Derivation of coupled mode equations

5.3.1 Intermodal beating

The superposition of the pump and Brillouin signals (each in a different linearly

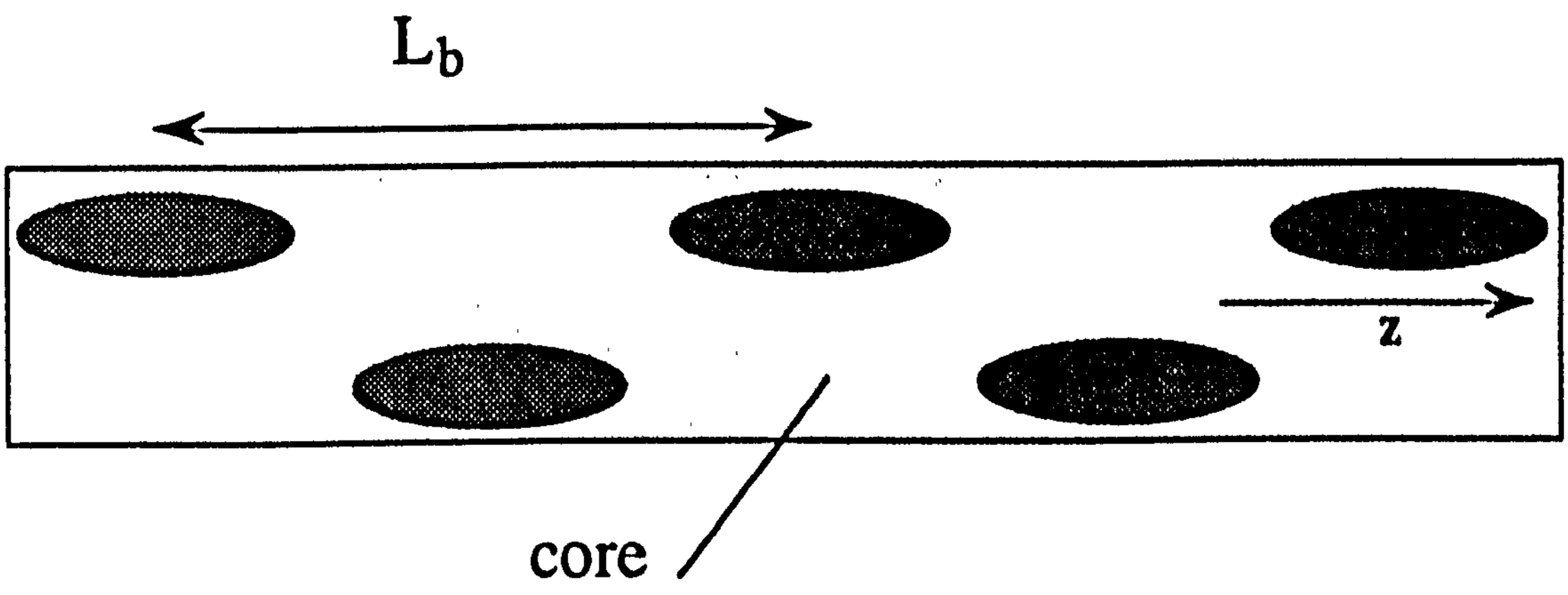

Figure 5.1

Schematic of intermodal beating. Constructive interference between the LP_{01} and LP_{11} modes occurs on alternate sides of the core at a spatial beat period L_b. During FSBS this pattern moves, its wavelength and phase velocity matching those of a flexural acoustic mode of the fibre.

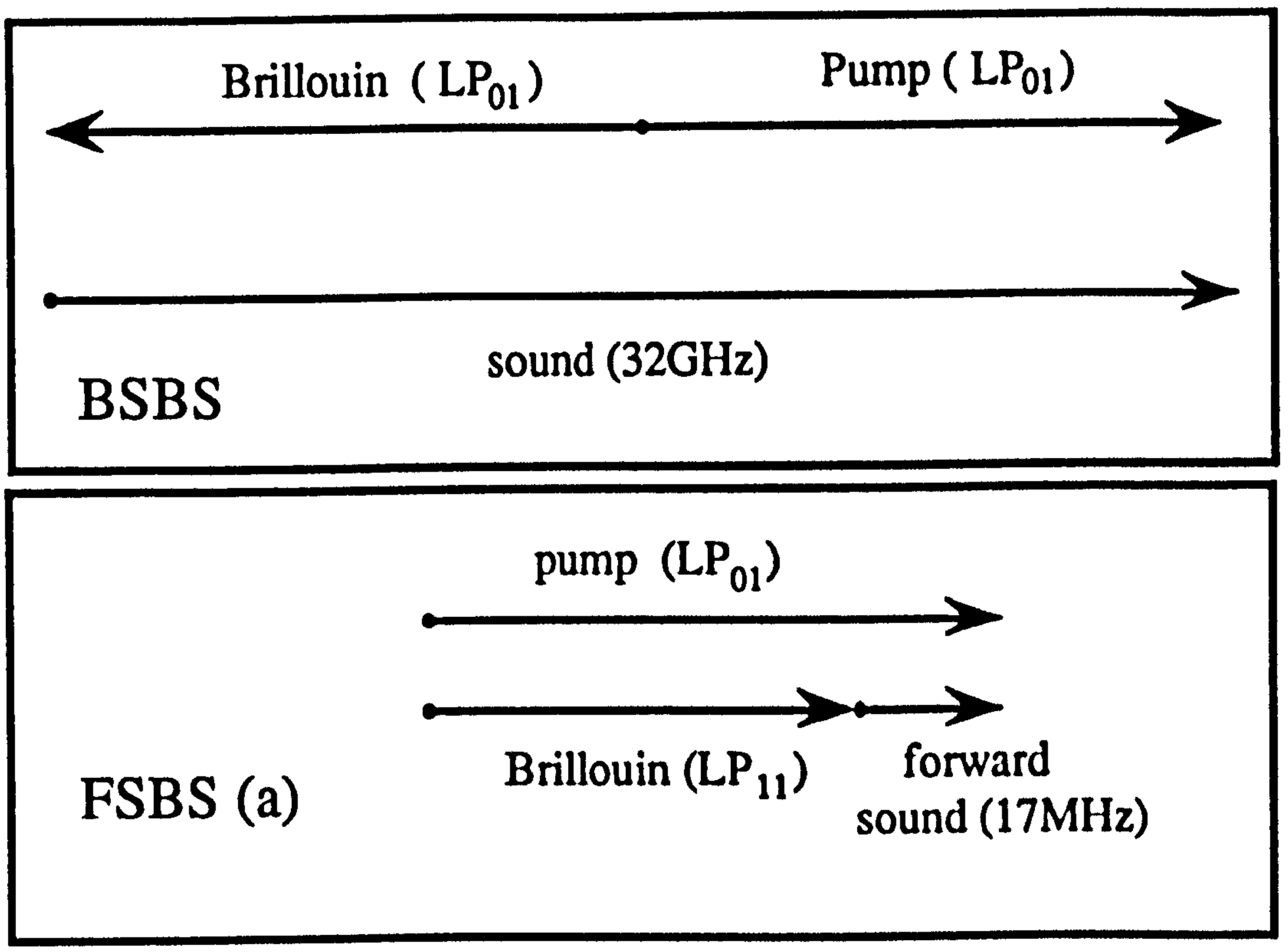

Figure 5.2

Wave vector conservation in normal backscattered SBS, LP_{01} - LP_{11} FSBS and LP_{11} - LP_{01} FSBS. The arrows represent (schematically) the wave vectors, pointing parallel to the phase velocities of each wave. Note that in FSBS (b) the acoustic phase velocity is negative.

polarised fibre mode) yields a total electric field given by:

$$E_{tot} = \frac{1}{2}\left[e_B(r,\phi)A_B(z)\exp\{-j(k_Bz - \omega_Bt)\}\right.$$
$$\left. + e_L(r,\phi)A_L(z)\exp\{-j(k_Lz - \omega_Lt)\} + \text{c.c}\right] \qquad (5.3.1)$$

where A_B and A_L are the electric field amplitudes and $e_B(r,\phi)$ and $e_L(r,\phi)$ the dimensionless transverse mode profiles which essentially describe the modal shape and are equal to $e_{01}(r)$ or $e_{11}(r,\phi)$ depending on the circumstances (see figure 5.3 for the co-ordinate system). The factor 1/2 is required so that A_B and A_L are real amplitudes. In contrast to BSBS it is noted that both the laser/pump and Brillouin signals are co-propagating. It is clear that the compound field will contain intermodulation components at frequency $\Omega_F = \omega_L - \omega_B$ with associated wave vector $K_F = k_L - k_B$. If K_F equals the wave vector at frequency Ω_F of a fibre flexural mode, these components will phase match to it. Acoustic gain is then possible via electrostriction and FSBS may occur. In order to treat the effect of electrostriction it is necessary to find the average energy per unit volume ($W = \varepsilon E_{tot}^2/2$)[11] and convert it into a change in pressure[12] where W is the energy stored per unit volume, ε the dielectric permitivitty and E_{tot} the total electric field. Neglecting those components that average to zero over one cycle and selecting those components of W that travel forward (for LP_{01} - LP_{11} conversion) at velocity Ω_F/K_F one obtains, in a similar manner to that described for BSBS:

$$W = \frac{1}{4}\varepsilon e_{01}(r)e_{11}(r,\phi)A_LA_B^{*}\exp\{-j(K_Fz - \Omega_Ft)\} + \text{c.c} \qquad (5.3.2)$$

For a uniaxial strain s along the fibre axis, electrostriction is governed by the parameter:

$$\frac{\partial\varepsilon_r}{\partial s} = 2n^2(1 - \chi) \qquad (5.3.3)$$

where $\varepsilon_r = \varepsilon/\varepsilon_0$ and $\chi = 0.22$[13] for fused silica yielding $\partial\varepsilon_r/\partial s = 3.3$. This leads to an

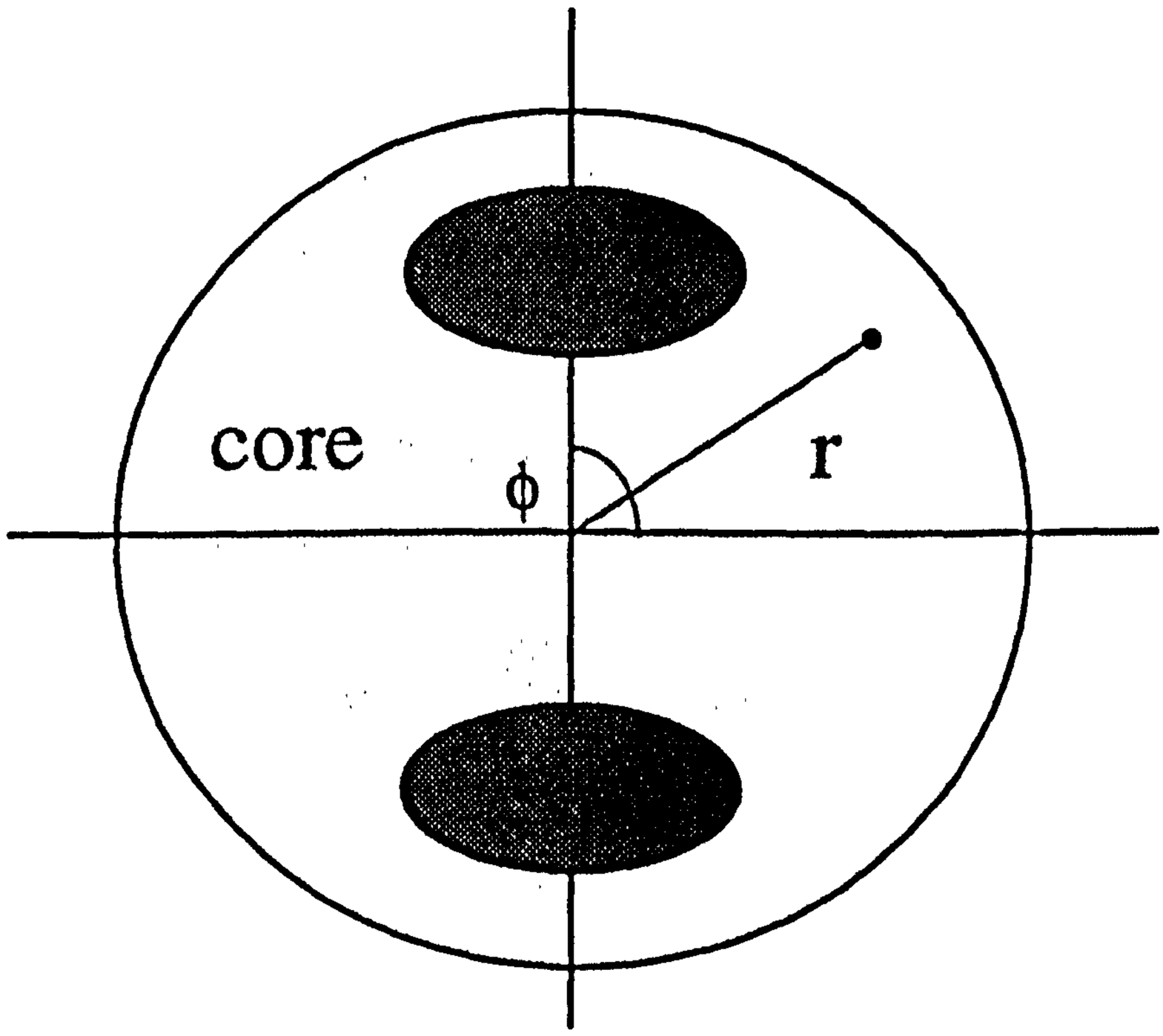

Figure 5.3

Co-ordinate system for the evaluation of the overlap integral $Q \approx r_{eq}/2a$. The elliptical shaded regions represent the intermodal beat pattern.

axial component of electrostrictive stress Δp in the form:

$$\Delta p\,(r,\phi,z,t) = \varepsilon_0 \frac{\partial \varepsilon_r 1}{\partial s 4}\{e_{11}(r,\phi)e_{01}(r)A_B{}^*(z)A_L(z)\exp\{-j(K_F z - \Omega_F t)\} + \text{c.c}\} \quad (5.3.4)$$

The stress wave in eqn.(5.3.4) is periodic, with a wavelength equal to the beat length between the LP_{01} and LP_{11} modes. When the background dc electrostrictive stress field is superimposed, regions of high stress alternate with z between the upper and lower hemispheres of the core (as already depicted in figure 5.1). The induced electrostrictive driving moment may be calculated as follows:

$$M_d(z,t) = \iint \Delta p(r,\phi) r^2 \cos(\phi) d\phi dr \quad (5.3.5)$$

where the integral is over the fibre cross section - see figure 5.3. This finally yields:

$$M_d(z,t) = \varepsilon_0 \frac{\partial \varepsilon_r}{\partial s}\frac{a}{4}\left[Q A_{eq} A_B{}^*(z)A_L(z)\exp\{-j(K_F z - \Omega_F t)\} + \text{c.c}\right] \quad (5.3.6)$$

where a is the fibre radius and the overlap integral, Q, is given by:

$$Q = \frac{1}{a A_{eq}} \int_{r=0}^{a} \int_{\phi=0}^{2\pi} e_{11}(r,\phi)e_{01}(r) r^2 \cos\phi dr d\phi \quad (5.3.7)$$

and e_{01} and e_{11} are defined such that the equivalent modal area (spot size) is given by:

$$A_{eq} = \iint e_{11}{}^2(r,\phi) r dr d\phi = \iint e_{01}{}^2(r) r dr d\phi \quad (5.3.8)$$

The overlap integral may be shown to be given approximately by $Q = r_{eq}/2a$ where $\sqrt{(A_{eq}/\pi)}$ is the mode spot radius.

5.3.2 Low frequency flexural wave equation with drive term

Low frequency flexural waves obey the equation[14]:

$$\rho A \frac{\partial^2 y}{\partial t^2} + EI \frac{\partial^4 y}{\partial z^4} = 0 \qquad (5.3.9)$$

where y is the transverse deflection, z the axial coordinate, E the Youngs modulus, ρ the mass density and $I = \pi a^4/4$ the second moment of inertia for a fibre of cross sectional area A. For small deflections $|y/a|^2 << 1$ the local moment may be expressed as:

$$M(z,t) = EI \frac{d^2 y}{dz^2} \qquad (5.3.10)$$

The condition for validity of eqn.(5.3.10) is[10]

$$af_F/v_t < 0.1 \qquad (5.3.11)$$

where $f_F \sim 17$MHz and $v_t = 3764 \text{ms}^{-1}$ the shear velocity in silica. In the reported experiment[1] this parameter has the value of 0.28, which places the waves in the transition regime between low and high frequency waves[10] and has implications on the overlap of acoustic and optical power; at higher frequencies the acoustic energy shifts from a bulk flexural disturbance to an acoustic surface wave, thus reducing the influence on the guided modes. Under these conditions the actual overlap integral will therefore be somewhat smaller than Q. A useful additional quantitative correction may be made by distinguishing carefully the group from the phase velocity and replacing them with accurate values from the more complete theory[10].

The phase velocity of the flexural waves described by eqn.(5.3.9) is:

$$v_F^2 = \frac{EIK^2}{\rho A} = \left[\frac{\pi a v_e}{\Lambda_F}\right]^2 \qquad (5.3.12)$$

where $v_e = \sqrt{(E/\rho)}$[10] is the extensional wave phase velocity. The general relationship for the group velocity of dispersive waves is [10]

$$v_{gF} = \left[v_F/(1 - \frac{\Omega_F \partial v_F}{v_F \partial \Omega_F}\right] \tag{5.3.13}$$

and may be used to show that for low frequency waves $v_{gF} = 2v_F$. Using $\partial^2/\partial t^2$ in eqn.(5.3.9) and substituting eqn.(5.3.10) yields:

$$M(z,t) - \frac{1}{K^4}\frac{d^4M}{dz^4} = M_d(z,t) \tag{5.3.14}$$

where the driving term $M_d(z,t)$ has been incorporated (eqn.(5.3.6)). Expressing the moment wave as:

$$M(z,t) = \frac{1}{2} A_F(z) \exp(-j(K_F z - \Omega_F t)) + \text{c.c} \tag{5.3.15}$$

where $A_F(z)$ is its slowly varying amplitude, substituting $M(z,t)$ into eqn.(5.3.14), neglecting all but first order spatial derivatives of A_F and collecting coefficients of $\exp(-j(K_F z - \Omega_F t))$ yields:

$$\pm\frac{\partial A_F}{\partial z} + \frac{\alpha_F}{2} = -\frac{j\Omega_F a}{4 v_{gF}}\left[\varepsilon_o Q A_{eq}\frac{\partial \varepsilon_r}{\partial s}\right] A_B^* A_L \tag{5.3.16}$$

where the expression in eqn.(5.3.6) has been substituted for M_d and a phenomenological absorption α_F (m^{-1}) incorporated. This absorption is related to the phonon lifetime τ_F and bandwidth Δf_F by $\alpha_F = \Delta f_F / v_F$. The upper sign is chosen if the acoustic wave copropagates with the optical waves, i.e., if the pump light is launched into the LP_{01} mode.

5.3.3 Intermodal coupling by flexural microbending

It is straightforward to show that the mechanical strain s due to the presence of a low amplitude flexural wave is:

$$s = r\cos\phi\frac{d^2y}{dz^2} = \frac{r\cos\phi}{EI}M(z,t) \qquad (5.3.17)$$

Using eqn.(5.3.3) one can translate, s, into a change in ε_r:

$$\Delta\varepsilon_r(r,\phi,z) = \frac{\partial\varepsilon_r}{\partial s}\frac{r\cos\phi}{2EI}A_F(z)\exp\{-j(K_Fz - \Omega_Ft)\} + \text{c.c} \qquad (5.3.18)$$

Incorporating $\Delta\varepsilon_r$ in Maxwell's equations for the fibre modes, and carrying out a standard coupled-wave analysis yields with some rearrangement:

$$\frac{\partial A_B}{\partial z} + \frac{\alpha}{2}A_B = \frac{-j\omega_B a}{4v_{gB}}\left\{\frac{Q}{EIn_B{}^2}\left(\frac{\partial\varepsilon_r}{\partial s}\right)\right\}A_F{}^*A_L \quad \text{(a)} \qquad (5.3.19)$$

and

$$\frac{\partial A_L}{\partial z} + \frac{\alpha}{2}A_L = \frac{-j\omega_L a}{4v_{gL}}\left\{\frac{Q}{EIn_L{}^2}\left(\frac{\partial\varepsilon_r}{\partial s}\right)\right\}A_FA_B \quad \text{(b)} \qquad (5.3.20)$$

where once again a phenomenological optical absorption $\alpha(\text{m}^{-1})$ has been added. The optical group velocities v_{gB} and v_{gL} arise from a more accurate treatment of the guided modes; they are distinguished from the phase velocities c/n_L and c/n_B (which they closely equal) for clarity. The FSBS process is now described by eqn.(5.3.16), (5.3.19) and (5.3.20). For full benefit it is necessary to normalise the amplitudes A_B, A_L, and A_F to the total power involved in the parametric process.

5.3.4 Power normalised coupled-wave equations

The power density in any guided wave is given by the average energy stored per unit volume (J) multiplied by the group velocity. This leads for flexural waves to a total power of[15]:

$$P_F = \frac{1}{2EI}|A_F|^2 v_{gF} = \frac{2\pi f_F^2 |A_F|^2 v_{gF}}{a^2 \rho v_F^4} \tag{5.3.21}$$

and in the case of the pump and Brillouin modes, the equivalent expressions are[16]:

$$P_L = \left[\frac{A_{eq} n_L^2 \varepsilon_o |A_L|^2}{2}\right] v_{gL} \tag{5.3.22}$$

$$\text{and } P_B = \left[\frac{A_{eq} n_B^2 \varepsilon_o |A_B|^2}{2}\right] v_{gB} \tag{5.3.23}$$

Defining the normalised amplitudes a_L, a_B, and a_F as

$$a_m = \sqrt{(P_m/P_{tot})} \tag{5.3.24}$$

where $m = L, B$ or F and P_{tot} the total incident power, the three coupled wave equations (5.3.16), (5.3.19) and (5.3.20) may be re-expressed in normalised form as follows:

$$\begin{aligned} &\frac{\partial a_L}{\partial z} + \frac{\alpha}{2} a_L = -j\,\kappa_L a_F a_B && \text{(a)} \\ &\frac{\partial a_B}{\partial z} + \frac{\alpha}{2} a_B = -j\,\kappa_B a_F^* a_L && \text{(b)} \\ &\pm\frac{\partial a_F}{\partial z} + \frac{\alpha_F}{2} a_F = -j\,\kappa_F a_L a_B^* && \text{(c)} \end{aligned} \tag{5.3.25}$$

where the upper sign is taken if the flexural wave co-propagates with the laser and Brillouin waves, and the lower if it counter propagates. If the laser is launched into the LP_{01} mode, the upper sign holds. The coupling constants are defined by:

$$\kappa_L = \omega_L/c_F; \quad \kappa_B = \omega_B/c_F \text{ and } \kappa_F = \Omega_F/c_F \tag{5.3.26}$$

and where the velocity c_F is given by the expression:

$$c_F = \frac{n_L n_B}{Q(\partial\varepsilon_r/\partial s)} \sqrt{\left\{\frac{2\pi v_{gL} v_{gB} v_{gF} E a^2}{P_{tot}}\right\}} \tag{5.3.27}$$

The approximations $v_{gL} \approx c/n_L$ and $v_{gB} \approx c/n_B$ are valid in these expressions. From the energy conservation requirement given in eqn.(5.2.1) it can be shown that:

$$\kappa_L - \kappa_F - \kappa_B = 0 \tag{5.3.28}$$

which may in turn be used to demonstrate the solutions of eqn.(5.3.25) conserve power.

5.3.5 Brillouin gain

Equation (5.3.25) may be re-cast in a mathematically more elegant form if each of the complex amplitudes is expressed in terms of the real valued quantities b_m and ϕ_m :

$$a_m = b_m \exp(j\phi_m) \tag{5.3.29}$$

where m is L, B or F. After some manipulation it is found that

$$b_F b_B b_L \cos\Psi = B_O \exp\{-(\alpha \pm \alpha_F/2)z\} \tag{5.3.30}$$

where B_O is set by the boundary conditions. Power conservation is expressed by the equation:

$$\frac{\partial(P_L+P_B \pm P_F)}{\partial z} + \alpha(P_L+P_B) + \alpha_F P_F = 0 \tag{5.3.31}$$

where $P_m = b_m^2$ is the normalised power in wave m. Finally the coupled wave equation set becomes:

$$\frac{\partial P_L}{\partial z} + \alpha P_L = -2\kappa_L b_L b_F b_B \sin\Psi \qquad \text{(a)}$$

$$\frac{\partial P_B}{\partial z} + \alpha P_B = 2\kappa_B b_L b_F b_B \sin\Psi \qquad \text{(b)} \qquad (5.3.34)$$

$$\pm\frac{\partial P_F}{\partial z} + \alpha_F P_F = 2\kappa_F b_L b_F b_B \sin\Psi \qquad \text{(c)}$$

where

$$\Psi = (\phi_L - \phi_B - \phi_F) \qquad (5.3.35)$$

is the relative phase and the +ve sign refers to the case where the flexural wave co-propagates with the light.

The boundary condition at $z = 0$ must be such that all the waves carry finite power, although of course the pump will overwhelmingly dominate since the Brillouin and the flexural waves are spontaneous. The maximum parametric gain is expressed when the relative phase at $z = 0$ is $\Psi = \pi/2$ or $3\pi/2$, which yields from eqn.(5.3.30) $B_O = 0$. This is the case of interest in FSBS, since Brillouin and flexural waves satisfying this phase relationship reach threshold first. From this point, therefore, $B_O = 0$ is assumed which implies that Ψ remains at $\pi/2$ or $3\pi/2$ throughout the interaction.

Although eqn.(5.3.34) may be solved numerically, it is instructive to follow the precedent set in many BSBS analysis[17] and treat the special case when $\partial P_F/\partial z$ is negligible. For validity this implies that the characteristic absorption length $1/\alpha_F$ must be smaller than the characteristic length for the FSBS process. This is a good approximation for BSBS, however, it is not necessarily true for FSBS, as we shall see. Adopting it for the present, the following differential equation pair may be obtained:

$$\frac{\partial P_B}{\partial z} = [-\alpha + g_{BF}P_L]P_B \qquad \text{(a)}$$

$$\frac{\partial P_L}{\partial z} = [-\alpha - g_{BF}P_B]P_L \qquad \text{(b)} \qquad (5.3.36)$$

where the Brillouin gain $g_{BF}(\text{m}^{-1})$ is given by

$$g_{BF} = (4\kappa_B\kappa_F/\alpha_F) \qquad (5.3.37)$$

and $\kappa_L \approx \kappa_B$ is used. The general solution of these equations is:

$$P_B(z) = P_{BO}\left\{\frac{(P_{LO}+P_{BO})\exp(-\alpha z)}{P_{BO}+P_{LO}\exp(-g_{BF}(P_{BO}+P_{LO})L_i)}\right\} \qquad (5.3.38)$$

where $P_L(z) = ((P_{BO}+P_{LO})\exp(-\alpha z) - P_B(z))$ and the effective interaction length

$$L_i = (1 - \exp(-\alpha z))/\alpha \qquad (5.3.39)$$

The quantities P_{BO} and P_{LO} are the initial values of P_B and P_L at $z = 0$. If pump depletion due to FSBS is neglected the solution becomes:

$$P_B(z) = P_{BO}\exp(-\alpha z + g_{BF}L_i) \qquad (5.3.40)$$

Which is formally identical with the expression derived in backward SBS, and makes no distinction as to whether the flexural wave is co - or counter-propagating.

In order to compare the gains in FSBS with those in BSBS, it is necessary to derive the coupling constants for the backward SBS interaction. They take a form similar to eqn.(5.3.26) and are expressed in eqn.(3.2.2), the only difference being the definition of C_O which is stated in eqn.(3.2.3). It is now possible to obtain an expression for the ratio g_{BF} to g_{BO}, the Brillouin gain at the same power level in backward SBS:

$$\frac{g_{BF}}{g_{BO}} = \frac{\alpha_o f_F v_{go}}{\alpha_F f_o v_{gF}}\left[\frac{2Qr_{eq}}{a}\right]^2 \sim \frac{\alpha_o \Lambda_o}{2\alpha_F \Lambda_F}\left[\frac{r_{eq}}{a}\right]^4 \qquad (5.3.41)$$

where $Q \sim r_{eq}/2a$. The reasons for this strong dependence on r_{eq}/a are i) that the acoustic power is distributed over the entire fibre cross section while the optical power is concentrated in the core, and ii) that the induced electrostrictive moment scales with r_{eq}. Point ii) is further clarified by noting that the axial electrostrictive force (pressure x area) depends only on the optical power whatever its intensity; enlarging the spot size

yields a higher moment since the moment arm lengthens while the electrostrictive force remains unchanged (see figure 5.4). The consequence is that, in peculiar contrast to all other non-linear effects, larger spot sizes of the optical mode increase the non-linearity. As in eqn.(3.2.4), it is usual to define explicit expressions for the Brillouin gain (gain per unit intensity) in units of m/W. These expressions, denoted by $\bar{g}_{BF}$ and $\bar{g}_{BO}$, take the form:

$$\bar{g}_{BF} = G_B \left\{ \frac{(r_{eq}/a)^4}{\Lambda_F \alpha_F} \right\} \tag{5.3.42}$$

and

$$\bar{g}_{BO} = G_B \left\{ \frac{2}{\Lambda_o \alpha_o} \right\} \tag{5.3.43}$$

where

$$G_B = \frac{(\pi \partial \varepsilon_r / \partial s)^2}{\lambda_B c n_L n_B E} \tag{5.3.44}$$

In the experiment described here, λ_B = 514.5nm and E = 73kNmm^{-2},[13] yielding G_B = $4.5\text{x}10^{-12}$ m/W where $n_L = n_B$ = 1.458, $c = 3\text{x}10^8 \text{ms}^{-1}$ and $\partial \varepsilon_r / \partial s$ = 3.3. Graphs of $\bar{g}_{BF}$ versus r_{eq}/a for various values of α_F are plotted in figure 5.5 for $L_b = \Lambda_F$ = 0.17mm and r_{eq} = 2.3μm. For comparison $\bar{g}_{BO}$ at $\Lambda_o = \lambda_B/2n$ = 176nm (eqn.(2.3.4)) and $\alpha_o = 1\text{x}10^6 \text{m}^{-1}$ is also plotted. Large values of r_{eq}/a significantly favour FSBS. If r_{eq} is varied, keeping a constant, a similar result is obtained, although the beat length $L_b = \Lambda_F$ at constant normalised frequency V (chosen to lie in the dual mode regime $2.405 < V < 3.832$), see eqn (5.6.3), will scale linearly with r_{eq} and reduce the quartic dependence on r_{eq} to cubic. Even so, under these circumstances increasing the spot size at constant pump power will still lower the FSBS threshold. The flexural phase velocity and frequency, together with the parameters af_F/v_t from eqn.(5.3.11) are plotted in figure 5.6 for the same case as in figure 5.5. The limits of validity of the low frequency flexural wave approximation are marked. The experiment in section 5.6 lies to the left of the region marked. Taking an acoustic loss of around 1m^{-1}, the ratio of forward to backward Brillouin gain is of the order 10^{-2}.

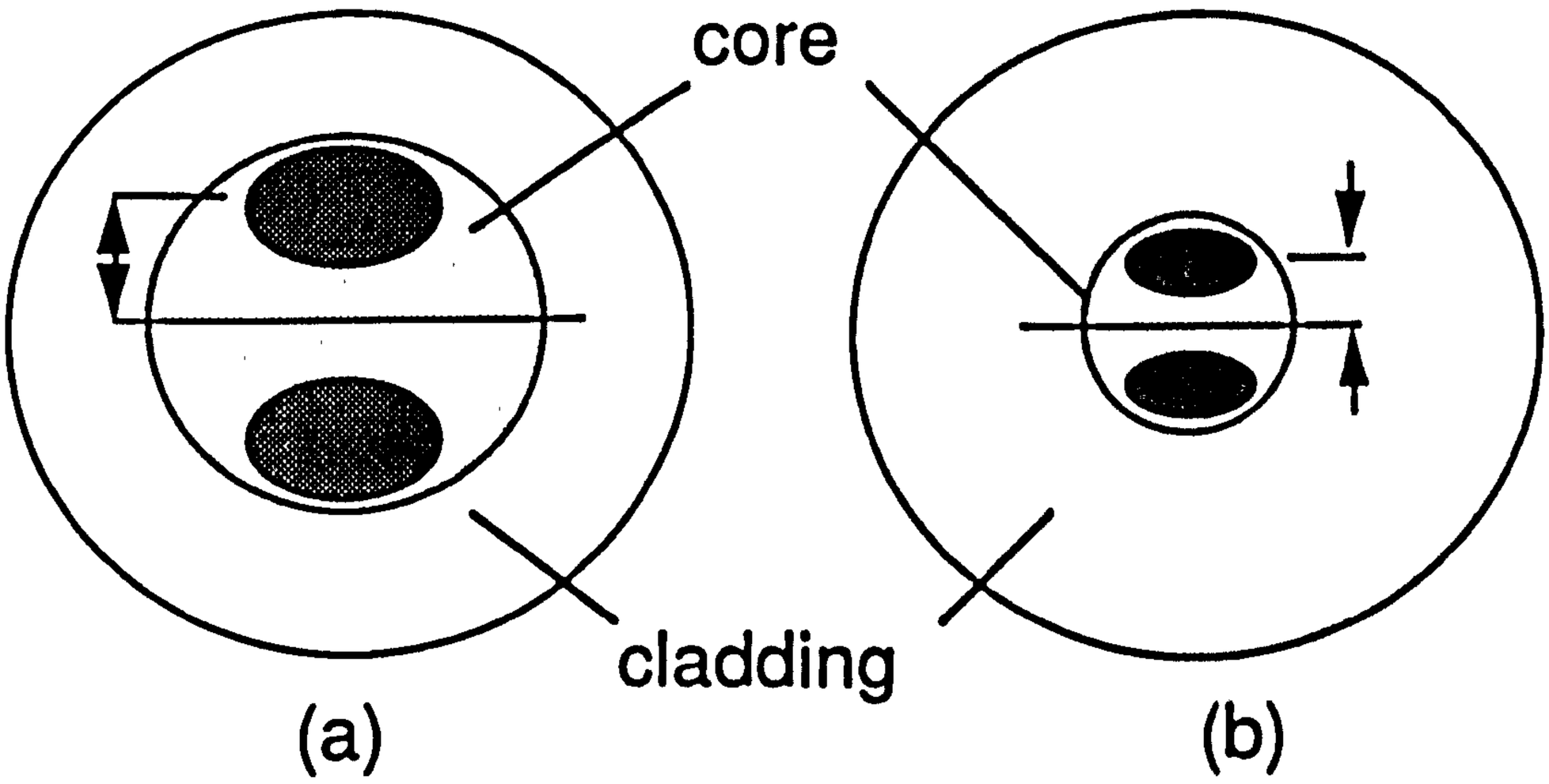

Figure 5.4

The electrostrictive moment arm for two different spot diameters in a fibre of constant cladding radius. Because the axial electrostrictive force depends only on the optical power, it is advantageous (at fixed optical power) to have as large as possible an optical spot size, in contrast to every other known non-linear effect. This is because the axial electrostrictive force is independent of the area of the elliptical regions, whereas the resulting moment is proportional to the moment arm (marked).

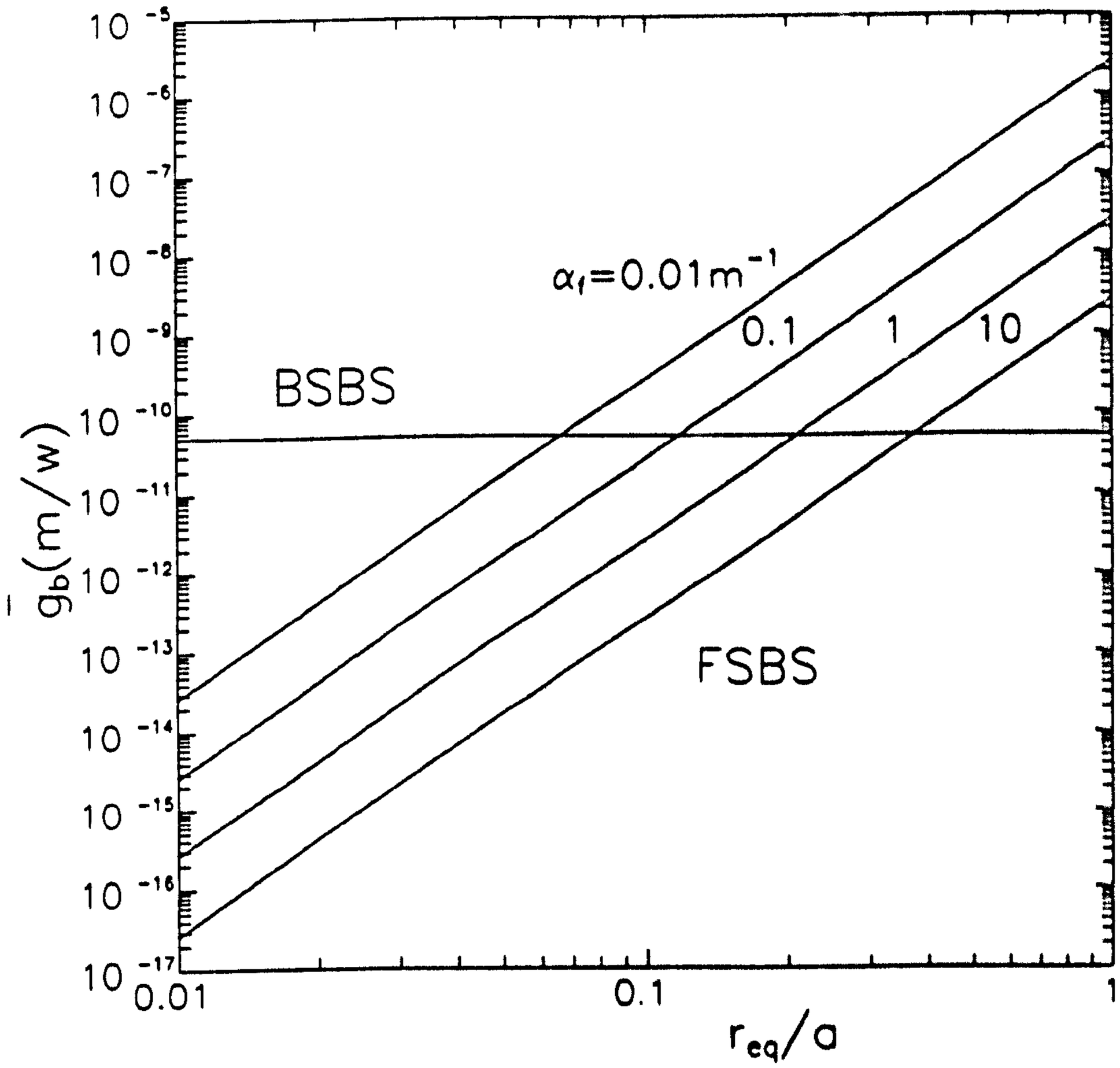

Figure 5.5

Brillouin gains in m/W plotted against the ratio of modal to cladding radii at different levels of flexural wave absorption α_F. The parameter values were Λ_F = 0.17mm and r_{eq} = 2.3μm. The equivalent BSBS gain is included for comparison.

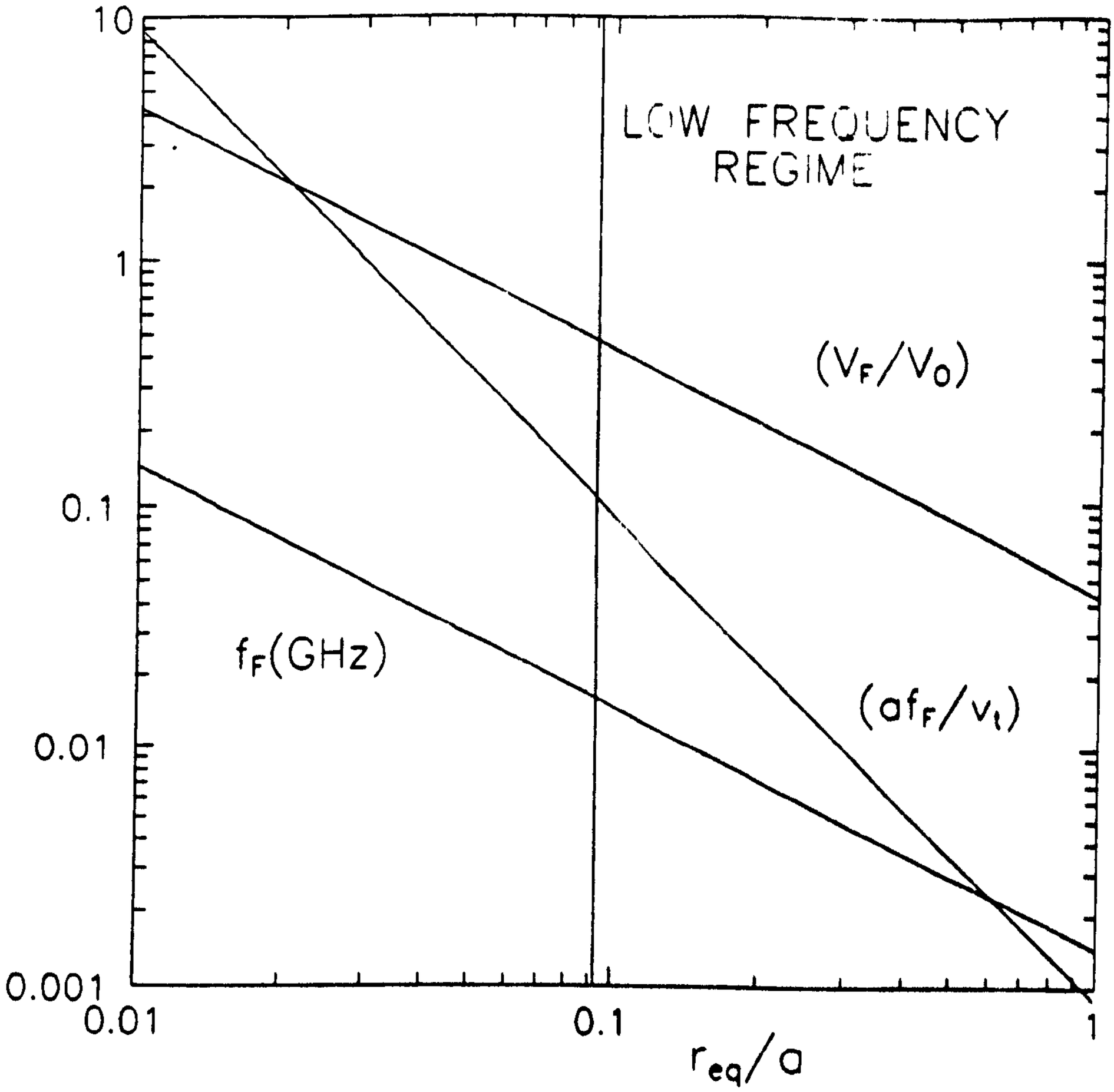

Figure 5.6

Various parameters plotted against r_{eq}/a for the FSBS case in figure 5.5. The analysis is valid in the low frequency region, where, from eqn.(5.3.11), the parameter $(af_F/v_t) \leq$ 0.1.

5.4 Threshold power for FSBS

Following, Smith[18], the spontaneous Brillouin signal (caused by scattering of pump light at thermally excited acoustic phonons) can be incorporated into eqns.(5.3.36) as follows:

$$\frac{\partial P_B}{\partial z} = -\alpha P_B + g_{BF} P_L (P_B + s_F) \qquad \text{(a)}$$

$$\frac{\partial P_L}{\partial z} = -\alpha P_L - g_{BF} P_L (P_B + s_F) \qquad \text{(b)} \qquad (5.4.1)$$

where the normalised spontaneous Brillouin power s_F is given by

$$s_F = \frac{f_B \Delta f_L K_B T}{f_F P_{tot}} \approx \frac{f_L \Delta f_L K_B T}{f_F P_{tot}} \qquad (5.4.2)$$

and K_B is Boltzman's constant. As before these expressions are only valid if $\alpha_F >> g_{BF}$. Although eqns.(5.4.1) may be numerically integrated, the threshold power can be found by neglecting non-linear pump depletion, i.e.setting $P_L(z) = \exp(-\alpha z)$ and integrating the first eqn.(5.4.1). This yields:

$$P_B(z) = (s_F g_{BF}/\alpha)\exp(-\alpha z) \int_0^Y \frac{\exp(g_{BF} y/\alpha)}{y+\exp(-\alpha z)}\, dy \qquad (5.4.3)$$

where y is the variable integral in the limit between $Y = 0$ and $Y = 1 - \exp(-\alpha z)$. Making the approximation that the integral is only significant in the range where $y \approx 1$ (assuming the fibre is long enough to allow $\exp(-\alpha z) << 1$) eqn.(5.4.3) may then be integrated. Following Smith in defining the threshold as occurring when the Brillouin signal equals $P_L(z) = \exp(-\alpha z)$, the threshold power P_{th} is a solution of :

$$P_{th} = \left(\frac{f_L \Delta f_L K_B T}{f_F}\right)\exp\left(\frac{\bar{g}_{BF} P_{th} L_i}{\pi w_{eq}^2}\right) \qquad (5.4.4)$$

where the exponential function is assumed to be much greater than 1. This shows that the growth from noise can be approximately modelled by means of an equivalent injected Brillouin power $P_{BF}(o) = (f_L \Delta f_L K_B T / f_F)$ at $z = 0$, which corresponds to an injected photon flux $K_B T / h f_F$ per mode within the pump/laser linewidth. For a laser linewidth $\Delta f_L = 25$MHz, $\lambda_L = 514.5$nm, $T = 293^{\circ}$C and $f_F = 17$MHz, the equivalent injected power turns out to be $P_{BF}(o) = 3.5\mu$W. This is in contrast to BSBS (see chapter 2.2) where, for $f_o = 32$GHz, the equivalent injected power is $P_{BO}(L) = 1.8$nW.

Computed threshold powers, obtained by iteratively solving eqns.(5.4.4) and eqn.(3.2.6) are presented in figure 5.7 as a function of a, the cladding radius, for $\alpha =$ 20db/km, $\alpha_o = 10^6$ per m, $r_{eq} = 2.3\mu$m, $L = 20$m and $\Lambda_F = 0.17$mm. The acoustic flexural wave loss α_F is varied as a parameter and account is taken of the variation of f_F with a. As expected, smaller values of a significantly favour FSBS. In the experiment[1] in section 5.6 a much lower threshold for FSBS than predicted by figure 5.7 was found. The implications of this will require further careful experimental study.

Since FSBS does not require a long coherence length (the Brillouin and pump waves co-propagate and are therefore closely correlated) the use of a multi-frequency laser line will suppress the BSBS signal in favour of FSBS.

5.5 Computer modelled solutions for full set of the cw equations

Numerical solutions allow the treatment of the case, clearly of importance in FSBS, when it is no longer valid to neglect $\partial P_F / \partial z$. This happens if the acoustic loss is small compared to the Brillouin gain, i.e. when $\alpha_F / g_{BF} << 1$. The consequence of an increased phonon lifetime is that an acoustic wave excited in one part of fibre may travel a significant distance without serious absorption to another section of the fibre where

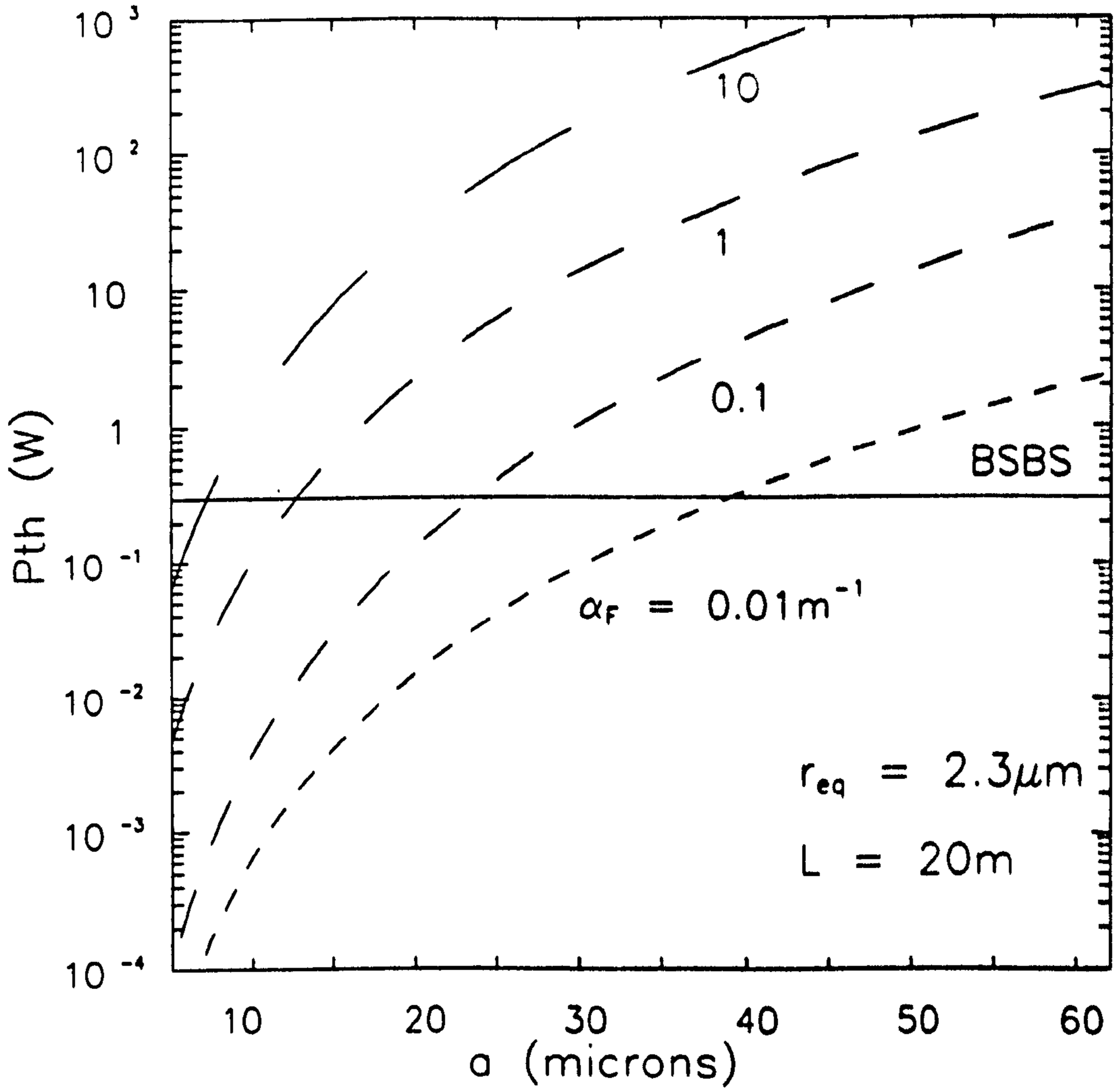

Figure 5.7

Threshold pump power levels in FSBS and BSBS, for different values of α_F, plotted against the cladding radius a at constant mode spot size r_{eq} = 2.3μm.

the relative phase Ψ is different. Graphs of the z dependence of P_F, P_B and P_L, eqn.(5.3.34), for a series of transition cases are plotted in figure 5.8. The travelling optical interference fringes that provide gain via electrostriction for the flexural wave in one section of the fibre flip their phase by 180° at the transition between one coupling cycle and the next (see figure 5.9 for a logarithmic plot of the case in figure 5.8c, including the acoustic wave power P_F). An acoustic wave that travels over this transition will immediately experience negative electrostrictive gain and begin to lose power, donating energy back to the Brillouin signal, which will then be up-converted back to the pump frequency. As the parameter α_F/g_{BF} falls in magnitude, the number of possible coupling cycles rises. As it rises in value, the solution eqn.(5.3.38) is approached when frequency up conversion of the Brillouin signal is impossible since the acoustic phonons are absorbed almost immediately after being created; they do not then travel far enough to experience the flip in phase just mentioned. Under these conditions it is expected that the approximate solution of eqn.(5.3.38) will become valid. To provide confirmation of this, the accurate and approximate solutions are compared in figure 5.10; eqn.(5.3.38) predicts a premature onset of the stimulated Brillouin process rather nearer the launch end than is correct. Otherwise the behaviour is very similar. The initial value of P_B was arbitrarily set to 10^{-9} for these calculations, $P_F(o)$ was set equal to $((2\kappa_F/\alpha_F)^2 P_{BO} P_{LO})$ and Ψ was set equal either to $\pi/2$ or $3\pi/2$ depending on the position in the coupling cycle.

5.6 Experimental observation

5.6.1 Intermodal beat length

FSBS is described by periodic optical coupling between two spatial modes in circular optical fibres. In an ideally unperturbed straight fibre, these two modes are orthogonal to each other and they do not exchange optical power as the light propagates along the fibre's length. However, should a mechanism exist that would allow periodic microbending such that the period matches the beat length, L_b, between the two modes

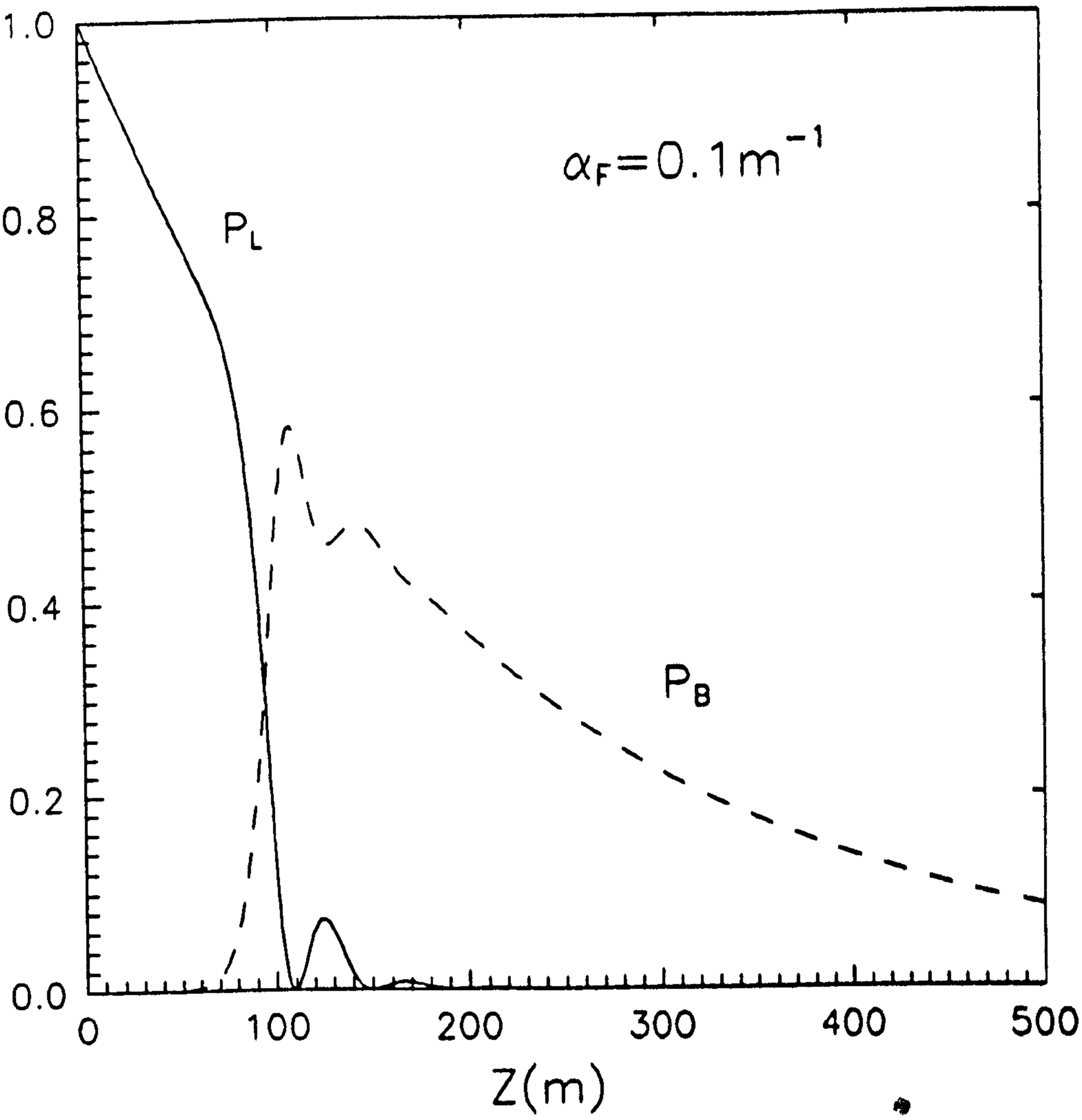

Figure 5.8 (a)

Growth of FSBS with distance, calculated by numerical integration of eqn.(5.3.34) at three different values of acoustic loss: (a) $0.1m^{-1}$ (b) $0.05m^{-1}$ and (c) $0.01m^{-1}$. The other parameter values are P_{tot} = 200mW, an optical wavelength of 514.5nm, r_{eq} = 5μm, a = 25μm and α = $0.005m^{-1}$, giving v_F = $1330ms^{-1}$ and f_F = 3.9 MHz. The Brillouin gain in each case is (a) $0.54m^{-1}$ (b) $1.1m^{-1}$ and (c) $5.4m^{-1}$.

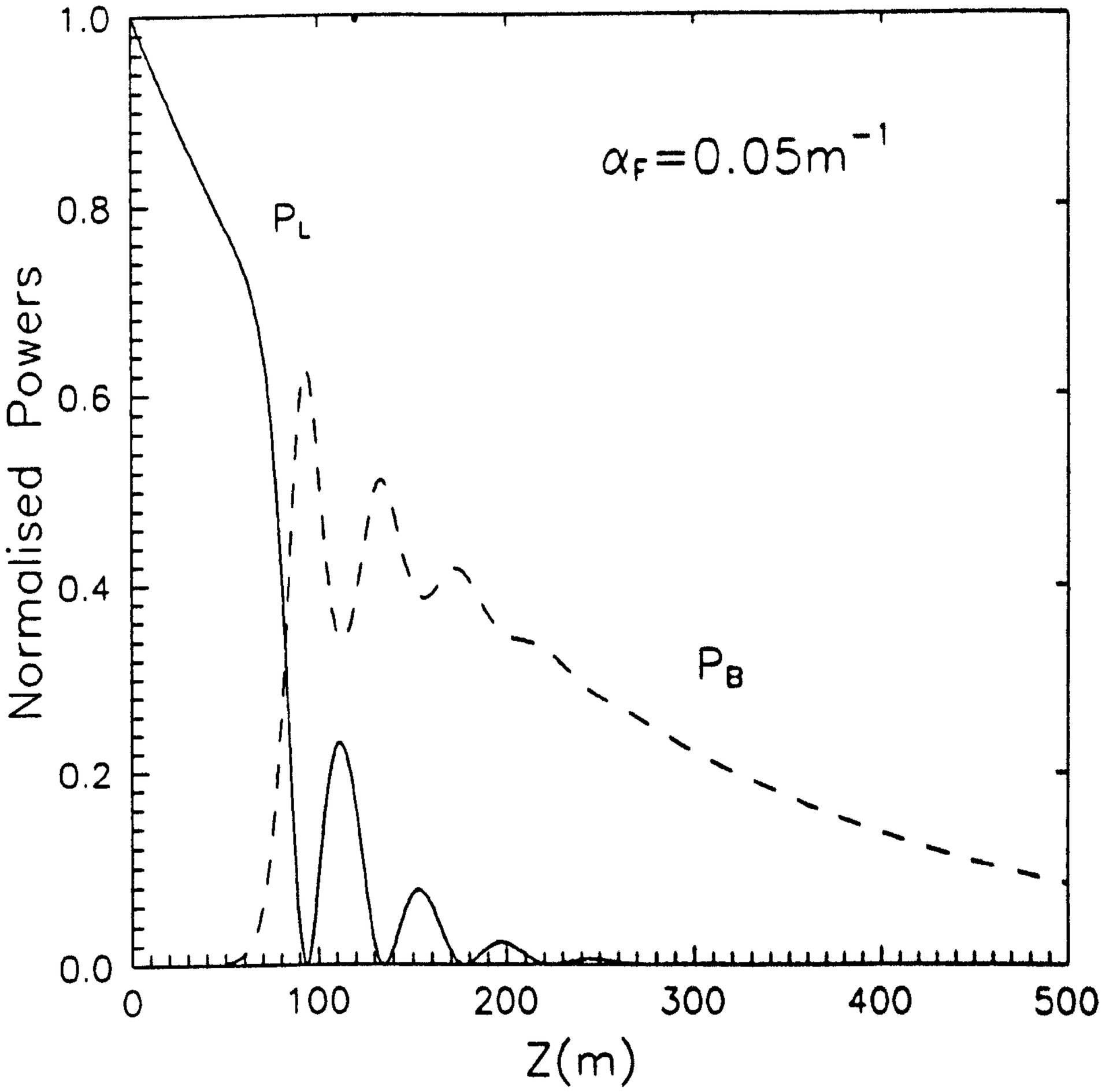
1.0
0.8
0.6
0.4
0.2
0.0
Normalised Powers
$\alpha_F = 0.05 m^{-1}$
P_L
P_B
0
100
200
300
400
500
Z(m)

Figure 5.8 (b)

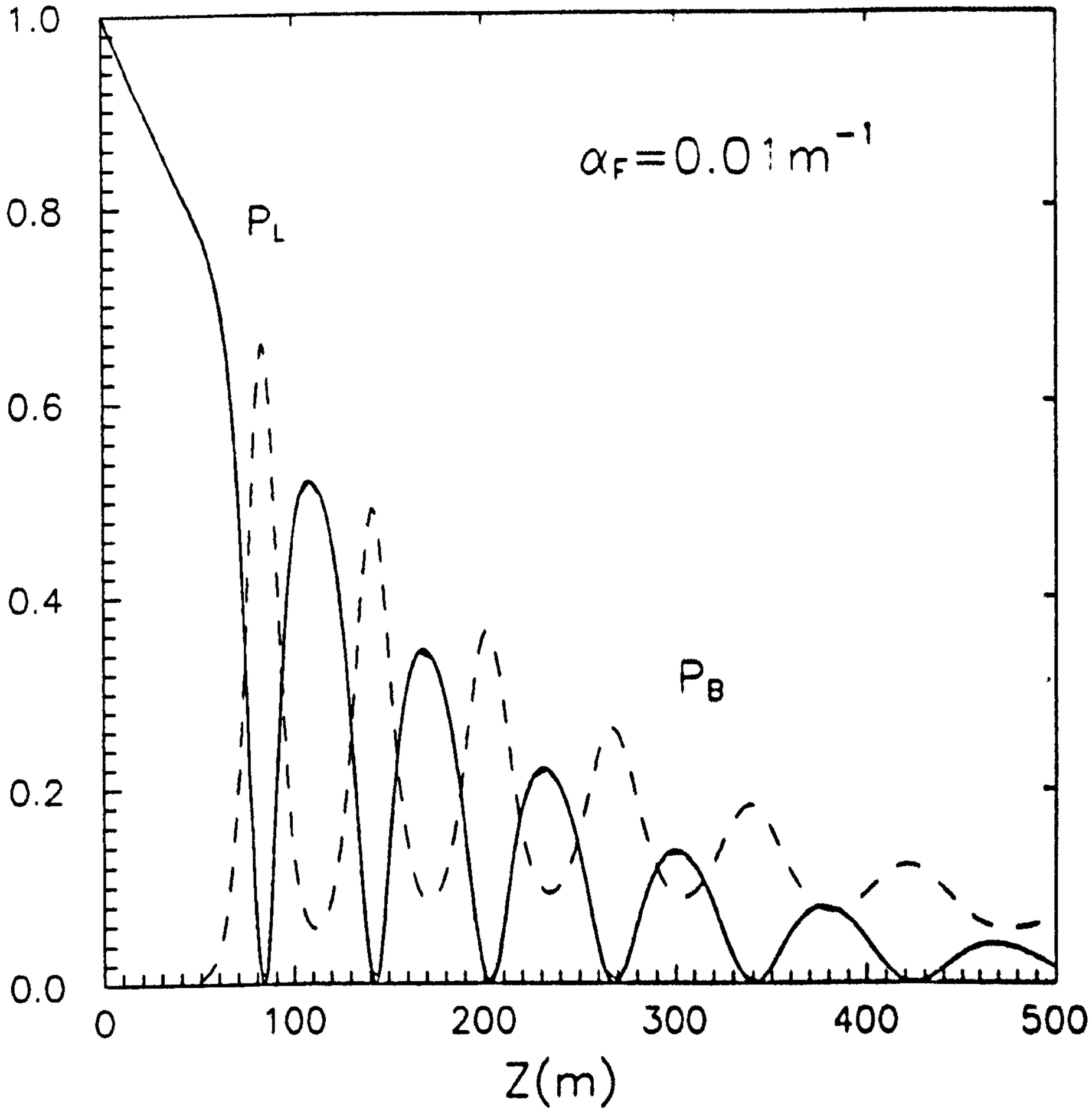
1.0
0.8
0.6
0.4
0.2
0.0
Normalised Powers
$\alpha_F = 0.01\,m^{-1}$
P_L
P_S
0
100
200
300
400
500
Z(m)

Figure 5.8 (c)

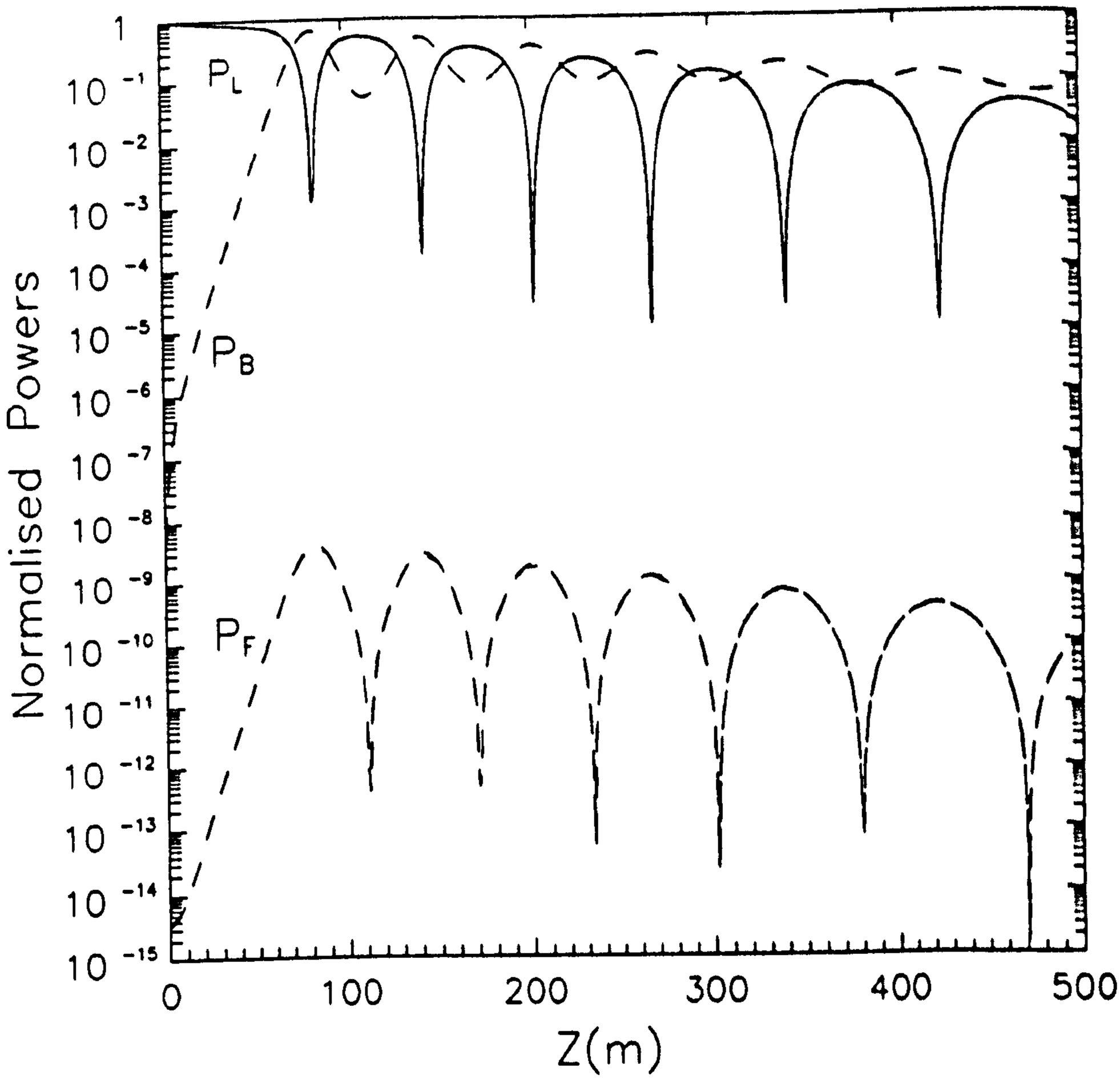

Figure 5.9

Plot in figure 5.8(c) rescaled logarithmically and including the flexural wave power P_F. The complex interdependence of the three parametrically coupled waves is clear.

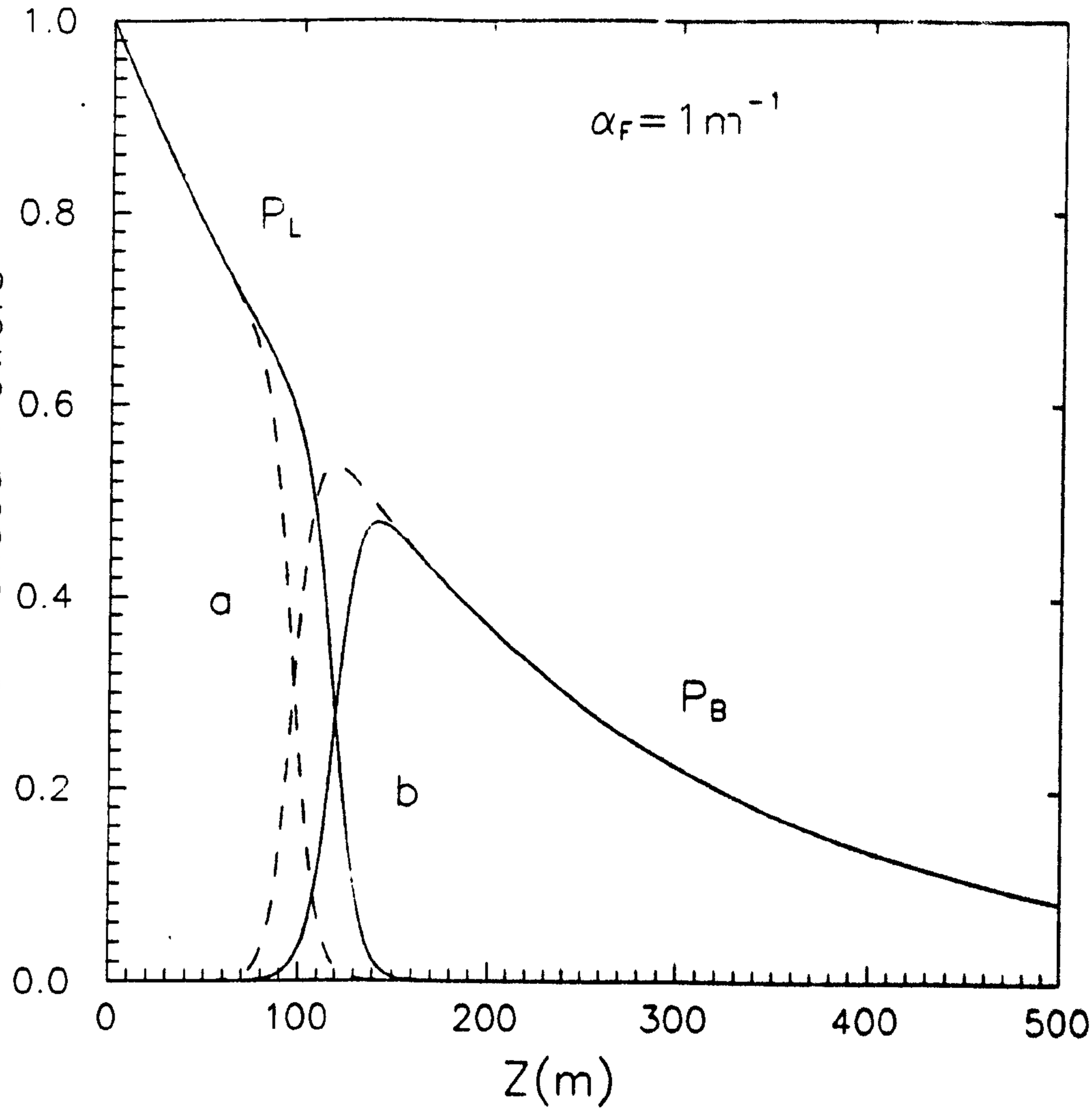

Figure 5.10

Comparison of (a) the approximate solution of eqn.(5.3.38) with (b) that resulting from numerical integration of eqn.(5.3.34). The other parameter values are the same as in figure 5.8, with the exception that the power level is 1W and $g_{BF} = 0.27m^{-1}$. The approximate solution underestimates the interaction length needed before the FSBS signal becomes significant.

then coupling between the two lowest order modes is made possible. In reality a spontaneous flexural wave satisfying the phase matching condition is inherent in the fibre on account of localised and environmental changes along the fibre length; it is because of this weak grating generated by the spontaneous flexural wave that intermodal coupling between the LP_{01} and LP_{11} modes exist. It is necessary to calculate the beat period between the first two modes of the fibre. The beat length, L_b, (Snyder and Love pg.228)[19] is given by:

$$L_b = 2\pi/(k_{01} - k_{11}) \tag{5.6.1}$$

where the propagation constants k_{01} and k_{11} are defined by:

$$k_{01/11} = \sqrt{(k_L^2 n_{co}^2 - (\mu_{01/11}/r_{eq}^2)} \tag{5.6.2}$$

and where k_L is the pump wavevector, r_{eq} the core radius, n_{co} the refractive index of the core, n_{cl} the refractive index of the cladding and μ the modal parameter defining cut-off for each of the two modes propagating in the core of the fibre[19]. The modal parameters of an optical waveguide depend on all of the physical quantities which define the waveguide, i.e. the refractive index profile and cross sectional geometry together with the frequency of the source of excitation. From these parameters the normalised waveguide parameter V can also be defined[19]:

$$V = 2\pi r_{eq}/\lambda_L \sqrt{(n_{co}^2 - n_{cl}^2)} \tag{5.6.3}$$

where the parameters have their previously defined meanings and V determines the number of modes the waveguide can support. A waveguide is said to be multi-mode if $V >> 1$ when many bound modes can then propagate. At the opposite extreme when V is sufficiently small so that only two polarisation states of the fundamental mode can propagate, the waveguide is said to be single mode. For example, the step index profile of circular fibre is single mode when $V < 2.405$. For the specified fibre parameters in

section (5.6.2) the intermodal beat length L_b, eqn.(5.6.1), is calculated as L_b = 0.17mm where n_{co} = 1.458, n_{cl} = 1.4535, and λ_L = 514.5nm and r_{eq} = 2.3 μm. From a point of completeness the V value indicates that for these fibre parameters the fibre is dual moded for a core radius of between 1.8μm and 2.7μm.

5.6.2 Experimental configuration

An argon ion laser running single mode at 514.5nm was used to deliver light to 500m of dual mode fibre, as shown in figure 5.11. To verify truly single frequency operation a part of the laser output was split off and monitored directly at the photo-diode and a confocal Fabry Perot (CFP). The laser was operated in single mode because "spurious side effects" were detected when the laser light was directly incident upon the photo-diode. This then made it impossible to distinguish the FSBS signal incident from the output from the fibre. Hence a shutter system allowed independent monitoring of the light to ensure no such spurious "side-effects" could be confused with the FSBS signal when the measurement was made. After careful adjustment of the launching conditions the frequency spectrum in figure 5.12 was obtained which shows a clear frequency component at 16.6MHz; no such signal was apparent at the laser output. For our fibre parameters the intermodal beat length has previously been calculated to be L_b = 0.17mm at 514.5nm; at f_F = 16.6MHz, a fibre cladding radius a = 62.5μm and a shear velocity v_t = 3764ms^{-1}, the parameter af_F/v_t [10] = 0.28, which places the interaction in the transition regime between high and low frequency flexural waves, see section 5.2. The full theory [10] then yields $v_F \approx 0.5v_o$ = 2880ms^{-1}. The product of L_b and f_F also gives an independent estimate of v_F = 2822ms^{-1} which is in excellent agreement and would seem to confirm that FSBS is taking place. The observed threshold power was recorded as 45mW whereas the theoretically predicted threshold for a flexural loss of α_F = 0.01m^{-1} is 250mW. Whilst it is possible that the signal was mistaken for spontaneous scattering, the result did suggest a threshold condition. This result will require further and careful experimental investigation.

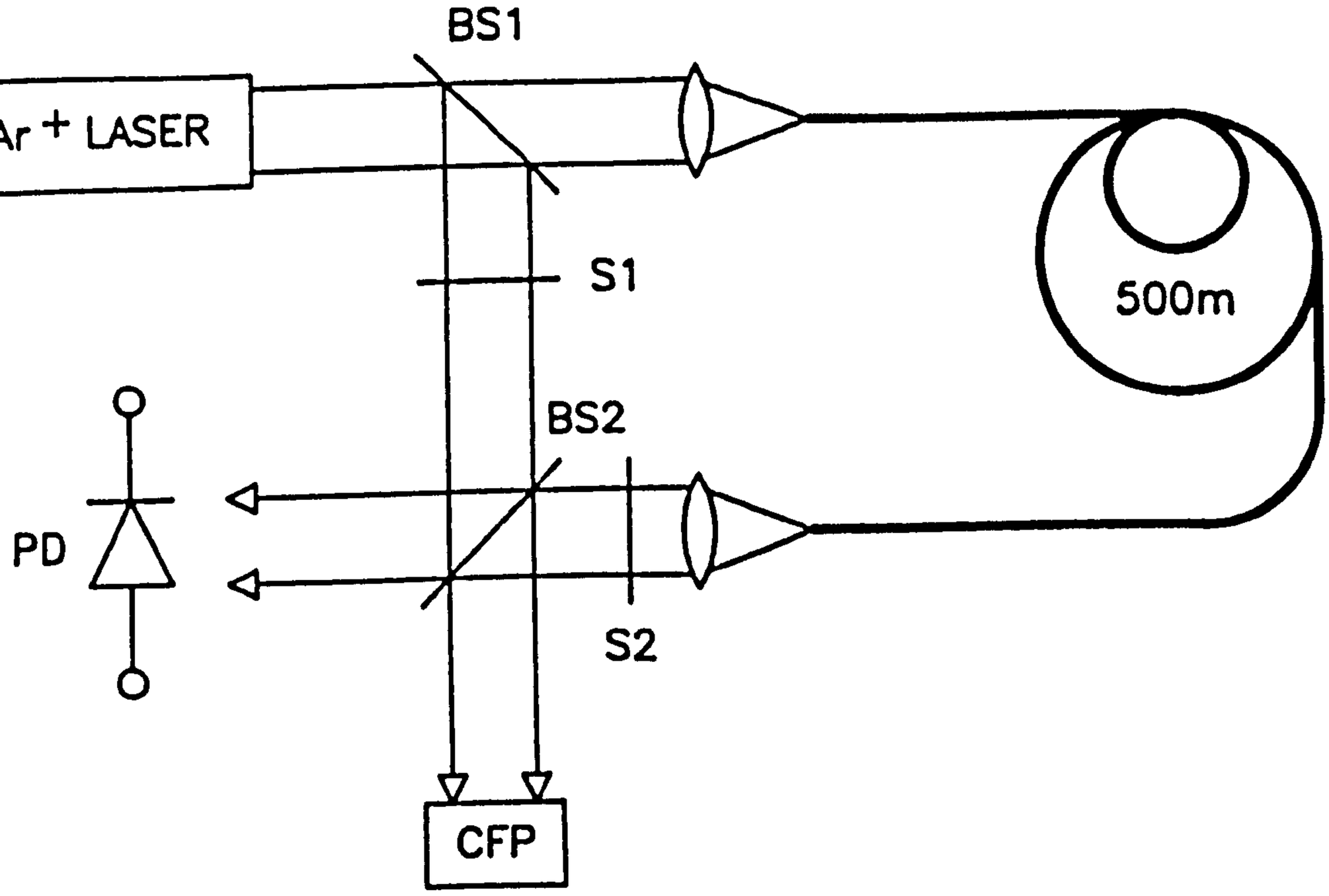

Figure 5.11

Experimental set-up for observing the frequency shifted FSBS signal. The single frequency laser beam at 514.5nm is monitored directly using both a confocal Fabry Perot (CFP) and a photo-diode (PD) to verify that no spurious frequency components are present. Light transmitted through the fibre is detected at the same PD, and a shutter system (s_1 and s_2) used to monitor the FSBS And laser signals independently.

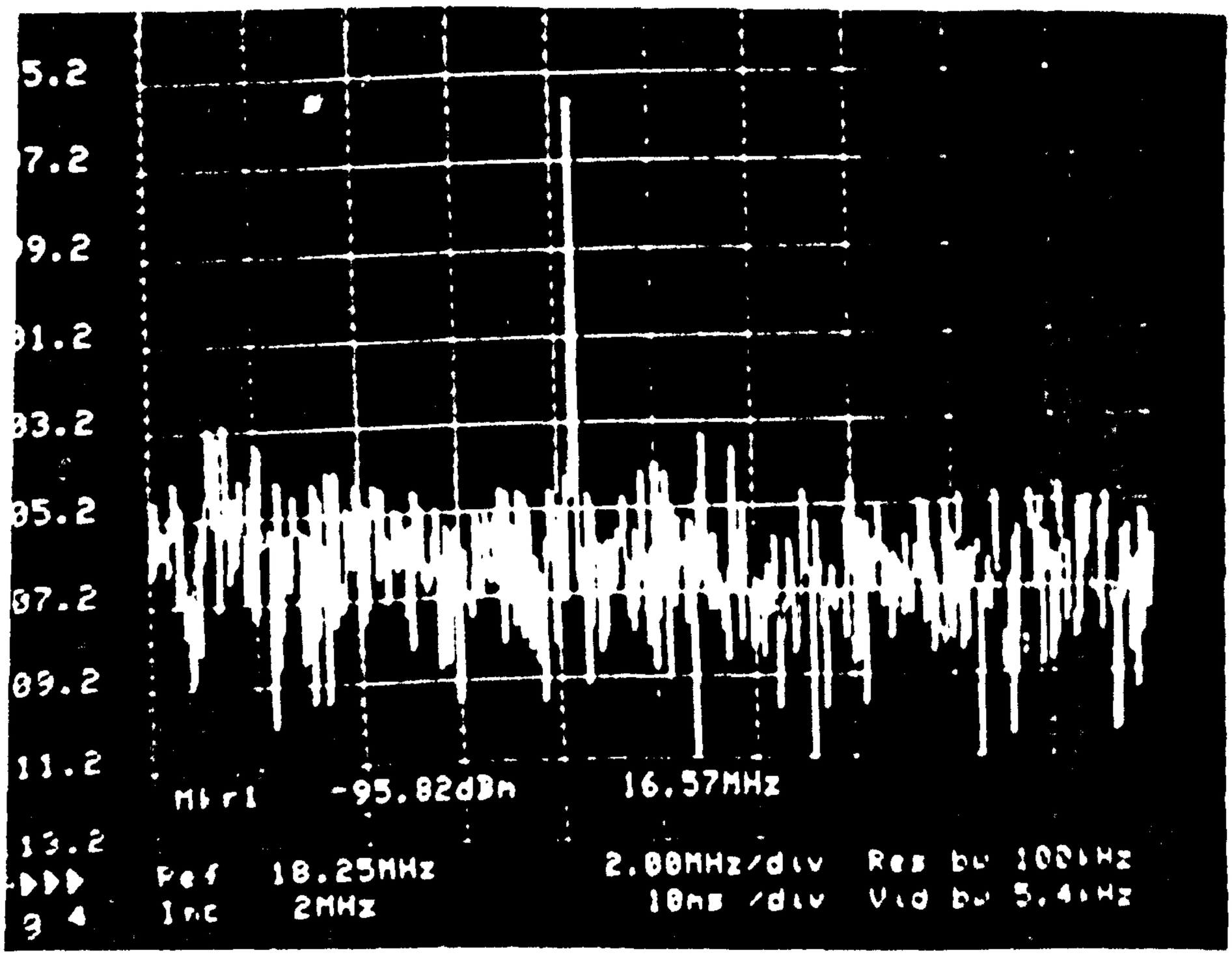

Figure 5.12

The spectrum obtained; a clear peak is apparent at 16.6MHz (2MHz/div). Its narrowness is an indication of the expected high degree of correlation between the co-propagating laser and Brillouin signals.

5.7 Discussion of unique features of FSBS

It is emphasised that the analysis presented is fully valid only in the flexural wave regime where the inequality in eqn.(5.3.11) holds. It will remain qualitatively valid outside this regime, however, with somewhat reduced values of acoustic/optical overlap and hence Brillouin gain. Within this restriction, the FSBS gain can be greatly enhanced by appropriate fibre design and employing a laser running single line but multi-frequency. It varies as $(r_{eq}/a)^4$ and hence is improved (at constant pump power) for larger modal spot sizes. FSBS is thus unique in being the only known non-linear effect which is enhanced by reducing the optical intensity while keeping the power constant. This odd behaviour arises because a) the axial electrostrictive force is independent of the spot radius r_{eq} and b) its moment arm increases with r_{eq}. The standard approximation used in BSBS - that the acoustic absorption length is much shorter than the Brillouin gain length - is no longer always valid in FSBS. The consequence is that non-localised acoustic wave coupling in both directions between the pump and the Brillouin modes can take place. Within the effective interaction length L_i, many cycles of coupling can take place. Experiments remain to be done on specially designed fibres with i) plastic coating removed to reduce α_F, ii) large dual mode spot sizes (requires small core/cladding refractive index step) and iii) large values of r_{eq}/a. Attention to these details will greatly reduce the FSBS threshold power level.

References: Chapter5

1. Russell, P.St.J., Culverhouse, D., and Farahi, F.: "Experimental observation of forward stimulated Brillouin scattering in dual mode single core fibre", Electron. Lett., vol.26, pp.1195-1196, 1990.
2. Shelby, R.M., Levenson, M.D., and Bayer, P.W.: "Guided acoustic wave Brillouin scattering", Phys.Rev., vol.B31, pp. 5244-5252, 1985.
3. Friberg, S.R., Silberberg, Y., Oliver, M.K., Andrejco, M.J., Saifi, M.A., and Smith, P.W.: "Ultra-fast all optical switching in dual core fibre non-linear coupler", Appl. Phys. Lett., vol.51, pp.1135-1137, 1987.
4. Trillo, S., Wabnitz, S., Stolen, R.H., Assanto, G., Stegeman, G.I., and Seaton, C.T.: "Experimental observation of polarisation instability in a birefringent optical fibre", Appl. Phys. Lett., vol.49, pp. 1224-1226, 1986.
5. Trillo, S., Wabnitz, S., and Stegeman. G.I.: "Nonlinear codirectional guided wave mode conversion in grating structures", J.Lightwave Techn., vol.6, pp 971-976, 1988.
6. Russell, P.St.J., and Payne, D.N.: "Nonlinear switching in strongly coupled periodic dual waveguide couplers", Paper FC2-1, Topical Meeting on Nonlinear Guided Wave Phenomena: Physics and Applications, Houston, 1989.
7. Kim, B.Y., Blake, J.N., Engan, H.E., and Shaw, H.J.: "All-fibre acoustooptic frequency shifter", Opt Lett., vol.11, pp. 389-391, 1986.
8. Kim, B.Y., Blake, J.N., Engan, H.E., and Shaw, H.J.: "Analysis of intermodal coupling in two-mode fibre with periodic microbends", Opt. Lett., vol.12, pp. 281-283, 1987.
9. Sabert, H., Dong, L., and Russell, P.St.J.: "In-line flexural wave optical modulator, filter and frequency shifter in dual-core fibre", Paper TuD9, Topical Meeting on Integrated Photonics Research, Hilton Head, South Carolina, March 1990.

10. Engan, H.E., Kim, B.Y., Blake, J.N., and Shaw, H.J.: "Propagation and optical interaction of guided acoustic waves in two-mode optical fibres", J. Lightwave Techn., vol. 6. pp.428-436, 1988.

11. See:Yarwood, J.:"Electricity and magnetism",pp.403-631,1984.

12 See: Landau, L.D., and Lifshitz, E.M.: "Electrodynamics of continuous Media", Course of Theoretical Physics, vol.8, Pergamon Press (Oxford, London, New York, Paris), 1963.

13. American Institute of Physics Hand Book, edited by D.C.Gray, McGraw - Hill Book co. Inc., New York, 1965 second edition.

14. Thurston, R.N.: "Elastic waves in rods and clad rods", J. Acoust. Soc. Amer., vol.64, pp.1-37, 1963.

15. Skinner, R.: "Mechanics", Blaisdell Publishing Co., p.527, 1969.

16. Elliott, R.S.: "Electrodynamics", McGraw - Hill Book Co., p.286, 1966.

17. For analysis of backward SBS see: Y.R.Shen, *The Principles of Non-linear Optics*, p.189 (Wilel Interscience, New York, 1984)

18. Smith, R.G.: "Optical power handling capacity of low loss optical fibres as determined by stimulated Raman and Brillouin scattering", Appl. Opt., vol.11 pp. 2489-2494, 1972.

19. Snyder, A.W., Love, D.: "Optical waveguide Theory", London: Chapman and Hall, p.228, 1983.

Chapter 6

Gain studies of stimulated Brillouin scattering in fibre ring resonators and its applications

6.1 Introduction

Stimulated Brillouin scattering (BSBS) in optical fibres is of interest for the development of fibre amplifiers[1] as well as fibre lasers[2-4]. In chapter 6 a new study of the fundamental properties of a BSBS laser is presented, as are also two applications; namely a discretely tunable, variable frequency, all fibre-optic frequency shifter and a tunable microwave generator. A detailed explanation of BSBS has been given in chapter 3, and the generation of BSBS in a fibre ring laser has been discussed in chapter 4. Figure 4.5, chapter 4, shows the arrangement with the pump propagating in a fibre ring resonator. If the pump frequency is held at the centre of a cavity resonance the pump intensity inside the ring resonator is enhanced. The resulting BSBS which propagates along the opposite direction will also be enhanced when there is a cavity resonance within the BSBS gain bandwidth. If the BSBS gain in the resonator is greater than the loss then BSBS lasing takes place. The threshold pump power for BSBS lasing can be very low - 35μW was achieved by Smith[5], whereas a threshold power of 165μW at λ_L = 633nm for a resonator with finesse 180 was measured in chapter 4.5. Nevertheless, in both these examples the pump power needed to achieve BSBS in an all fibre ring resonator is small compared to that for long fibre lengths.

Efficient modulation of light at microwave frequencies is important for low loss transmission of microwave signals along optical fibres and optical locking of microwave oscillators[6,7]. Direct current modulation of laser diodes has been demonstrated for frequencies greater than 10GHz at 0.83μm[8] and 1.3μm[9]. In sub-section 6.2.1 an alternative technique is discussed where a tunable microwave signal is generated by mixing the output from a BSBS ring resonator laser with the original

pump source. In sub-section 6.2.2 it is shown that by increasing the optical power density within the resonator, the BSBS gain exceeds the lasing threshold for several modes of the ring laser cavity to be excited and the BSBS gain profile can be traced. In sub-section 6.3.1 a discretely tunable all fibre frequency shifter based on mixing the outputs of two stimulated Brillouin scattering ring resonator lasers is described. The observed temperature dependence of the frequency shift is as expected, with the discrete frequency jumps being equal to the free spectral range of the resonator. In chapter 4.4 it was argued that the spectral width of the laser line can be very narrow since the fibre cavity can be described as a relatively quiet cavity. Because of this the BSBS laser linewidth can be much narrower than the pump spectral linewidth; a measurement giving an upper limit in the optical domain is given in sub-section 6.3.2, and where an estimate for the linewidth of the beat generated by two such signals is also resolved electronically.

6.2 BSBS laser for microwave generation and gain studies

6.2.1 BSBS resonator for microwave generation

It has been shown in chapter 4.2 eqn.(4.2.10) that the finesse of the ring resonator is given by $F = \pi\sqrt{k_r}/(1 - k_r)$, where $k_r = (1-\gamma_o)\exp(-\alpha L)$ is the optimum coupling coefficient, γ_o the lumped loss of the device, α the fibre attenuation coefficient and L the loop length; k_r is hence shown to be completely dependent upon the loss of the device. For commercially available optical fibres the losses at 1300nm and 1500nm are the lowest at typically < 0.3dB/km and < 0.1dB/km, respectively. Hence rings with the highest finesse should be realisable at these wavelengths. For the device to be used in high resolution studies, as in this case, it is also necessary to fabricate the resonator with a long fibre length - again militating against the use of fibres at short wavelengths. For example, at 633nm where the fibre loss ~8dB/km, assuming $\gamma_o = 0.01$, the maximum achievable finesse in a 40m ring is ~37, whereas at 1300nm for an identical lumped loss and loop length, a finesse greater than 240 is possible.

A microwave generator can be realised providing a resonant cavity mode falls under the spontaneous gain curve. It can be made tunable by either heating the resonator or by varying the frequency of the pump laser since the Brillouin frequency shift depends on both the optical frequency of the pump and the temperature of the scattering medium (see eqn.(2.3.4)). The experimental configuration is shown in figure 6.1. The pump source for the SBS ring laser is a single frequency Nd:YAG laser (linewidth 5KHz) operating at 1320nm. The light was coupled into the ring resonator by a polished coupler with a 50:50 splitting ratio. The ring resonator was manufactured from Optical Fibre fibre (cut-off wavelength 1300nm) with a 40m loop length; the free spectral range (FSR) of the resonator was 5MHz. The finesse was measured as 200, equivalent to an optical resolution of 25KHz. The loop length was chosen such that several resonances of the ring laser cavity fell under the spontaneous Brillouin gain curve (typical linewidth 15MHz at 1300nm)[10].

The ring resonator was temperature stabilised using a thermal enclosure and additional stabilisation was provided by active servo control thus ensuring that the enhanced circulating intensity maximised the generation of SBS. At 1300nm the Brillouin frequency shift is ~12GHz (see eqn.(2.3.4)). The backward propagating output from the Brillouin laser was mixed with the pump beam available at the second port of the input coupler and the beat frequency signal observed at the output of the third coupler. The beat signal was detected using an HP11928A detector. The spectrum of the photodiode current was measured with an HP 70206A spectrum analyser. A typical spectrum is shown in figure 6.2 where the beat frequency is at 12.164 GHz. The efficiency was measured as 12%, i.e. a 250μW (r.m.s) microwave beat signal was generated for 2mW of input optical power injected into the ring resonator.

6.2.2 BSBS gain studies

By increasing the optical power density within the ring resonator shown in figure 6.1, the BSBS gain exceeded the lasing threshold for several modes of the ring laser cavity as indicated in figure 6.3. A simple computer programme was then used to

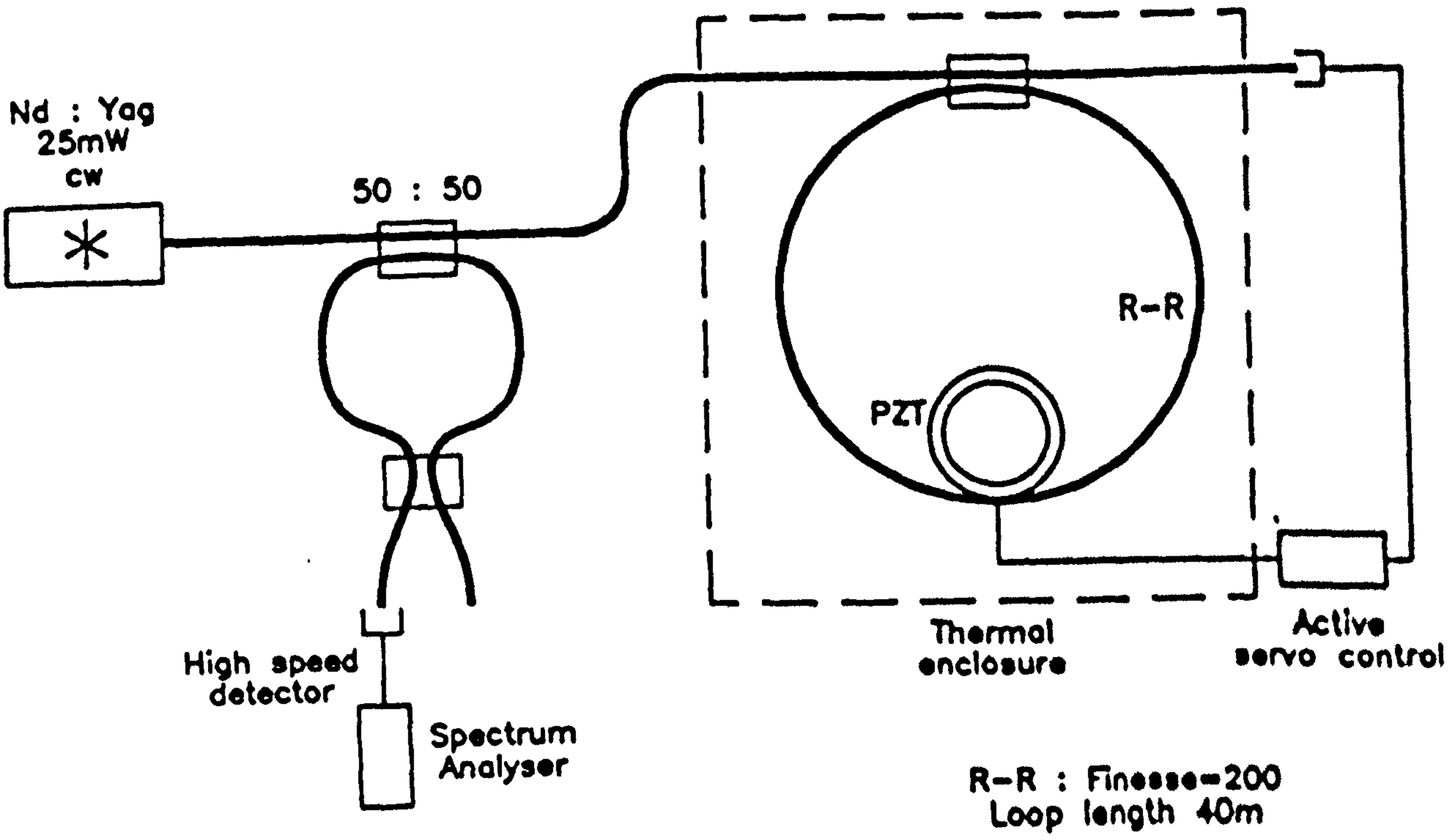

Figure 6.1

Experimental configuration for the generation of microwaves at 12.5 GHz.

PAGE NUMBERING AS ORIGINAL

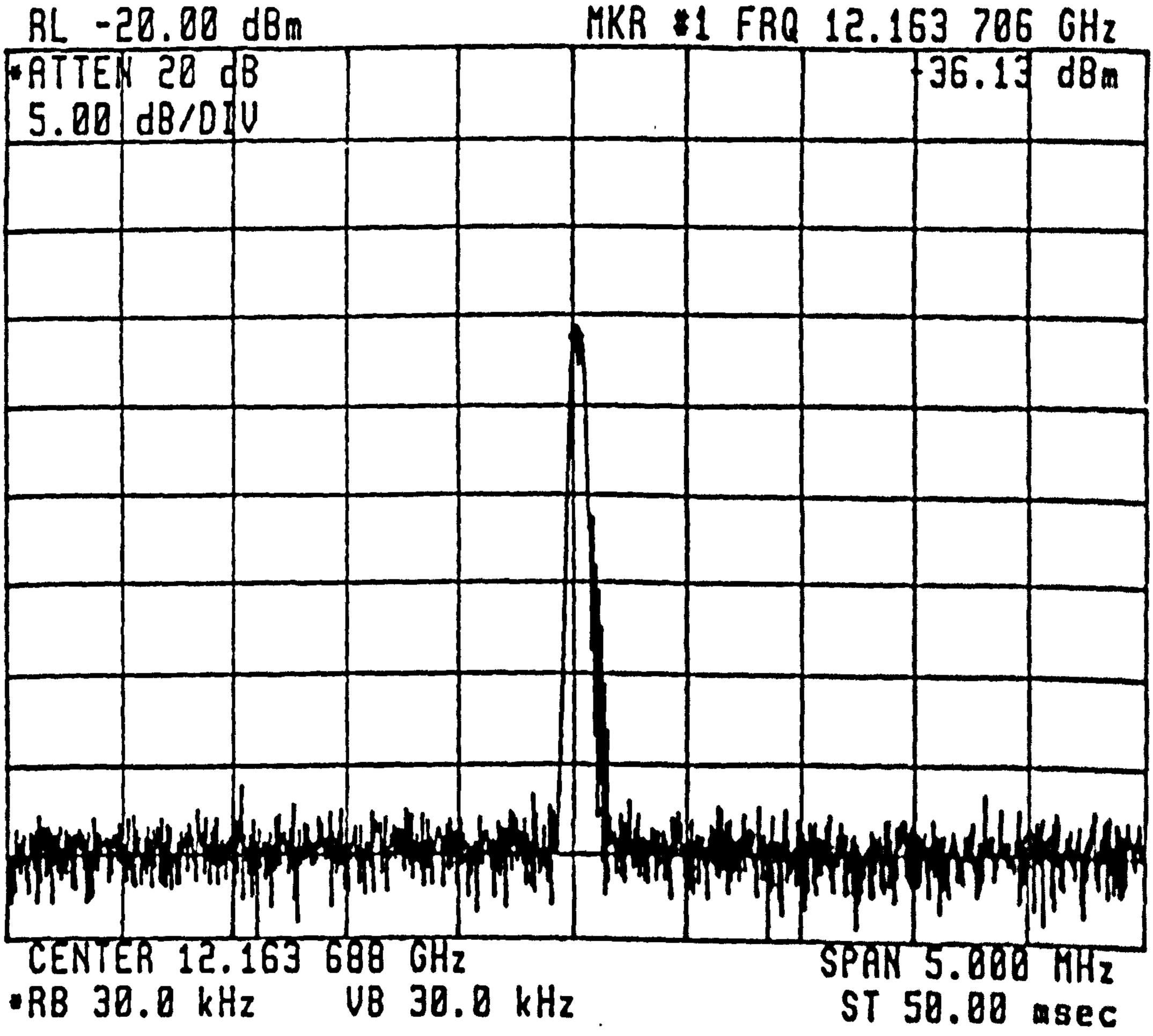

Figure 6.2

The 12.164 GHz beat frequency generated at the photodiode.

generate the Lorentzian curve within which the modes could oscillate. This computer generated curve is also shown in figure 6.3 and represents the gain curve of the laser. The fitted linewidth was 15 MHz (±1MHz). When the resonator is heated both the frequency of the SBS gain curve and the absolute resonant frequencies of the ring change, as shown in figure 6.4, hence the microwave frequency in figure 6.2 can be varied. When the enclosed temperature of the ring resonator was changed from room temperature by ~7°C the spontaneous Brillouin curve was seen to shift by 0.96MHz per °C with respect to the resonator lines. The change in frequency is dependent on the fibre characteristics (see chapter 2.3). In the results shown in figures 6.3 and 6.4 several microwave frequencies are generated, but in a practical system the power of the pump laser would be adjusted to be such that only a single microwave frequency was generated.

6.3 Fibre frequency shifter and linewidth narrowing of BSBS laser

6.3.1 Discretely tunable all fibre frequency shifter

The development of fibre optic based sensor systems[11] has created a need for an all fibre tunable frequency shifter in order that efficient heterodyne signal processing can be effected. Several methods have been reported in which an acoustic wave of wavelength equal to the beat length of the fibre is used to couple a guided optical beam from one mode to another, in either a dual moded fibre (LP_{01} to LP_{11}) or in highly birefringent fibre[12.13]between the non-degenerate LP_{01} modes.The acoustic wave is generated by acoustic horns, acoustic torsional generators or surface acoustic waves[12.14.15]. Although all these devices show promise, the fact that they must operate at fixed frequencies will tend to limit their applicability. In this section, the use of BSBS generated in two high finesse ring resonators in order to realise a tunable fibre frequency shifter in the range 10 - 60 MHz is discussed. This arrangement has the added advantage that it provides complete suppression of any unshifted light.

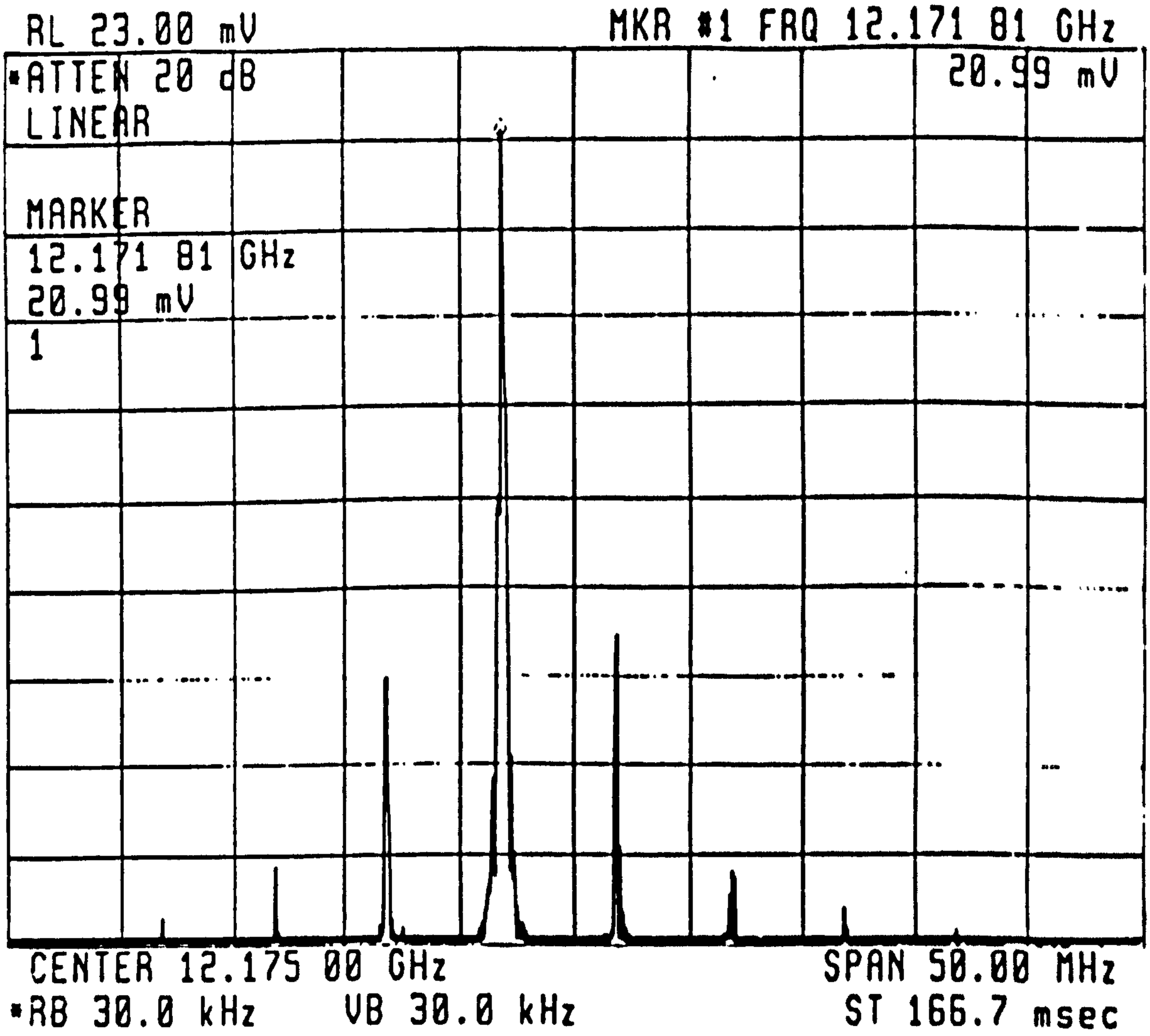

Figure 6.4

The change in optical frequency of the BSBS modes for a temperature difference of 7°C. The shift to 12.17181GHz shown above, compared to 12.16506GHz shown in figure 6.3, indicates a sensitivity of 0.96MHz per°C.

For a typical single mode laser at 633nm the frequency shift is ~30GHz (see chapter 2 section 3) a frequency that is too high for general purpose signal processing. However, an equivalent optical shift in the region 10 - 60 MHz should be achievable by mixing the outputs from two BSBS ring resonator lasers. For BSBS signals generated in long lengths of fibre the beat frequency Δf_B is given by:

$$\Delta f_{BT} = \frac{2(n_1 v_{o1} - n_2 v_{o2})}{\lambda_L} \qquad (6.3.1)$$

and Δf_{BT} is continuously tunable by varying the temperature of one fibre with respect to the other (see chapter 3.6.2). The situation is more complex in the case of mixing the outputs of two BSBS lasers as these lasers can oscillate only at frequencies f_{LN} where the BSBS gain curve coincides with the resonant frequencies of the ring laser cavities. Hence a discretely tunable, variable frequency, all fibre-optic frequency shifter should be realisable by simply varying the temperature of one ring resonator laser with respect to the other. The advantage of this approach is that much lower optical powers, typically <100μW[5], are required for the generation of BSBS in ring resonators; this is in comparison with tens of milliwatts required for its generation in long fibre lengths.

The experimental configuration is shown in figure 6.5. The output beam from the single mode He-Ne pump laser of output power 800μW was initially injected into a monomode fibre of cut-off wavelength 600nm. The beam was launched into two ring resonators fabricated "in-house" through a tunable polished coupler (see appendix A). Ring resonator 1, 2.4m in length (FSR~85.5MHz) was fabricated from Light Wave Technology (L.W.T) fibre, whereas ring resonator 2, 2.36m in length (FSR~87 MHz) was fabricated from York fibre. The finesse of both rings was in excess of 400. Servo controlled piezo-electric stretchers (PZT) were incorporated into each ring resonator such that they could be independently locked at the resonance peak corresponding to the pump frequency. A polarisation controller was included in each resonator to ensure that the SBS laser would oscillate only in one polarisation state. This ensures that the power

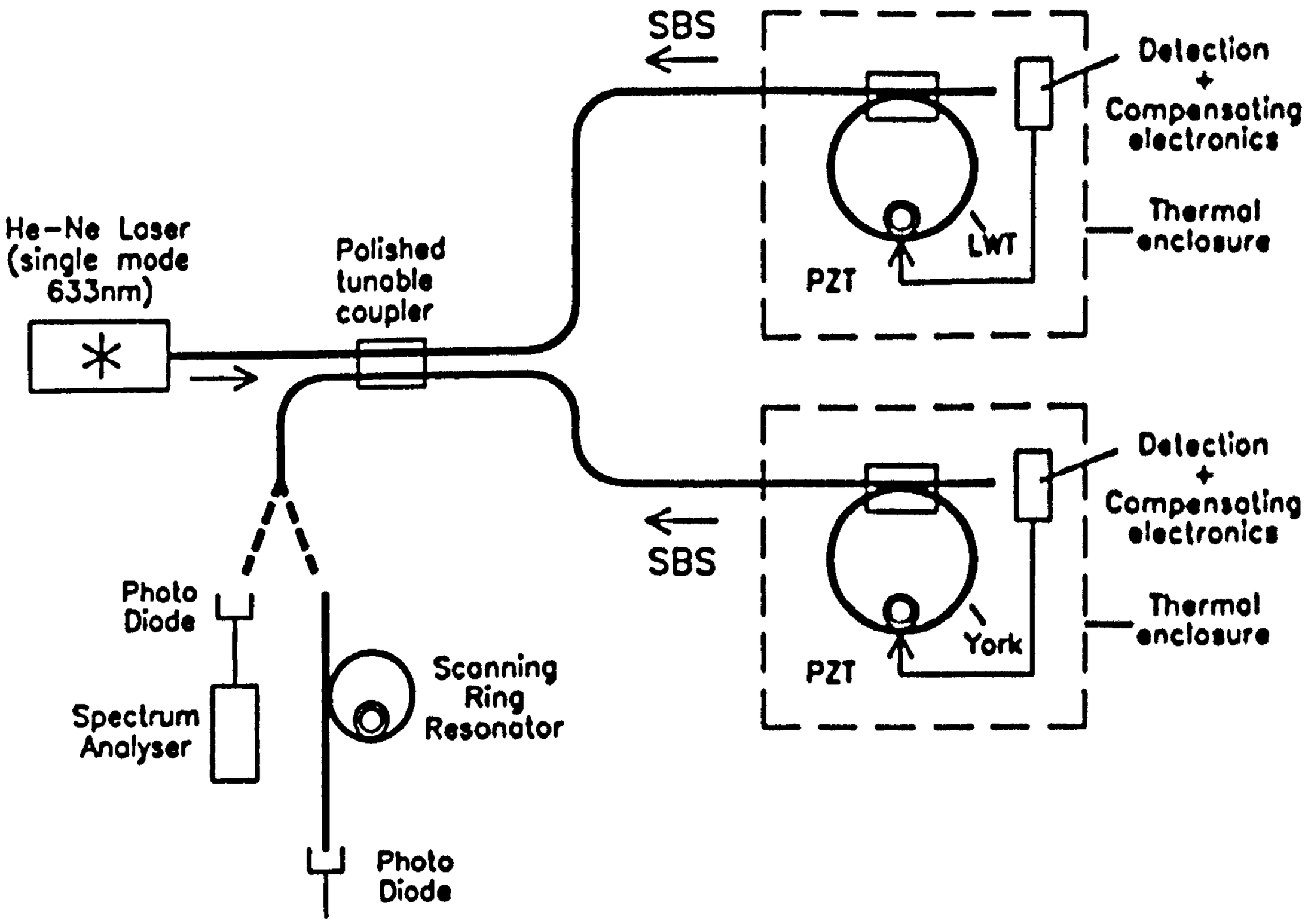

Figure 6.5

Experimental configuration for the all - fibre frequency shifter.

circulating in the ring is at a maximum and hence the SBS threshold is at a minimum. Each ring was placed in a thermal enclosure to maximise frequency stability. For the data shown in figure 6.6, 210 and 280 μW of input power were injected into the rings 1 and 2 respectively. The overall optical efficiency of the fibre network was ~68%, and SBS thresholds were experimentally observed at 140 and 110 μW for rings 1 and 2 respectively.

The backward propagating SBS signals were then transferred by the tunable coupler and subsequently analysed in two ways: first with a photo-diode, the resulting beat note, Δf_{BT}, generated at the photo-diode being detected with a high frequency spectrum analyser, and second by a third ring resonator (finesse 530, linewidth 260kHz), which resolved the generated SBS signal directly in the optical domain.

From the manufacturer's data the values of the indices of the fibre cores were 1.4619 and 1.460; hence the predicted beat frequency from eqn.(6.3.1) is ~35.8MHz at 20°C. The observed beat frequency, figure 6.6, was in fact 20 MHz, indicating that the resonators' frequencies did not coincide with the peak of the SBS gain curve. The beat signal power was ~45μW giving an overall frequency conversion efficiency of ~10%.

To achieve a different beat frequency the temperature of ring 1 was continuously varied relative to that of ring 2, which was held at room temperature. The variation of the beat frequency as a function of the temperature difference of the rings is shown in figure 6.7. The observed behaviour is predictable from the known value, 3MHz/°C[16.17], of the variation of the BSBS gain peak with temperature. A temperature change of ~ 10°C will cause a significant change in the absolute frequency of the BSBS gain peak, causing the fibre ring resonator to mode hop and oscillate at $f_{LN} \pm$ FSR. As anticipated, Δf_{BT} is virtually independent with temperature, undergoing a discrete frequency jump at a finite temperature difference. The slight variation in Δf_{BT} with temperature before and after the mode hop can be attributed to the limitation of the servo. In an ideal experimental arrangement the resonance peaks of the ring resonators would be stabilised by the servo controlled piezo electric stretchers. For small temperature fluctuations this system proved adequate and allowed the rings to be

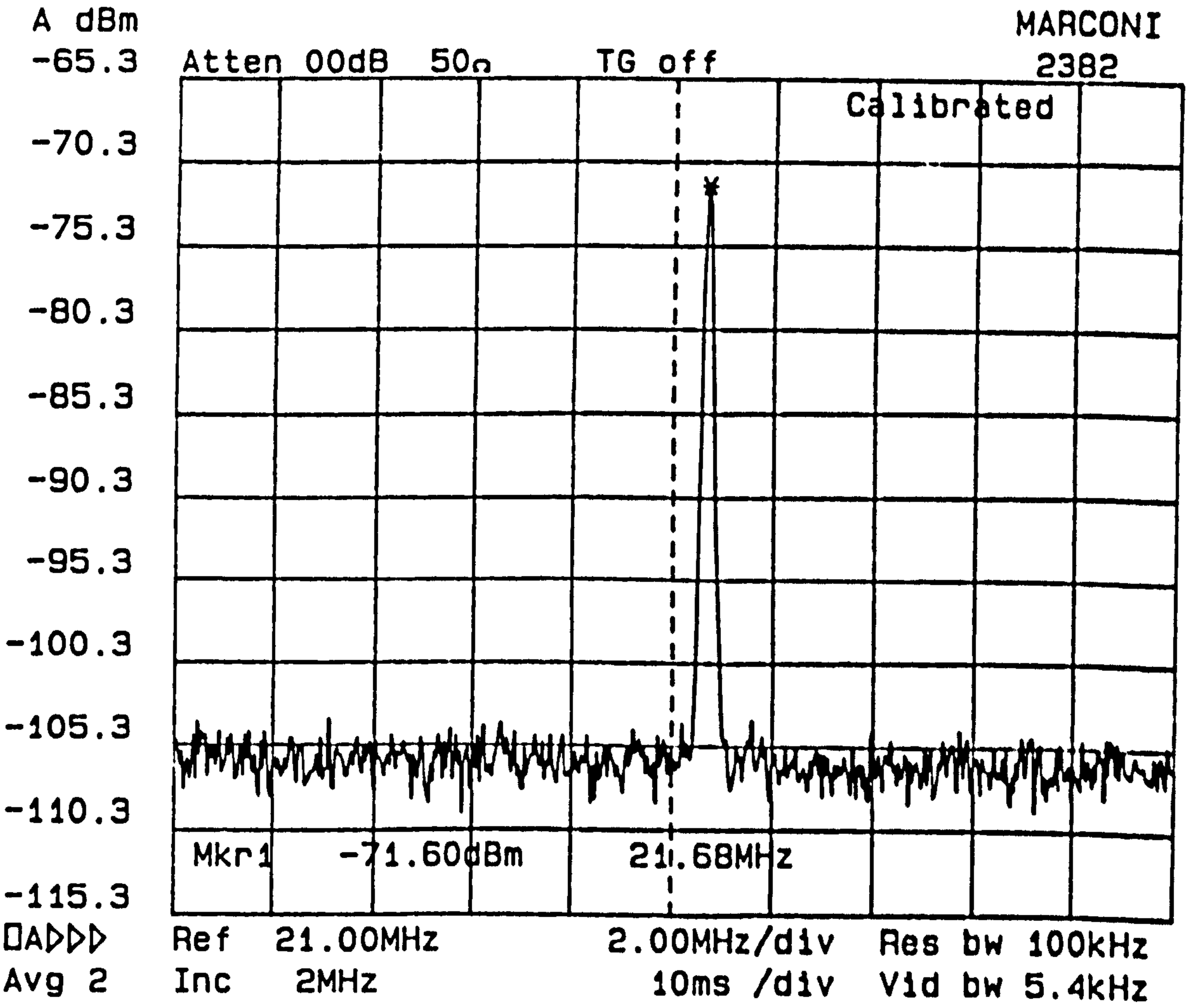

Figure 6.6

SBS beat note generated at 20 MHz by mixing the output from two SBS ring resonator lasers.

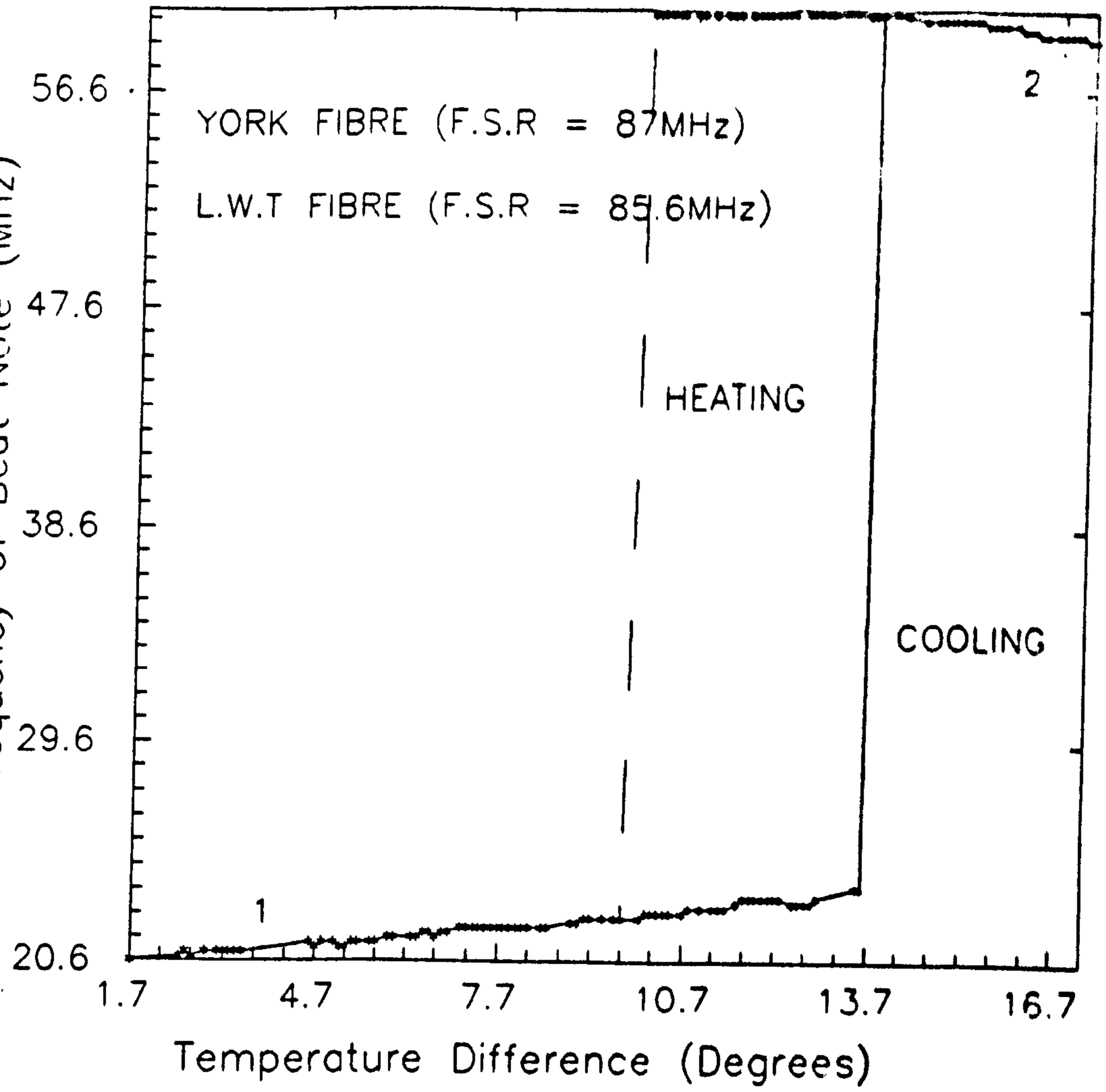

Figure 6.7

Variation of the beat frequency as a function of the temperature difference on the cooling and heating cycles. The frequency jump of 33 MHz was the same whether the ring was heated or cooled; the transition temperature difference, however, was different, being 13.7°C (cooling) and 9.7°C (heating).

locked at resonance for time periods in excess of 20 minutes. However, for the temperature changes imposed on the rings during this experiment it was found that the resonators had to be re-locked every thirty seconds and hence satisfied a new cavity length at each lock attributed to the change in FSR of the resonator for a small change in the refractive index with temperature. The change in refractive index with temperature can be reliably taken to be 1 part in 10^5 per^{o}C[18]. For a BSBS frequency shift of ~27GHz and a ring resonator of FSR~85.5MHz, the downshifted Stokes wave can be expected to appear in the 316th order. Whilst the frequency shift of the gain curve itself increases for increased temperatures (as it is directly proportional to the fibre refractive index) the FSR of the resonator will decrease with increased temperatures as it is inversely related to the refractive index. Hence the beat note can be theoretically expected to show a temperature gradient of 0.27MHz per^{o}C. The positive gradient of the beat note observed before the frequency jump in figure 6.7 is explained by the absolute frequency shift of the Stokes line generated in ring resonator 1 being smaller than that generated in ring resonator 2 at room temperature. Consequently by heating ring resonator 1 the difference between the absolute shifts is increased and this gives a positive temperature gradient. After the frequency jump, however, the absolute frequency shift in ring resonator 1 is greater than ring resonator 2 and the difference between the absolute values will now decrease as ring resonator 1 is heated. The beat note will now show a negative temperature gradient as indicated. The temperature gradient shown in figure 6.7 is observed to be 0.3MHz per^{o}C which is in excellent agreement with the theoretically predicted value. It can also be observed from figure 6.7 that the beat note remains constant at regular intervals. This indicates the success of the servo and its ability to hold the resonator at resonance as it is heated.

A priori it is not possible to predict the value of the new beat frequency as one of the rings is heated, because the absolute value of the SBS gain peak will decrease with temperature; hence the new beat will be either $\Delta f_{BT} = (f_{LN1} + \mathrm{FSR}) - f_{LN2}$ or $\Delta f_{BT}` = (f_{LN1} - \mathrm{FSR}) - f_{LN2}$. Assuming that the temperature of the ring increases in the same sense, all subsequent frequency changes will be equal to the FSR. The data

shown in figure 6.7, where the frequency jump is 33MHz, corresponds to Δf_{BT}`. The spectra observed in the optical domain confirm these results. Figure 6.8 shows the BSBS generated in ring resonator 1. On heating, the Stokes line is clearly seen to shift by ~84.7MHz, i.e. the FSR of ring resonator 1. In figure 6.9 the two BSBS lines are seen to be separated by 21.3MHz ($\Delta T = 4.2°C$) and 58.4 MHz ($\Delta T = 17°C$).

At the transition temperature it was possible to observe two beat signals momentarily, as indicated in figure 6.10, which means that the fibre laser was mode hopping. These experiments were performed several times; the observed behaviour was repeatable and occurred when the ring was heated or cooled.

6.3.2 Linewidth narrowing of BSBS ring resonator laser

The experimental configuration shown in figure 6.5 is a suitable arrangement in which to determine: a) an upper bound optical limit for the BSBS linewidth generated in ring resonator 1, and b) the linewidth of the beat note generated by mixing the BSBS outputs from ring resonators 1 and 2 and resolving the signal electronically.

The optical measurement is made by locking ring resonator 1 at a resonance peak such that the intense circulating pump leads to the generation of a backward propagating BSBS signal. The downshifted Stokes wave is then resolved by scanning ring resonator 3. The result is shown in figure 6.11 where a finesse of 530 is measured and this sets an upper optical limit for the BSBS linewidth. The upper limit is measured to be 260KHz. The explanation for the narrowing of the BSBS signal is given in chapter 4.5.1. This narrowing is found to be a function of the finesse, or the number of circulations of the light in the resonant cavity. A measurement of the beat note, resolved electronically, is attempted in figure 6.12. This measurement is seen to be severely limited by the servos holding the cavities 1 and 2 at resonance. An upper bound limit for the linewidth is seen to be ~10KHz and this is consistent with the results achieved by Smith[19] where a linewidth for the beat of ~3KHz was measured. Hence these results, as expected, confirm that the BSBS signal is narrowed when generated in a fibre ring resonator.

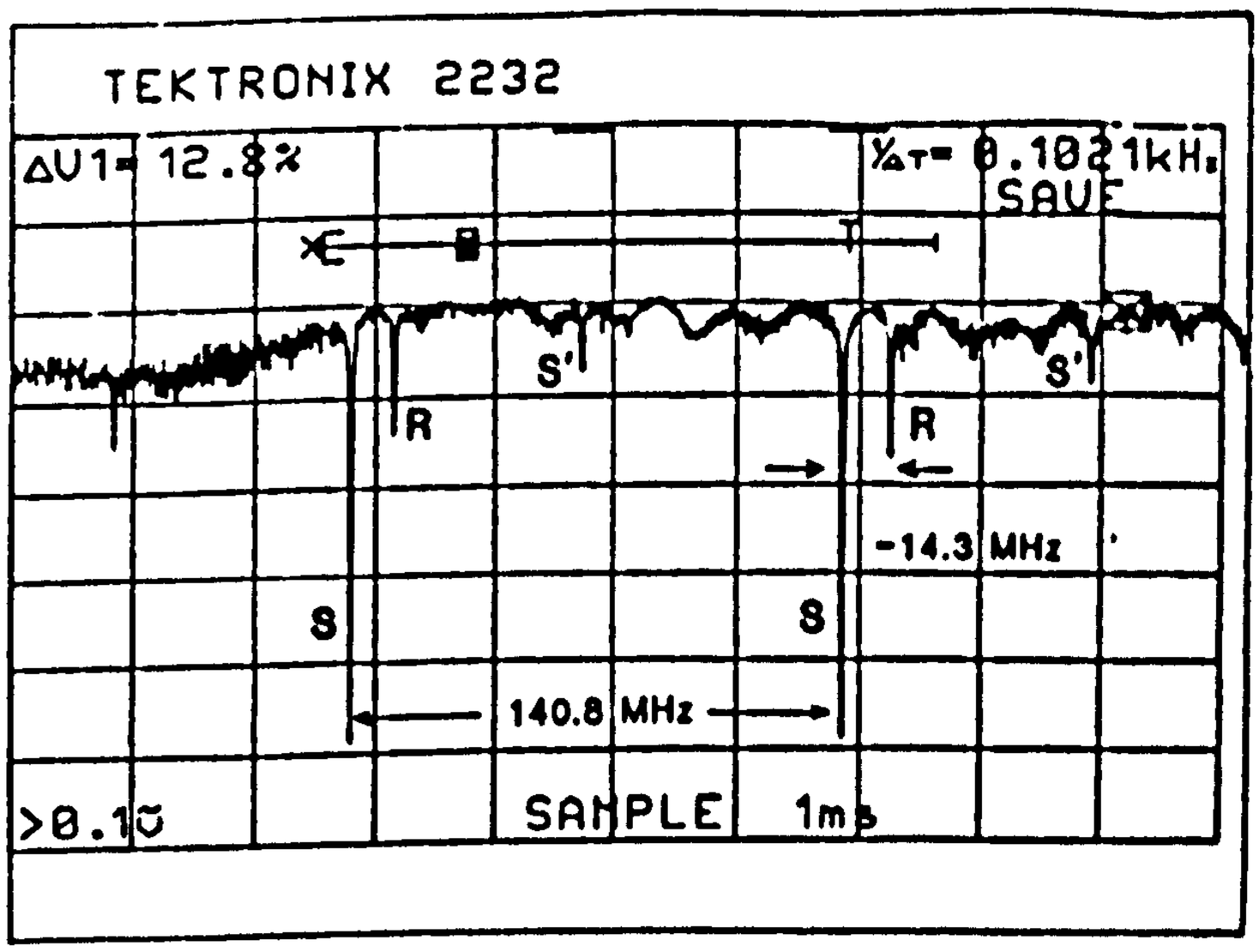

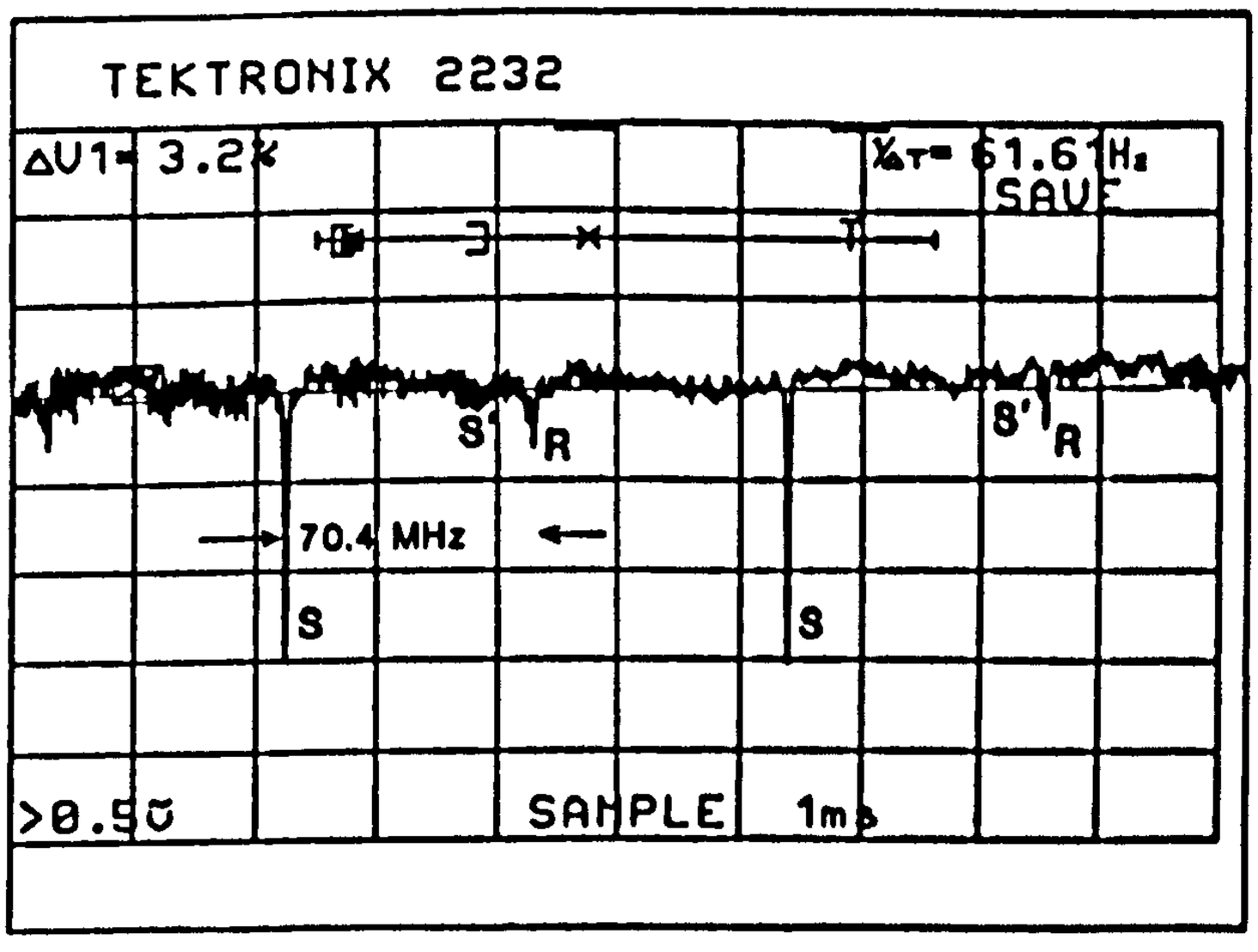

Figure 6.8

Optical spectrum of the SBS signal generated in ring resonator 1 analysed with ring resonator 3, with a FSR of 140MHz: top, before heating when the relative shift of S to R is -14.3MHz; bottom, after heating, when the relative shift from S to R is 70.4MHz, corresponding to a frequency jump 84.7MHz (i.e., the FSR of resonator 1). R, the Rayleigh line; S,S` the SBS signals corresponding to the polarisation modes of the fibre.

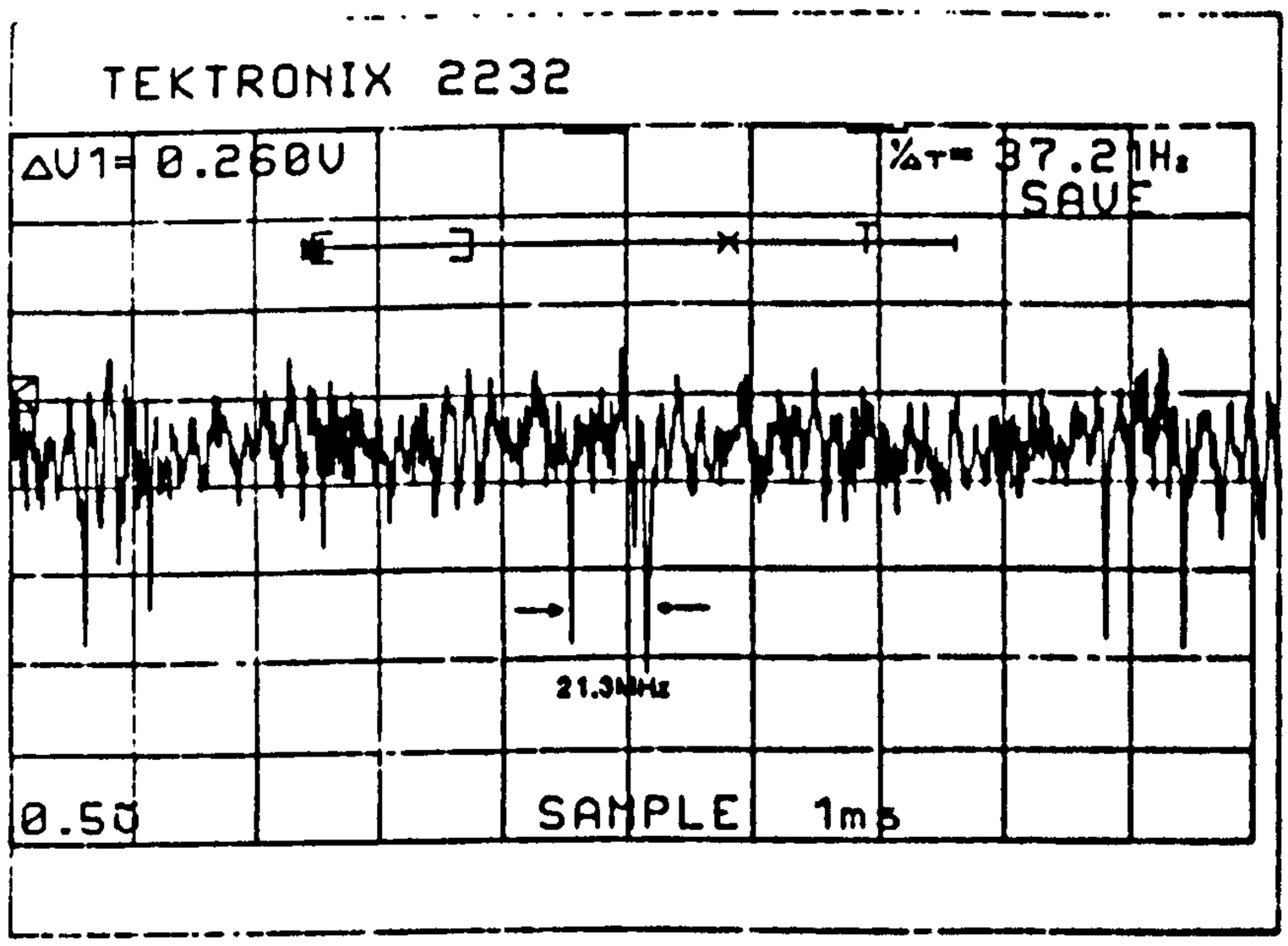

Figure 6.9

The optical spectra of the SBS signal generated in ring resonators 1 and 2. SBS separated by top, 21.3MHz (ΔT = 4.2°C) and bottom, 58.4MHz (ΔT = 17°C), corresponding to points 1 and 2 on figure 6.7.

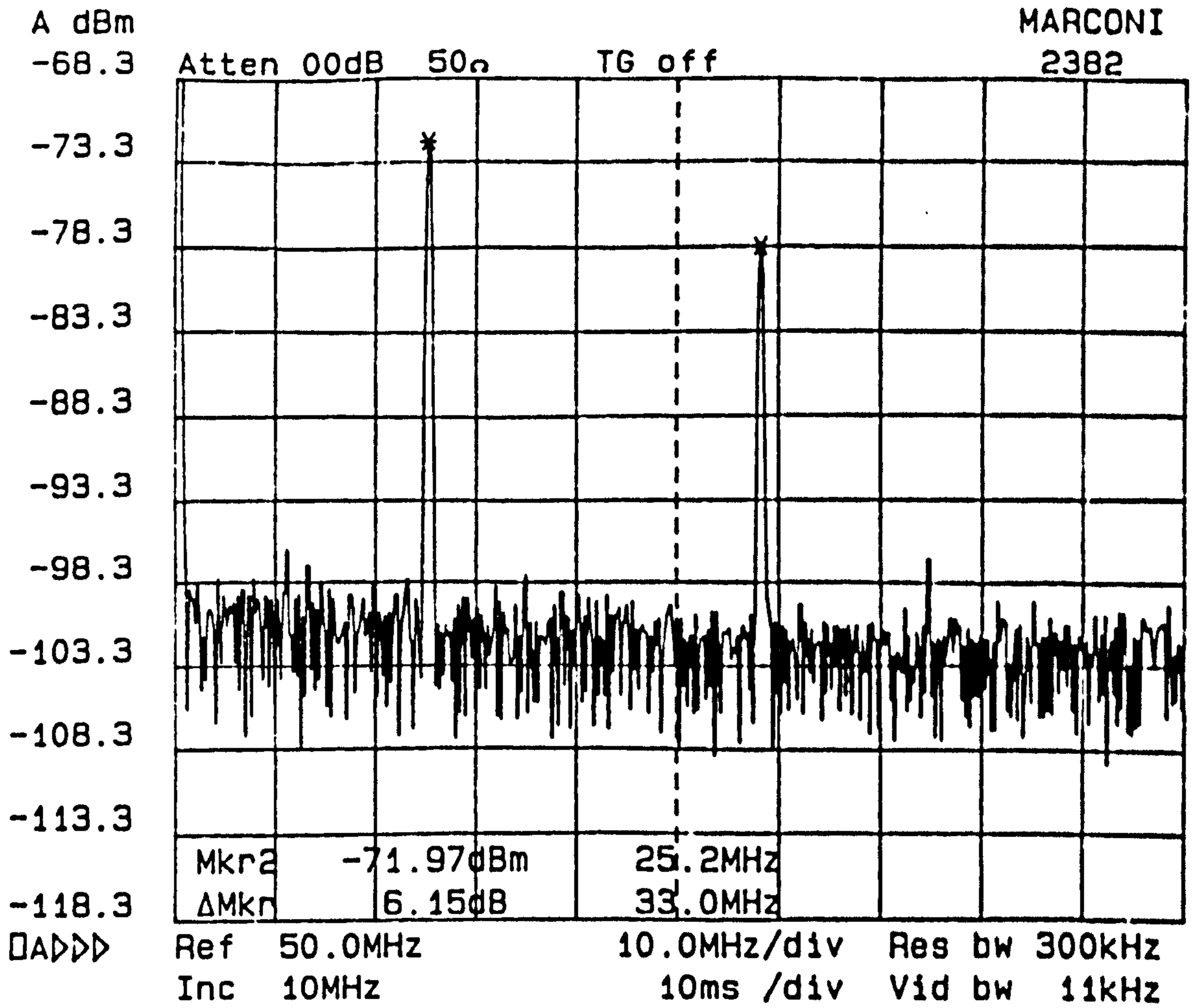

Figure 6.10

Two SBS signals observed electronically at the transition temperature.

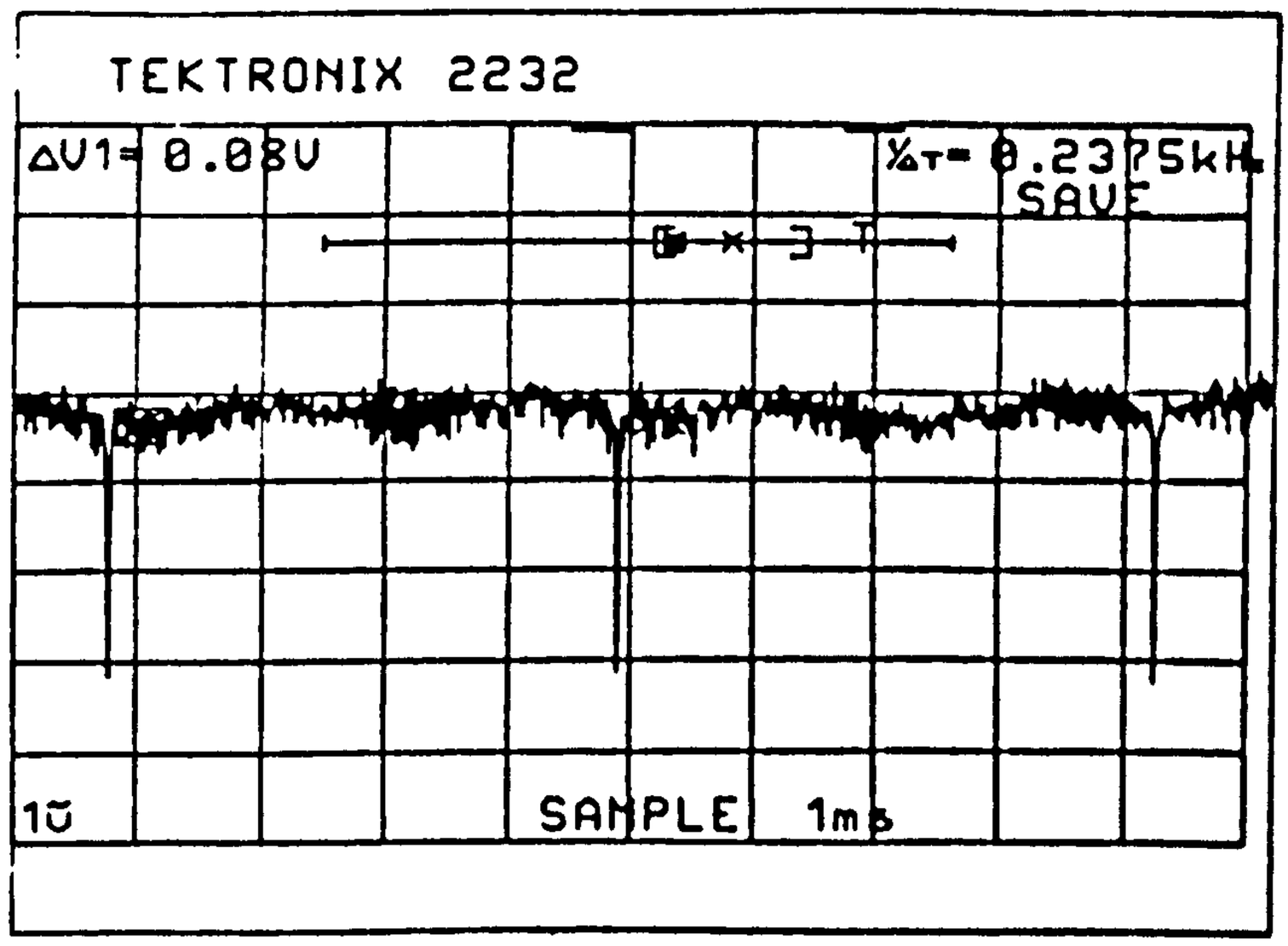

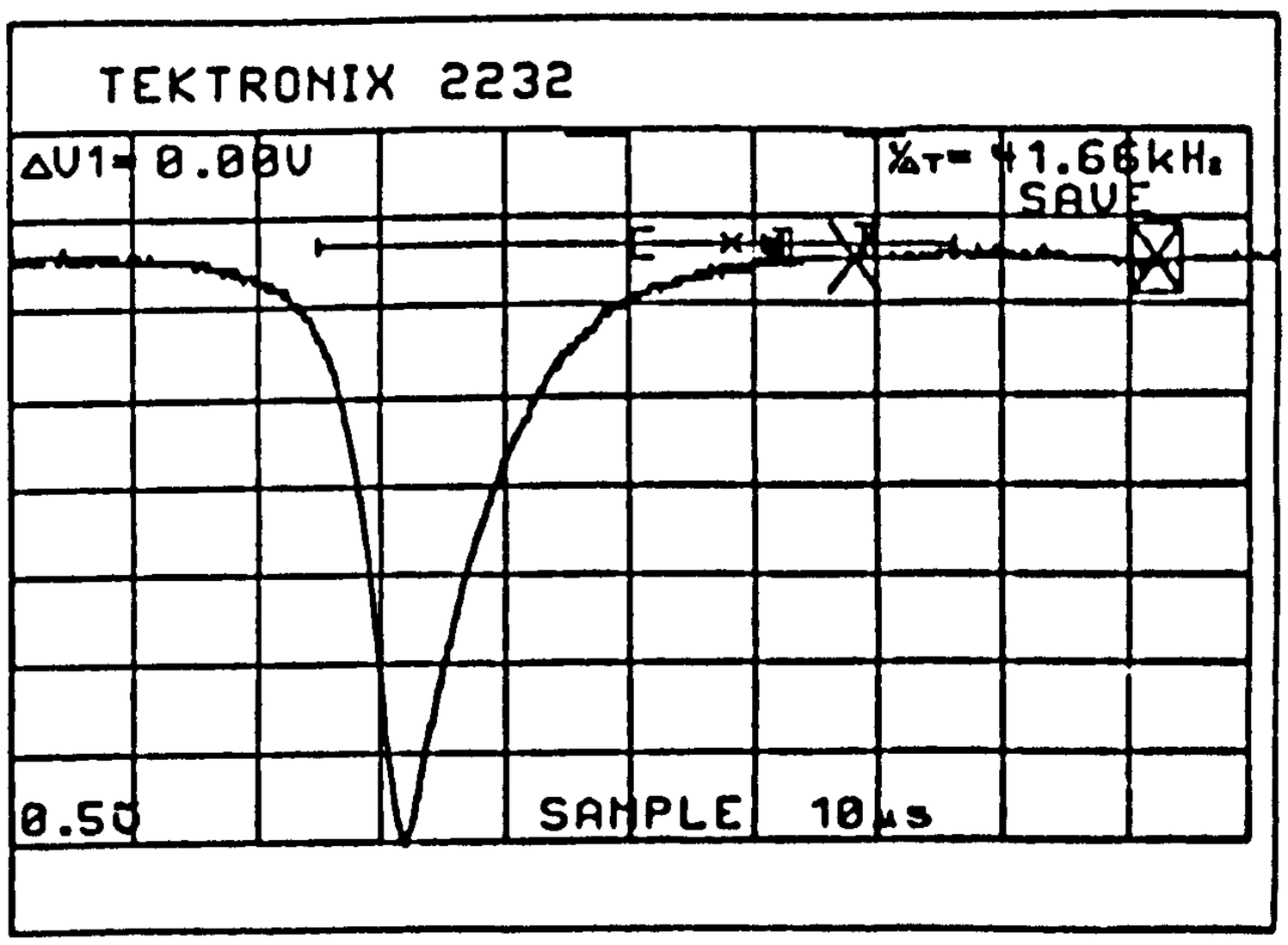

Figure 6.11

SBS linewidth narrowing when generated inside a fibre ring resonator. Upper trace: backward SBS generated by ring resonator 1 (figure 6.5) scanned by ring resonator 3. Lower trace: as above, but on a 10μs per division setting, thus giving a finesse of 530 and an upper bound optical limit of 260KHz for the SBS linewidth.

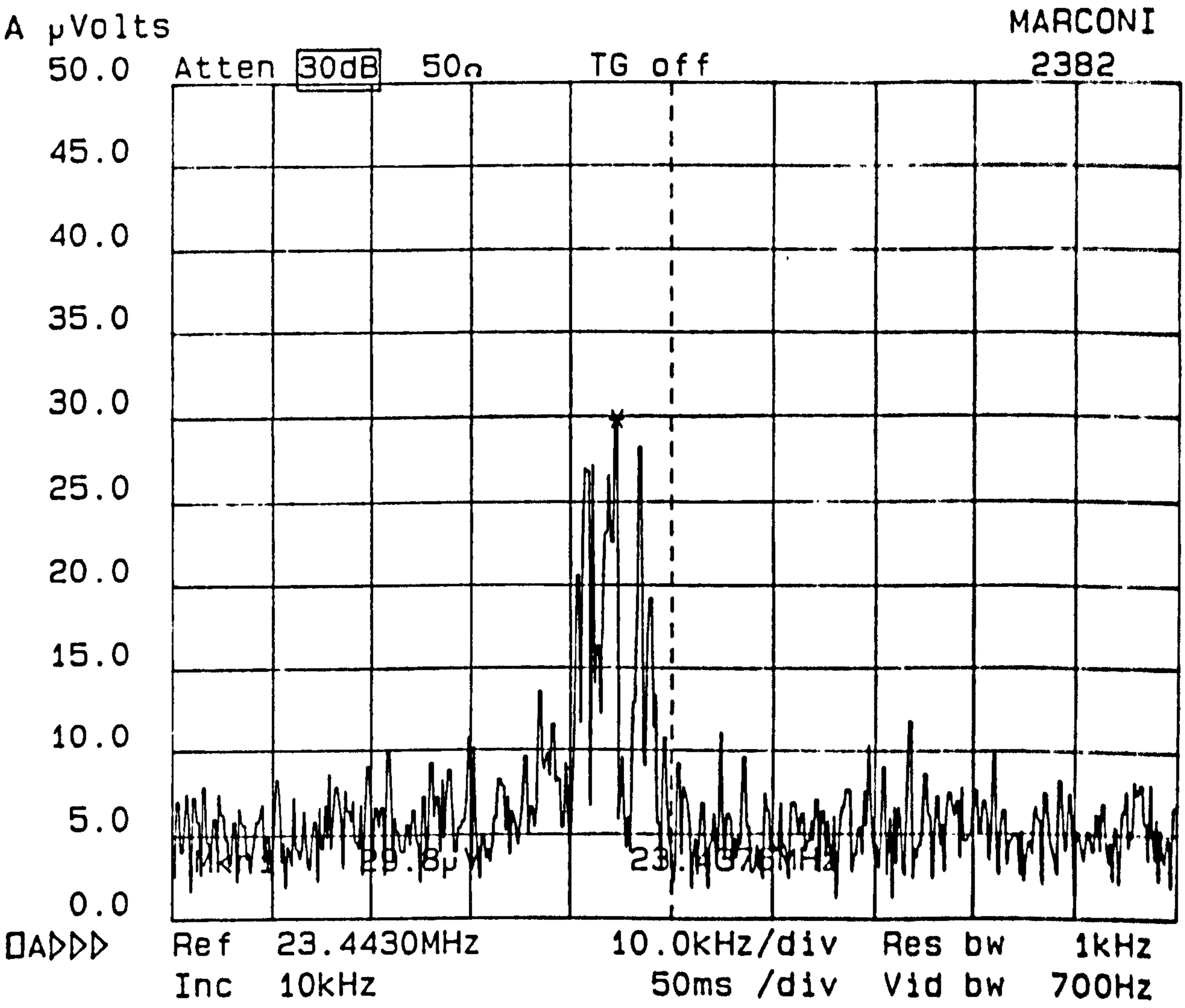

Figure 6.12

SBS beat note, resolved electronically, and generated by mixing the SBS signals from ring resonators 1 and 2. An upper bound limit of 10KHz is restricted by the servo controlled stabilisation of the ring resonators.

6.4 Conclusions

The generation of a continuous microwave signal at 12.16GHz by mixing the outputs of a BSBS ring laser with the original pump source has been demonstrated. The conversion efficiency of the optical pump power into the electronic microwave signal is ~12%. The gain profile of the SBS laser has a halfwidth of ~15MHz and the upper bound limit for the linewidth of the individual mode is <50KHz. By varying the temperature of the resonator the frequency of the microwave signal can be tuned over a narrow frequency range.

Also for the first time, an entirely new topology for an all fibre frequency shifter has been demonstrated. Although the frequency conversion efficiency was only ~10%, increased efficiencies can be anticipated if higher power single frequency lasers are used to generate the SBS signals.

References: Chapter 6

1. Agrawal, G.P.: "Nonlinear Fibre Optics", Academic Press, 1989.
2. Eziekel, S., Davis, J.L., and Hellwarth, R.W.: "Observation of intensity - induced non reciprocity in a fibre-optic gyroscope", Opt. Lett., vol.7, p.457, 1982.
3. Bayvel, P., Halley, J., Kadiwar, R., and Giles, I.P.: "Theoretical and experimental investigation of an all fibre Brillouin laser", ECOC Con. Proc., Pt.1, pp.123-126, 1988.
4. Garmire, E., Pandarese, E., and Townes, C.H.: "Coherently driven molecular vibrations and light modulation", Phys.Rev.Lett.vol.11, p.160, 1963.
5. Smith, S.P., Zarinetchi, F., Ezekiel, S.: "Stimulated Brillouin fibre optic laser gyroscope", Opt.Lett.,vol.16, no.4, 1991.
6. Salles, A.A., and Forrant, J.R.: "Initial observation of optical injection locking GaAs metal semi-conductor field effect transistor oscillators", Appl.Phys. Lett.,vol.38, pp.392-394, 1981.
7. Goldberg, L., Raucher, C., Weller, J.F., and Taylor, H.F.: "Optical injection locking of x-band FET oscillator using coherent mixing of Ga.Al.As. lasers", Elect.Lett., vol.19, pp.848-850, 1983.
8. Lau, K.Y., and Yariv, A.: "Ultra-high speed semi-conductor lasers", IEEE J. Quantum Electron., vol.QE-21, pp.121-137, 1985.
9. Lanzisera, V., Powinik, W., Meland, E., Olshansky, R., and Lauer, R.B.: "15GHz direct modulation bandwidth of vapor phase regrown 1.3μm lnGaAsP buried heterostructure lasers", Conference on lasers and electro-optics, paper WH-3, 21-24, May 1985.
10. Cotter, D.: "Stimulated Brillouin scattering in monomode optical fibre", J.Opt.Comm., vol.4, pp.10-19,1983.
11. Jackson, D.A.: "Monomode optical fibre interferometer for precision measurement", J.Phy.E., vol.18, p.981, 1985.

12. Kim, B.Y., Blake, J.N., Engan, H.E., and Shaw, H.J.: "All fibre acoustic optic frequency shifter", Opt.Lett., vol.11, p.389, 1986.

13. Berwick, M., Pannell, C.N., Russell, P. st J., and Jackson, D.A.: "Demonstration of birefringent optical fibre frequency shifter employing torsional acoustic waves", Electron. Lett., vol.27,p.713, 1991.

14. Risk, W.P., and Kino, G.S.: "Acousto-optic fibre optic frequency shifter using periodic contact with a co-propagating surface acoustic wave", Opt.Lett., vol.11, p.336, 1986.

15. Greenhalgh, P.A., Ford, A.P., and Davies, P.A.: "All-fibre frequency shifter using piezoceramic saw device", Electron.Lett., vol.25, p.1206, 1989.

16. Kurashima, T., Horiguchi, T., and Tateda, M.: "Thermal effects on the Brillouin frequency shifts in jacketed optical fibres", Appl.Opt., vol.29, p.2219, 1990.

17. Pine, A.S.: "Brillouin scattering study of acoustic attenuation in fused quartz", Phys.Rev.,vol.185, p.1187, 1969.

18. Jeunhomme, L.B.: "Single mode fibre optics: principles and applications", Marcel Dekkar, Inc., New York, p.243, 1985.

19 Smith, S.P., Zarinetchi, F., and Ezekiel, S.: "Narrow linewidth stimulated Brillouin fibre laser and applications", Opt.Lett., vol.16, no.6, 1991.

Chapter 7

Conclusions and future work

This thesis is comprised of an experimental and theoretical investigation of stimulated Brillouin scattering in optical fibres. It includes a comprehensive analysis of backward stimulated Brillouin scattering (BSBS) in optical fibres whilst its generation in low loss high finesse all fibre ring resonators is also studied. This has led to various experimental configurations for microwave generation and frequency shifting devices. The more recent phenomenon of intermodal forward stimulated Brillouin scattering (FSBS) in dual moded fibres has similarly been investigated.

It has been verified experimentally that a strong heterodyne beat signal with a narrow linewidth can be produced by mixing two BSBS signals generated in separate optical fibres. The beat frequency is shown to vary rapidly with temperature (5MHz per degree Celsius) and is also shown, as expected, to depend on the physical properties of the fibre. This phenomenon has been exploited in order to demonstrate a discretely tunable all fibre frequency shifter based upon mixing the outputs from two stimulated Brillouin scattering fibre ring resonator lasers. The beat signal in these experiments was 45μW, giving an overall efficiency of 10%. The frequency tuning was achieved by differentially heating the rings and the observed temperature dependence was as expected, with discrete frequency jumps being equal to the FSR of the resonator. Furthermore, a novel tunable method of microwave generation at a frequency ~12GHz, based upon mixing the output from an BSBS ring resonator with the original pump source at 1300nm, has been developed. The efficiency was measured as 12%, i.e. a 250μW (r.m.s) microwave beat signal was generated for 2mW of input optical power injected into the ring resonator.

The use of an all fibre ring resonator as a high resolution optical spectrum analyser has also been demonstrated; an upper limit has been placed on the BSBS linewidth in the optical domain of 260KHz for a pump wavelength at 633nm, a fibre

length of 2.4m and a finesse in excess of 400. This is in contrast to optical resolutions in the order of MHz that can be achieved with Fabry Perot interferometers. Finally the fibre ring resonator has also been used to determine the Lorentzian profile of the spontaneous Brillouin gain spectrum. With the ring resonator fabricated from a 40m fibre loop, (i.e. FSR = 5MHz), and using an optical power density within the resonator such that several modes were excited, the Lorentzian linewidth at 1300nm has been measured as 15 MHz.

Intermodal forward stimulated Brillouin scattering in dual moded fibre has also been investigated for the first time. In contrast to BSBS, where frequency shifts are in the order of GHz, FSBS results in a forward propagating Stokes wave that is downshifted in frequency by typically 17MHz; the wavelength of the acoustic flexural wave in this case is equal to the intermodal beat length between the LP_{01} and LP_{11} modes. FSBS is thus unique in being the only known non-linear effect which is enhanced by decreasing the optical intensity while keeping the power constant. This odd behaviour arises because a) the axial electrostrictive force is independent of the spot size r_{eq} and b) its moment arm increases with r_{eq}. Experiments remain to be done on specially designed fibres with i) the plastic coating removed in order to reduce the acoustic flexural wave loss, ii) a large dual mode spot size (requires small core/cladding refractive index step) and iii) large values of (r_{eq}/a). Attention to these details will greatly reduce the FSBS threshold power level.

Appendix A

Fabrication of the directional coupler and ring resonator

A.1 Introduction

The single mode all fibre ring resonator has important practical and potential uses. For example they can be used as an all fibre resonator interferometer[1], as a passive fibre gyroscope[2,3] and as an all fibre ring laser[4]. This last example is more fully described in chapter 4 whilst the application of the SBS laser and its exploitation in order to realise both microwave generation and frequency shifting devices has been described in chapter 6.

The resonator studied in the forementioned chapters is the same as that studied by Stokes et al[1,4] and requires a single mode directional coupler whose coupling coefficient is close to unity. A schematic of such an optical fibre ring resonator is shown in figure 4.1 where it is shown, with the application of a low loss coupler, that a fibre ring can be closed in a low loss manner. However, the nature of the all fibre coupler places tight tolerances on these components because of the small diameter of the fibre core. This appendix reports the development of a direct fibre-fibre directional coupler which transfers a desired fraction of the power from one single mode fibre to another while preserving the propagation direction. It is a four port junction and is the fibre analogue of an optical beam splitter. The coupling of optical power between two parallel fibres is made possible by the evanescent fields which extend just outside the fibre cores[5]. Much of the cladding must be removed to bring the fibre cores sufficiently close to cause the fields to overlap. For this purpose etching techniques have been proposed by Giallorenzi[6], but here a mechanical lapping technique is described which has the added advantage of retaining most of the cladding for mechanical stability and durability. The manufacturing process is described in section A.2 and the experimental results are given in section A.3. In sub-section 3.1 the "oil drop experiment" in order to

monitor the depth of polishing to the core/cladding interface is discussed whilst in sub-section 3.2 the tuning characteristics denoting the coupled power as the two coupler halves are transversely moved across one another is shown. The tuning characteristics for different oil indices is included in sub-section 3.3. Finally, in subsection 3.4 the application of the directional coupler such that a single length of single mode fibre can be closed in a low loss manner in order to demonstrate an all fibre ring resonator is shown. Conclusions are drawn in section A.4.

A.2 Manufacturing process of the fibre directional coupler

The technique is straightforward in principle, but requires care in practice. The optical fibres are first stripped of their jackets such that the exposed cladding sits neatly into a groove cut in a silica glass block, see figure A.1. The groove is 140μm in depth at the centre of the block, but deeper at the edges as the slot is cut with a concave downward curvature and this imparts a curvature to the path of the fibre as shown. The radius of curvature is ~25cm and controls the length of the interaction region[7]. It should be cut with a diamond impregnated saw as this ensures the cut is smooth and free from jagged splinters of glass. The dimensions of the blocks are shown in figure A.1, but 2-3mm of the jacket should protrude either side into the block in order to secure the final device. A quick set epoxy is then used to glue the fibres at the end of the blocks and then left for 24 hours before a suitable glue is applied in order to bond the fibre cladding to the block. The glue should be hard and like the quartz block polish at roughly the same rate as the fibre. Electronix ND351, a heat curing resin, proved to be the most suitable glue and boro silicate glass (not soda glass) the best material in order to support the fibres. The glass block was secured at the base of the Logitech polishing machine by using a soft dental wax which had previously been heated and then allowed to cool. The block was then ground by using a Logitech lapping plate (composed of iron) and lubricated with a cerium oxide solution and which has a particle size of ~10μm. The substrate is first ground to within a few microns (typically 15 μm) of the

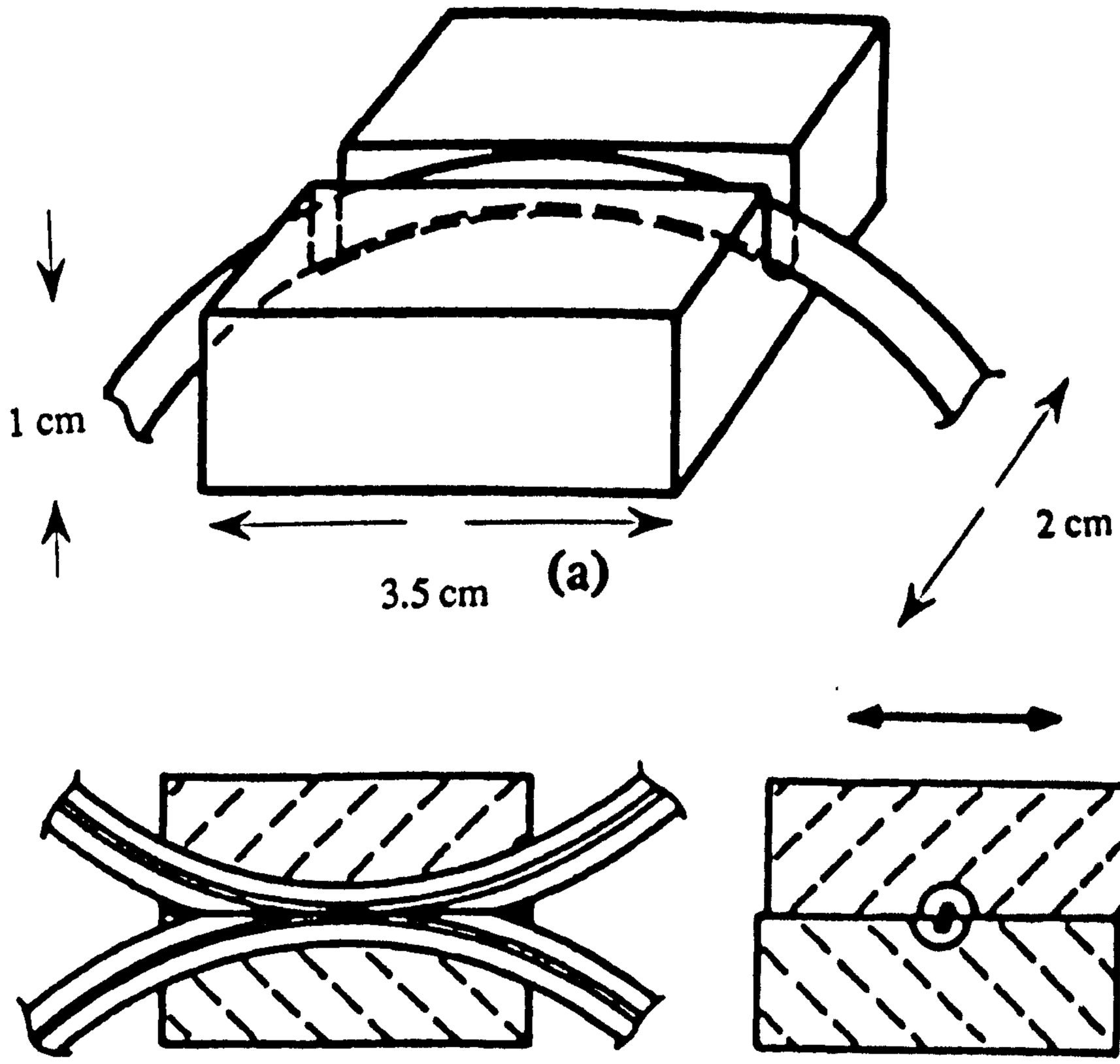

Figure A.1

Geometry of the curved-fibre optical coupler showing (a) the position of the fibre in its quartz substrate and (b) a longitudinal and transverse cross section of the assembled coupler.

core/cladding boundary. This corresponds to the polished region, which polishes down in the form of an ellipse because of the concave nature of the groove, being approximately 9mm in length and is measured with a travelling microscope. The lapping plate is then exchanged for a polyeurothane polishing wheel and a smaller particle lubricant, an opaline grade solution of particle size 1 micron. This powder breaks down with time to a third of its original size during the polishing process and ensures a smooth finish at the end of the polishing stage. Other solutions such as syton with a smaller particle size exist, however, they were found to crystallise and destroy the final product. The coupler half is then further polished until the core/cladding thickness has the desired value. This thickness, crucial to the fabrication of the all fibre ring resonator, was determined via an oil drop experiment. The liquid drop method involves measuring the throughput attenuation in dB's when a drop of liquid is placed on the polished section of the fibre. A throughput attenuation is observed providing the evanescent field has been exposed as result of polishing close to the core/cladding boundary. The measurement is time consuming and requires laser light to be launched into the fibre and monitored at the output with a detector; measurements are continuously made as the fibre is polished. Ideally one requires a maximum attenuation of the throughput and this is best achieved by first trying a range of oils from $n = 1.455$ to 1.465. The best oil will be the liquid which has a refractive index, n_{eff}, of the fibre guided mode. For this case the velocities of the bulk optic wave in the liquid and the guided wave in the fibre are identical and the guided wave is coupled out of the fibre. For lower indices the liquid still acts as a mode stripper, but with a reduced efficiency. In these experiments an oil with refractive index $n = 1.46$ was found best at $\lambda_L = 633$nm. The fibre used was York Technology single mode lo-bi fibre. It should also be included that the refractive index of the oil changes with temperature which can have a dramatic effect on the final result and so should always be done at room temperature. This and the oil drop experiment are discussed in section A.3. For the the cross coupled ring resonator discussed in chapters 4 and 6 the oil drop experiment should give ~32dB attenuation of laser light into the oil in order to give a coupling ratio tending to unity

when the coupler halves are finally mated. Although the process can be time consuming, the result is very accurate. In practise a resonator will take between 2-3 days to fabricate once the technique has been learnt; this took me just less than 1 year.

Once the manufacture of a directional coupler with a coupling efficiency tending to unity can be achieved, it is then possible to apply the same manufacturing process to two blocks, but on the same length of fibre. The single mode fibre can then be closed in on itself as shown in chapter 4 figure 5 in order to realise a high finesse all fibre single mode resonator. The result is shown in figure A.6

A.3 Experimental results

A.3.1 The oil drop experiment

The change in the attenuation of the coupler half as the material is removed is shown in figure A.2. These results were achieved using a 633nm He-Ne laser and monitoring the attenuation of the fibre output before and after an oil of refractive index equal to the fibre guided mode (see section A.2) was placed on the polished region. The fibre has an outside diameter of ~125μm and a concentric core diameter of ~4.6μm and was held in a 25cm radius of curvature cut in a boro-silicate glass block. As can be seen from figure A.2, there is no attenuation until a critical point approximately 6μm from the core cladding interface. From this point the index oil acts to strip the light from the evanescent field. As further cladding is removed the attenuation steadily increases until all of the light appears to be coupled into the oil. The attenuation was found to be independent of the film thickness for a refractive index $n = 1.46$. Hence from these results there is a well defined relationship between the amount of cladding material removed and the attenuation of the half coupler when an index matching oil is applied[7]. At three stages of throughput attenuation of light into the oil, i.e. 5dB, 35dB and 40dB, the two coupler halves were mated and tuning curves taken. These results are shown in subsection 3.2.

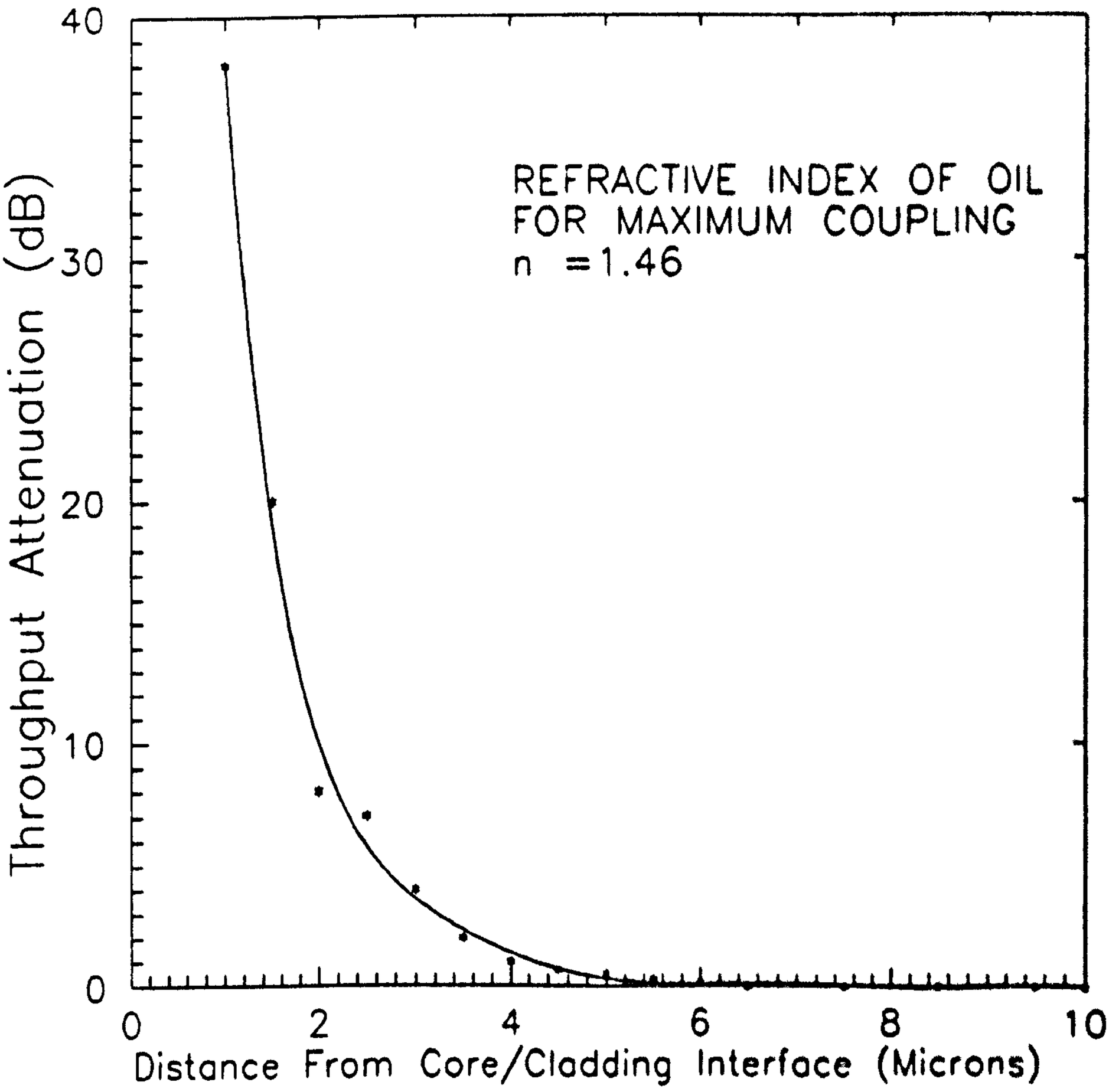

Figure A.2

Throughput attenuation measured as a function of the distance from the core/cladding interface. An oil of refractive index $n = 1.46$ is placed on the polished region and the amount of cladding removed from the fibre cross section recorded. Coupling curves at three stages (5dB, 35dB and 40dB) are recorded in figures A.3 and A.4.

A.3.2 Tuning curves

In section A.2 an oil of refractive index equal to the core was described in order to achieve maximum coupling into the oil. For the purpose of tuning the two coupler halves, an oil index between that of the core and cladding is necessary in order that the light can be most efficiently coupled from one coupler half to another and reduce what would otherwise exist as a loss in the device. Lateral translation (see figure A.1b) of the upper substrate is also made easier by the intermediate layer of liquid and its movement is accurate to 0.5 microns because of the differential micrometers providing smooth and easy adjustment. Their movement also provides an artificial means of varying the core to core spacing. The tuning curves are for the same fibre parameters previously described. After carefully aligning the fibres parallel to each other and superposed, the top fibre was translated parallel to itself by a few microns until the coupled power vanished. It was then translated step by step backwards then beyond the bottom fibre and both coupling data and lateral fibre position recorded. The three tuning curves taken are shown in figures A.3 and A.4, and each is applicable to a throughput attenuation monitored in figure A.2. Figure A.3 illustrates a maximum coupling coefficient of 100% and is an over coupler and corresponds to a throughput attenuation of 40dB as shown in figure A.2. Whilst a coupling coefficient tending to unity can be satisfied with this device, it will be too lossy and have implications on the finesse when configured as a ring resonator. Also, because of the large number of coupling points satisfying 100% coupling it will be very sensitive to tuning. In figure A.4(b) the data points for an under coupler corresponding to 5dB attenuation of light into the oil in figure A.2 is shown. This illustrates a maximum coupling coefficient of 8% and falls far short of the desired 100% coupling coefficient needed. However, in figure A.4(a) data for a coupling coefficient tending to unity is shown (in fact it is marginally an over coupler) and corresponds to a throughput attenuation of 35dB when an index of $n = 1.458$ is inserted between the coupler halves as illustrated in figure A.2. The loss measurements for various tuning positions are also clearly shown and the data from figure A.2 indicates that the cladding is polished until ~1μm from the core/cladding interface. The

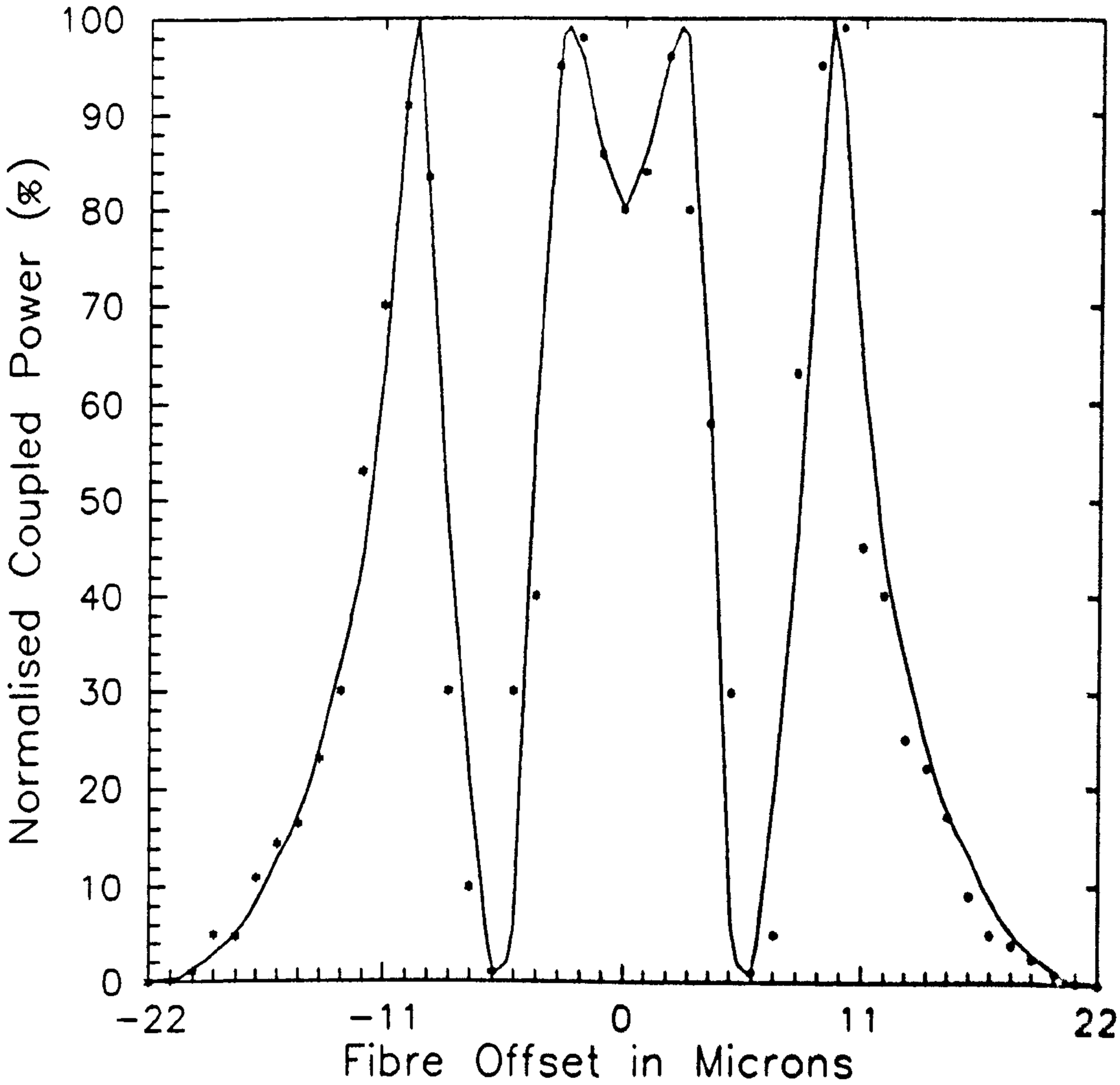

Figure A.3

Tuning curve representing the normalised coupled power as a function of the fibre offset in microns. The curve is characterised by 40dB of attenuation of light into the oil as measured by figure A.2, and the oil used for tuning has refractive index $n = 1.458$. A directional coupler of this kind would make a ring resonator difficult to tune and more importantly of low finesse because of the high insertion loss attributed to polishing too close to the fibre core.

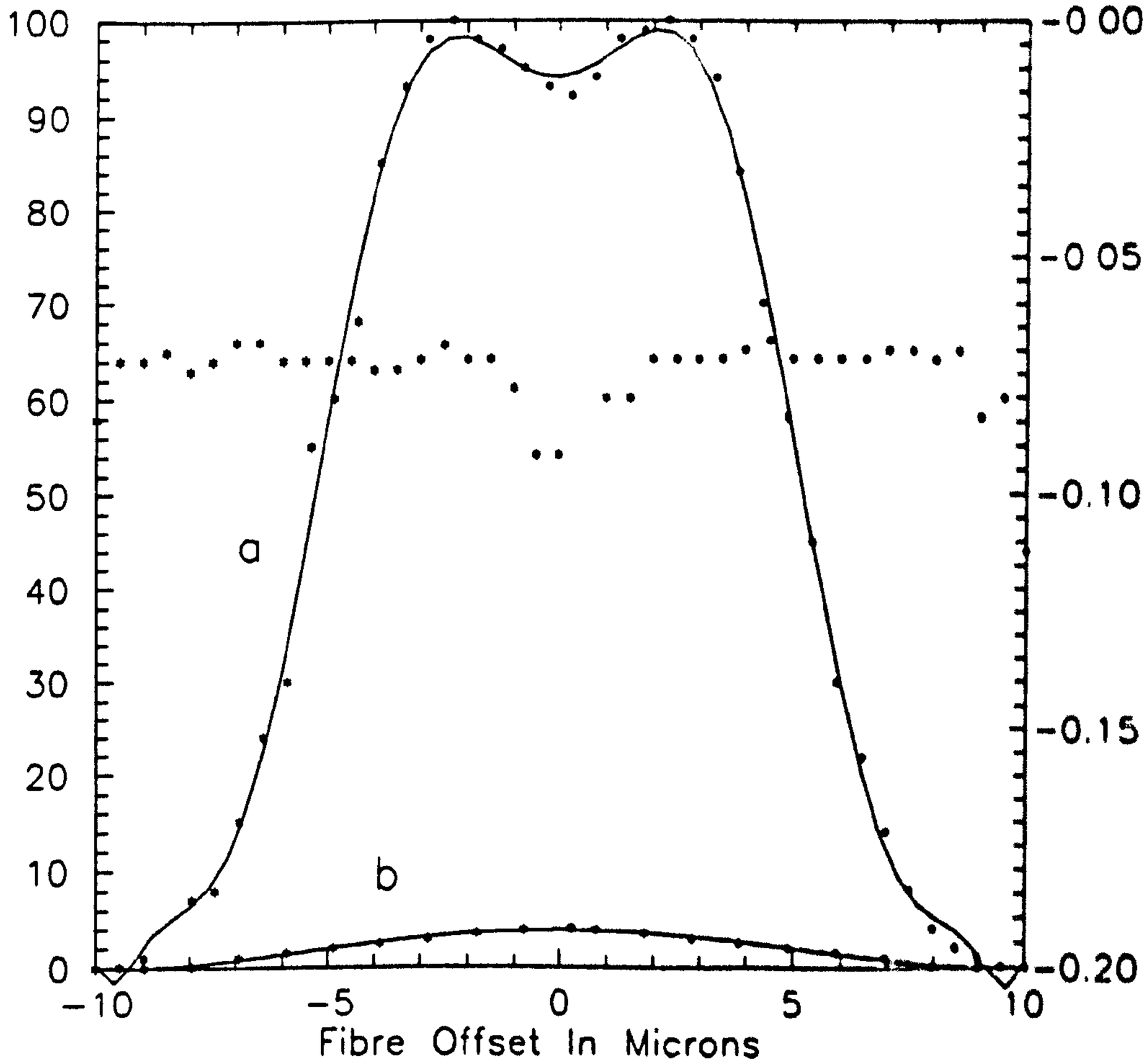

Figure A.4

Tuning characteristics as the upper block of a directional coupler is translated across the lower block: figure (a) indicates a 100% coupler (slightly an over coupler) and corresponds to 35 dB attenuation of light into the oil as measured in figure A.2. The coupler loss for this curve is also indicated. Figure (b) illustrates an under coupler and corresponds to 5 dB attenuation of light into the oil in figure A.2. Figure (a) demonstrates the coupling necessary to realise a low loss high finesse ring resonator whilst (b) would not satisfy a coupling coefficient tending to unity.

value of the index oil used for tuning can be changed providing it is within the limits set by the core/cladding boundaries. A higher refractive index oil will strengthen the coupling ratio and a lower refractive index oil will weaken the coupling ratio. Consequently should the coupler halves be slightly over or under polished then fine tuning in order to obtain the necessary coupling ratio can, to some extent, be achieved by changing the refractive index of the tuning oil. Coupling can be further enhanced by applying pressure on to the coupler halves in order to improve the fibre contact and in practice this is often necessary.

A.3.3 Refractive index oil used for tuning

Since the layer of index matching oil present between the two substrates seemed to play a significant role in the coupler behaviour, it was interesting to investigate the influence of the liquid refractive index on the coupling characteristics in more detail. Rather than trying different oils and the possibility of encountering reproducibility problems in the mating of the fibre substrates, it was preferred to modify the liquid index by changing its temperature which was made relatively easy by the large $\Delta n/\Delta T$ of most liquids, i.e. the large change of refractive index, Δn, with a change in temperature, ΔT. Temperature measurements were performed in the following manner. The fibre coupler assembly was set on a hot plate provided with a temperature control and covered with a thermal isolator to minimise temperature gradients within the substrates. A thermo-couple temperature gauge was placed against the bottom substrate and connected to a digital read out. A light signal (λ_L = 633nm) probed the coupler as the temperature was changed from room temperature up to 40°C. To eliminate thermal effects the coupler was aligned to produce maximum coupling at each temperature increment to neutralise any mechanical induced lateral offset. Data was taken along the cooling cycle for the coupler displaying a 100% coupling ratio as it was slower than the warming cycle. As expected, it was observed that the maximum coupled power increased as the temperature decreased from ~40°C to room temperature (figure A.5). A temperature increase of the liquid reduces its refractive index which in turn reduces the

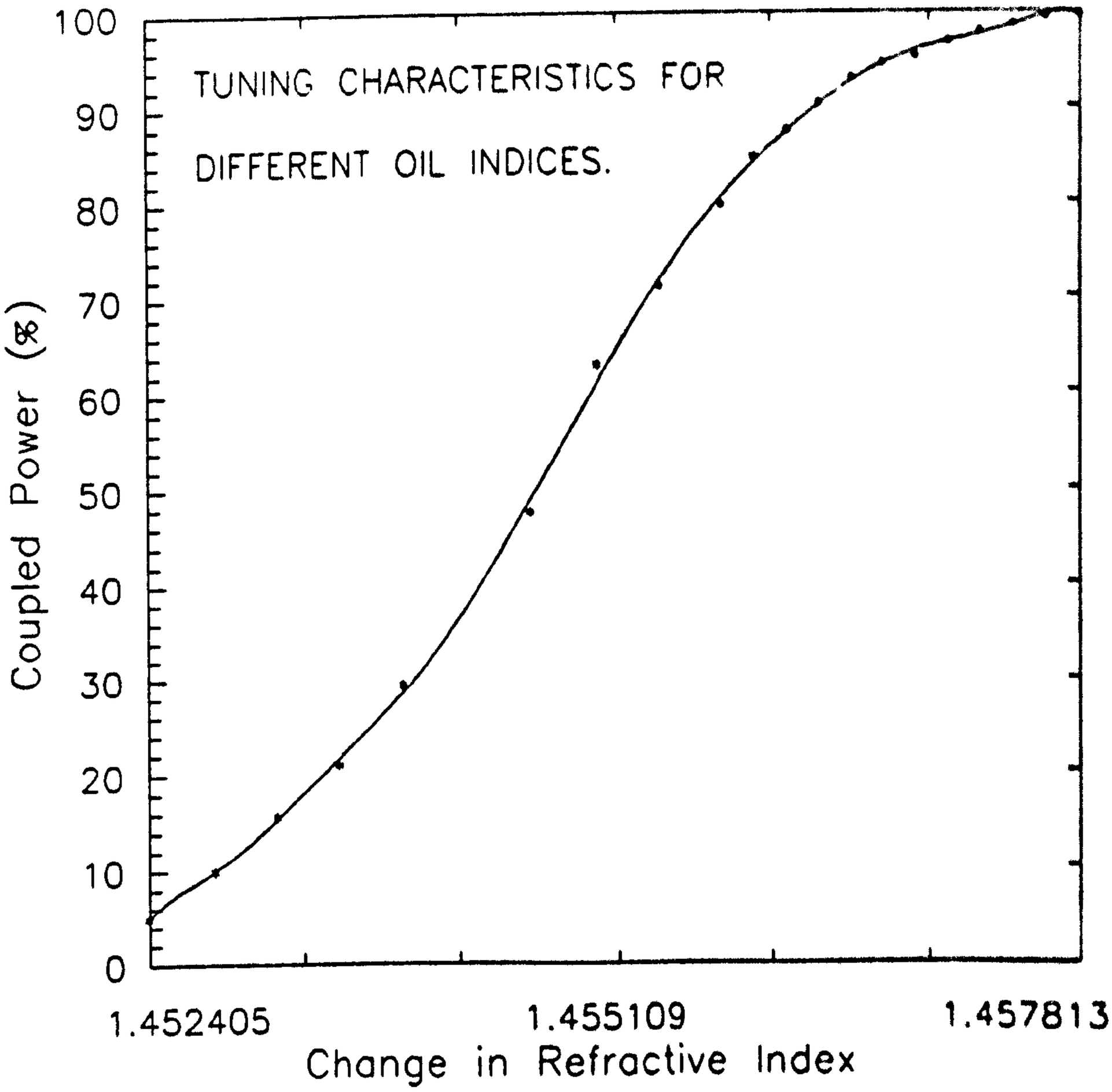

Figurre A.5

Tuning characteristics for the directional coupler using different oil indices for tuning. Coupling is optimised when the refractive index of the oil lies within the boundaries of the core and cladding. Whilst lower indices, as indicated, reduce the efficiency of coupling, greater indices increase the lumped loss of the device as more light is then scattered into the oil.

penetration depth of the fibre mode into the neighbouring waveguide and thereby lowering the coupling strength of the coupler. Such an effect is noticeable over a relatively small temperature gradient because of the large temperature dependence of the liquid index ($\Delta n/\Delta T \sim 4\text{x}10^{-4}{}^{o}\text{C}^{-1}$).

At this stage, having established the appropriate oil for the oil drop experiment at $\lambda_L = 633\text{nm}$ ($n_{eff} = 1.46$), the correct depth of polishing (32dB attenuation of light scattered into the oil) and the appropriate oil for tuning ($n = 1.458$) a position is now reached whereby a single length of fibre can be closed on itself in a low loss manner in order to form a resonant cavity. These results are explained in section 3.4.

A.3.4 The all fibre ring resonator

The experimental configuration given in figure 5 chapter 4 is for a cross coupled ring resonator of length 2.4m and which was fabricated from York lo-bi fibre and which has a 4.6μm core diameter. As shown part of the length was wound around a piezo-electric cylinder that can expand radially to modulate the phase. A polarisation controller consisting of two rotatable fibre loops, each acting as a 1/4 wave plate, was used to counter any birefringence induced in the ring resonator. Thus the polarisation entering the coupler from laser port 1 and the fibre ring, port 2, will be the same. A single frequency long coherence He-Ne laser ($\lambda_L = 633\text{nm}$) was used to excite the resonator. A low frequency triangular wave (50Hz) was applied to the phase modulator and the output of port 4 was monitored by a photo-diode. In this way the fibre resonator behaves like a scanning Fabry Perot interferometer. The oscilloscope trace shown in figure A.6(a) shows the resonant behaviour, output dropping to zero, twice during each linear stretch of the fibre. The observed finesse can be easily determined from figure 6(b) and shows a finesse of 180. The theoretical explanation for the all fibre ring resonator is clearly explained in chapter 4.

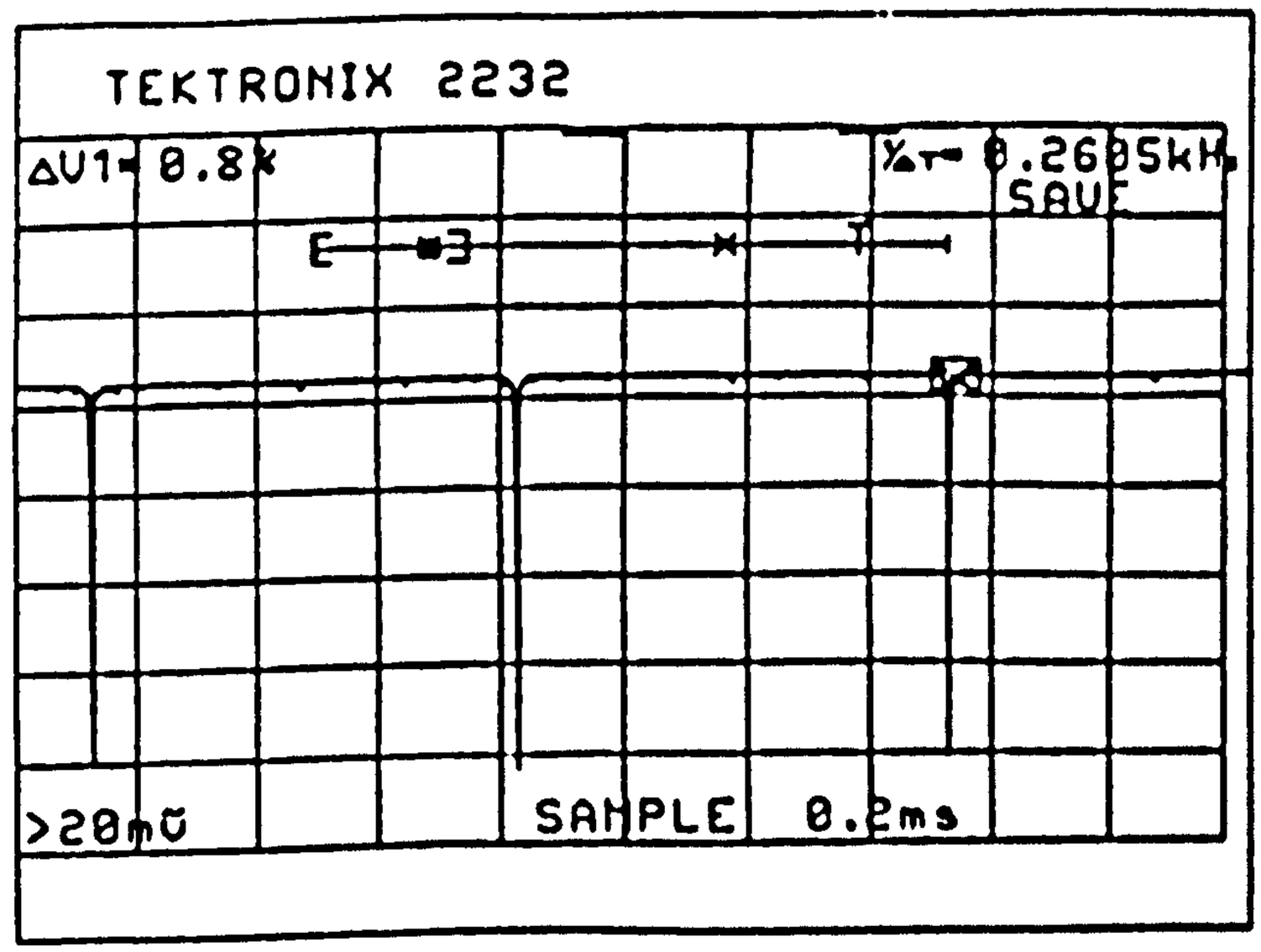

Figure A.6

Upper trace: transfer function detected at the output of a scanning fibre ring resonator. The resonance dips to zero twice during each cycle. See chapter 4 for more details. Lower trace: as above, but with the oscilliscope on a 20μs time scale. This allows the full width at half maximum for the resonance dip to be calculated such that the observed finesse for the device can be calculated to be ~180.

A.4 Conclusions

The aims of this appendix have been clearly defined as the manufacture of an all fibre ring resonator. A more detailed and theoretical investigation of the all fibre ring resonator and the implications of the directional coupler loss and a varying coupling coefficient are dealt with in chapter 4. Although the all fibre ring resonator has many applications, its principal applications to this thesis are the exploitation of the high circulating power densities in order to generate SBS and also as a spectrum analyser on account of the high resolutions that can be reliably achieved.

References: A.1

1. Stokes, L.F., Chodorow, M., and Shaw,H.J.: "Sensitive all single mode fibre resonant ring interferometer", IEEE J.Lightwave Technol., vol.LT-1, pp.110-115, 1983.
2. Mayer, E., Ezekiel, S., Stowe, D.W., and Tekippe, V.J.: "Passive fibre optic ring resonator for rotation sensing", Opt. Lett., vol.8, pp.644-646, 1983.
3. Bergh, R.A., Lefevre, H.C., and Shaw, H.J.: "An overview of fibre optic gyroscope", IEEE J.Lightwave Technol., vol.LT-2, pp.91-107, 1984.
4. Stokes, L.F., Chodorow, M., and Shaw,H.J.: "All fibre stimulated Brillouin ring laser with submilliwatt pump threshold", Opt.Lett., vol.7, pp.509-511, 1982.
5. Snyder, A.W.IEEE trans., vol.MTT-17, p.1130, 1969.
6. Sheem, S.K., and Giallorenzi, T:G.:Opt.Lett., vol.4, p.29, 1969.
7. Digonnet, M.J.F., and Shaw, H.J.: "Analysis of a tunable single mode optical fibre coupler", IEEE J.Quantum Electron., vol.QE-18, no.4, 1982.

Publications

Kalli, K., Culverhouse, D.O., Jackson, D.A.: "Fibre frequency shifter based upon stimulated Brillouin scattering generation in high finesse ring resonators", OFS-8, '92, California, P.28, Jan.1992.

Culverhouse, D.O., Kalli, K., Jackson, D.A.: "Stimulated Brillouin scattering ring resonator laser for SBS gain studies and microwave generation", Electronics letters, vol.27, no.22, pp.2033-2035, Oct.1991.

Kalli, K., Culverhouse, D.O., Jackson, D.A.: "Fibre frequency shifter based upon stimulated Brillouin scattering generation in high finesse ring resonators", Optics Letters, vol.16, no.19, pp.1538-1540, August 1991.

Russell, P.St.J., Culverhouse, D.O., Farahi, F.: "Theory of forward stimulated Brillouin scattering in dual-moded single-core fibres", I.E.E.E Journal of Quantum Electronics, vol.27, no.3, March 1991.

Russell, P.St.J., Culverhouse, D.O., Farahi, F.: "Experimental observation of forward stimulated Brillouin scattering in dual-moded single-core fibres", Electronics Letters, vol.26, no.15, July 1990.

Culverhouse, D.O., Farahi, F., Pannell, C.N., Jackson, D.A.: "Exploitation of stimulated Brillouin scattering (SBS) as a sensing mechanism for distributed temperature sensors, and as a means of realising a tunable microwave generator", OFS-6, '89. Paris, Proc.44, pp.552-559, September 1989.

Culverhouse, D.O., Farahi, F., Pannell, C.N., Jackson, D.A.: "Potential of stimulated Brillouin scattering as a sensing mechanism for distributed temperature sensors", Electronics Letters, vol.25, no.14, August 1989.

Culverhouse, D.O., Farahi, F., Pannell, C.N., Jackson, D.A.: "Stimulated Brillouin scattering. A means to realise a tunable microwave generator or distributed temperature sensor", Electronics Letters, vol.25, no.14, August 1989.